EFFECT OF CONICAL DISTRIBUTORS ON EVAPORATOR AND SYSTEM PERFORMANCE

BY

MICHAEL ANDREW FAY

THESIS

Submitted in partial fulfillment of the requirements
for the degree of Master of Science in Mechanical Engineering
in the Graduate College of the
University of Illinois at Urbana-Champaign, 2011

Urbana, Illinois

Adviser:

Professor Predrag Hrnjak

Abstract

This thesis presents the results of the study to experimentally examine effects of the distribution of refrigerant and air in the evaporator using a conical distributor on system COP and capacity.

Several conditions at the distributor inlet are varied including quality, mass flux, and orientation in gravity and the resulting superheat profiles of the evaporator circuit outlets are recorded. To examine possible effect of cone misalignment feeder tubes are switched in several steps and the data shows that there is imbalance in both the evaporator and distributor. It is observed that the imbalanced refrigerant distribution does not change over various operating conditions and is the result of complex interactions between the distributor and the evaporator.

Valves are installed on the feeder lines to create an ideal refrigerant distribution, indicated by uniform superheats at the outlets of the evaporator circuits, by adding a pressure drop in order to quantify the reduction in COP and capacity due to imperfect distribution. Using the valves to make the outlet superheat profile uniform improves the system and recovers most of the lost performance.

Additionally, the air distribution is made poor by blocking parts of the evaporator face. The impact of air imbalances on system performance is smaller than those of refrigerant. COP declines faster than capacity. Blocking entire refrigerant circuits rapidly deteriorates performance, compared to the same blockage area spread over all circuits. Moreover, the performance of the evaporator in terms of UA, LMTD, epsilon, and NTU, declines faster than overall system performance in terms of COP and capacity.

Table of Contents

List of Figures

List of Tables

Nomenclature

C	nozzle friction factor
Cmin	smaller heat capacity rate
cp	specific heat
$Drip$	weight of condensation collection bucket, g/s
dh_r	maximum possible enthalpy change of refrigerant in evaporator
LMTD	log mean temperature difference
$\dot{m}_{air}$	mass flow rate of air
M_r	measured mass flow rate of refrigerant
M_w	measured mass flow rate of condenser water
$\dot{m}_{w,out}$	mass flow of water in air through evaporator
NTU	dimensionless heat transfer units
P_{tun}	pressure drop across evaporator
P_{noz}	pressure drop across calibrated air flow nozzles
SL	suction line
SH	superheat, difference between measured temperature and saturation temperature
Q	heat load, kW
$T_{chwallin}$	interior of the environmental chamber wall
$T_{chwallout}$	exterior of the environmental chamber wall
T_{dew}	dew point of the environmental chamber air
$T_{shellbot}$	temperature near the bottom of the side of the compressor shell exterior
$T_{shelltop}$	temperature at the top of the compressor shell exterior
TXV	thermostatic expansion valve
UA	heat transfer coefficient times the heat exchanger area
W	measured electric power
Y	gas expansion coefficient
ε	heat exchanger effectiveness
ω	humidity ratio
σ	standard deviation, specifically of the evaporator circuit outlet superheats

Subscripts

aei	evaporator air in
aeo	evaporator air out
atm	atmospheric
auxhtr	electric heater
ave	average
comp	compressor
cri	condenser refrigerant in
cro	condenser refrigerant out
cwi	cooling water in
cwo	cooling water out

erdi	evaporator refrigerant distributor in
erdif	differential pressure across distributor
erin	refrigerant conditions entering evaporator
ero	evaporator refrigerant out, suction line
ers[i]	at the outlet of an individual circuit
fan	wind tunnel blowers
h1	electric heater
outlet	electric heater
r	refrigerant
sat	saturation
steam	steam injected for humidity

1 Refrigerant Maldistribution

1.1 Introduction

As evaporators increase in size there is a need to increase the number of circuits to maintain the refrigerant pressure drop across the evaporator at reasonable values and to balance pressure drop and heat transfer. Typically the quality exiting the thermal expansion valve is in the range of 0.10 to 0.30. Even distribution, assuming each circuit has equal load, of the liquid and vapor phases is difficult because both respond differently to inertial and gravity forces.

Two opposite, but both correct in principle, options for distribution are shown in Figure 1.1.

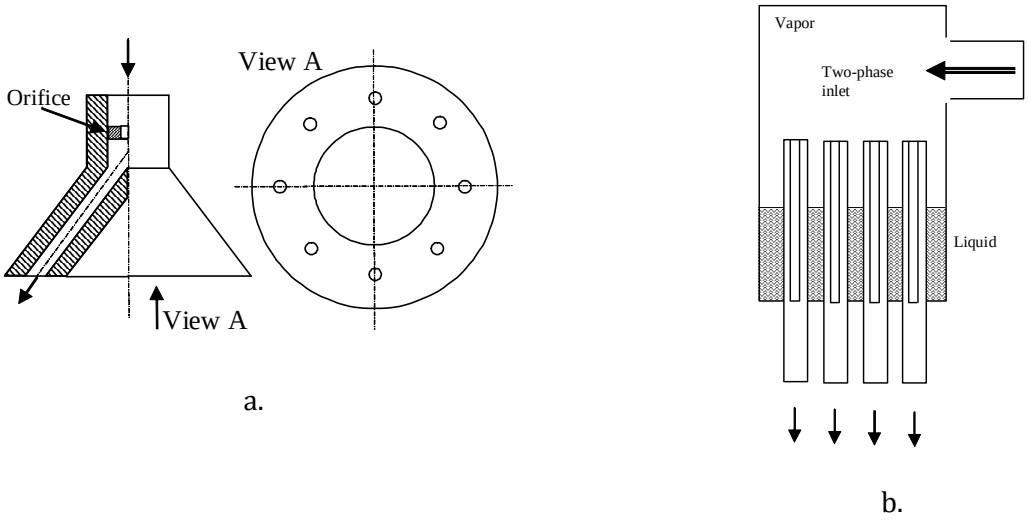

Figure 1.1: Two strategies for two phase flow distribution: a. homogenize and distribute and b. separate and distribute

The widely used way of distributing the two phases is as shown in Fig, 1.1.a. namely to homogenize the mixture and then immediately distribute it, feeding each circuit individually. In this

way the two phase flow is mixed and behaves like a single phase, at least temporarily before the two phases separate again.

The homogenization is done in expansion valve and helped with an orifice. The increase in velocity and the contraction through the orifice in addition to some liquid flashing as the pressure decreases mixes the two phases together. The orifice effuse is then directed into the evaporator feeder lines as a "single phase". To ensure equal flow rates through each branch it is essential that flow resistances are equal. In principle, ideal distribution does not require equal flow rates but adequate flow rates because thermal loads on each circuit may not be identical.

When this process does not perform correctly, maldistribution occurs as some of the evaporator circuits are overfed with liquid while another part is deprived. The circuit with insufficient feeding results in higher superheat and thus lower overall heat transfer. In the bigger picture, maldistribution impacts system performance as the non-ideal evaporator requires a larger temperature difference causing the suction line conditions to shift to less favorable for the compressor.

There is not much research in the open literature about conical distributors or maldistribution. Mueller [1988] wrote a review of maldistribution in heat exchangers, however much is not relevant to evaporators and one aspect, change in circuit pressure drop due to the laminar-turbulent transition, that is occurs at a flow rate much smaller than encountered.

Li et al. [2005] studied several methods to simulate two phase flow in distributors and found that the predictions for distribution and separation were similar for all the models. The study then used the simulation to test different distributor shapes and found that a spherical distributor base with an orifice located close to the base provided the best flow and distribution.

Wen et al. [2008] compared a conical distributor against a smooth tube Venturi and a Venturi connected to a microfinned spiral tube and found that the microfinned Venturi outperformed the distributor in COP and uniform distribution.

Kim et al. [2009] studied the optimization of evaporators with individual circuit control. The study built and validated a simulation that determined that control upstream of the evaporator was superior to below. Further, they calculated that improving refrigerant distribution would recover much of the loss in load and COP due to air side imbalances.

Studying evaporator circuitry, Liang et al. [2001] found that optimal coil design decreases the required heat transfer area by about 5%. Lee et al. [2003] found that different patterns of air maldistribution impact the heat transfer rate by up to 6%. Mueller et. al [1987] suggests that maldistribution generally reduces performance by 5 to 15%.

Shen et al. [2009] looked at ways to improve modeling with one aspect being refrigerant distribution at off-design conditions, the study found that the functioning of the distributor orifice was sensitive to the mass flow rate.

1.2 Equipment/Method

1.2.1 Lab System

The refrigeration system was part of a commercial rooftop air conditioning system running a vapor-compression cycle with a scroll compressor. The unit used refrigerant R410A. The evaporator nominal design capacity is 5 Ton or about 17.5 kW at air flow rate through evaporator 1.8 kg/s (2000 SCFM). The AC system was comprised of only a compressor, condenser, TXV, distributor, and evaporator. There were also high and low pressure safety switches.

The environmental chamber facility, interior dimensions 14’ x 7’ x 7’, was not large enough to accommodate the rooftop unit so parts were removed from the system and reconstructed as a new facility, Figures 1.2 and 1.3.

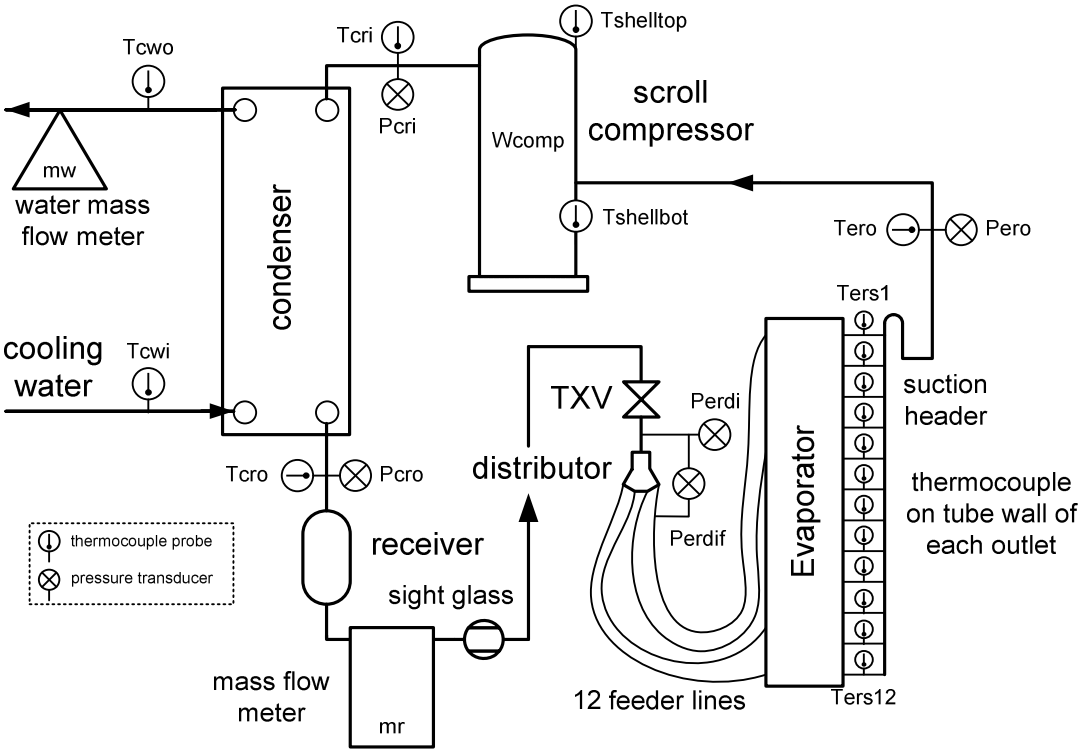

Figure 1.2: System diagram of the refrigerant loop

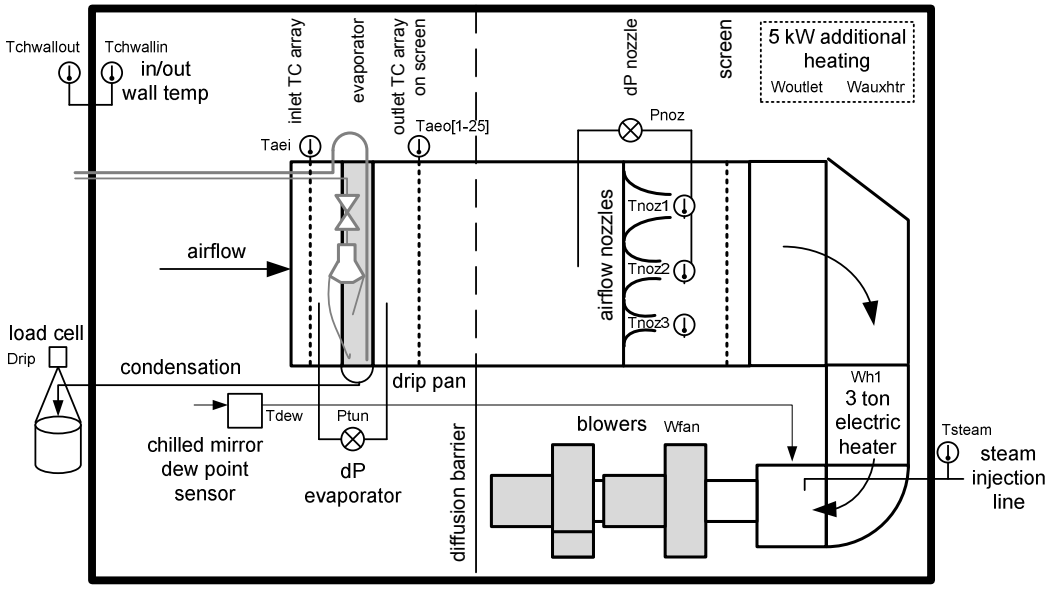

Figure 1.3: System diagram of the environmental chamber and wind tunnel

The compressor was a scroll type, Copeland Scroll ZP49K5E-TFE-130, with electronics compatible with the lab, 220 V/60 Hz. For experimental simplicity and with no effect on the evaporator distribution it was decided to use a water cooled a flat plate heat condenser.

The evaporator was removed from the unit by cutting the liquid line and suction line, keeping the Thermostatic Expansion Valve (TXV) and conical distributor, flowing down, as well as the suction header and some of the suction line undisturbed as one piece with the evaporator. It was installed at the inlet of a wind tunnel of the same cross section. The wind tunnel was constructed to standard ASHRAE 41.2-1987.

A drip pan emptying to a bucket on a load cell was built into the wind tunnel underneath the evaporator to collect condensation. Nozzles, one each of 3, 5, and 6 inches throat diameter, downstream were installed for airflow measurement.

1.2.2 Wind Tunnel

Figure 1.3 is an overview of the air loop of the facility. The wind tunnel was constructed to standard ASHRAE 41.2-1987. The inlet is 8 inches long and has the same cross section as the evaporator, 32" tall and 33.75" wide. There is a 3x3 fishing line grid 6" before the evaporator with nine thermocouples averaged together. Six inches downstream from the evaporator is a screen in a window screen frame of the same cross section as the tunnel. There is a differential pressure sensor measuring the pressure across the evaporator from points in the center of each of the four walls two inches from the evaporator both up and down stream. There are 25 thermocouples arrayed on the screen as prescribed by the ASHRAE standard.

Further downstream there are three calibrated nozzles, 6", 5", and 3" in diameter, visible in Figure 1.5. The pressure difference across the nozzles correlates to a volumetric flow rate of air. There is a thermocouple in the outlet stream of each nozzle.

From that point, the wind tunnel turns downward into an electric heater of 3 tons, 10.5 kW. As it rounds another corner, there is a steam injection tube. There are two identical 3.5 kW blowers,

Dayton model 4C329 with 3.5 kW motors model Dayton Wattrimmer 3KW33A drawing air from the end of the tunnel. With radially straight blades, the fan curve is stiff. The blowers exhaust laterally. There are three 1500 W electrical heaters arrayed around the blowers to further heat the air.

A chilled dew point sensor is mounted below the evaporator drawing air from just below the inlet. The low pressure side of the sensor is attached to the end of the wind tunnel to draw air through. A drip pan emptying to a bucket on a load cell was built into the wind tunnel underneath the evaporator to collect condensation.

1.2.3 TXV and Distributor

Both the TXV and distributor are mass produced commercial units, Figure 1.4. The TXV, Sporlan model BBIZE-4-GA, has a non-adjustable spring and is externally equalized. The sensing bulb is mounted in an 8-4 position (following clock hour sign locations) on the suction line.

The inlet of the distributor (Sporlan distributor Type 1115) is 13mm (1/2 inch) diameter tube. The orifice is 5mm (0.199 inch) in diameter and 6mm (0.250 inch) long. The orifice points toward a triangular cone. The feeder lines are recessed in a ring around the base of the cone. The twelve feeder lines are 4.75 mm (3/16 inch) OD, 3.34 mm (0.1315 inch) ID, and about 500 mm in length.

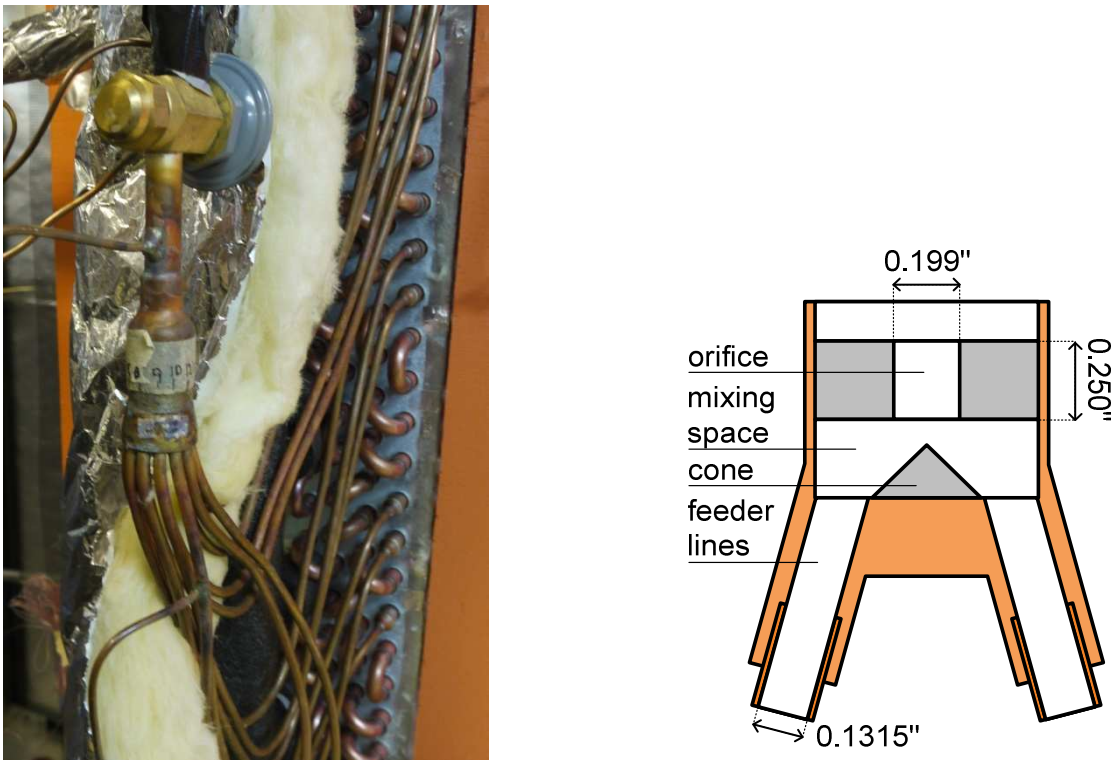

Figure 1.4: Left, a photo of the conical distributor and TXV along with pressure taps. Right, a cut-away view of the distributor from the manufacturer's catalogue

1.2.4 Evaporator

Figure 1.5 is a photograph of the evaporator in the wind tunnel. The round tube plate fin evaporator is approximately 813 mm (32 inches) tall and 857 mm (33.75 inches) wide. There are four slabs of refrigerant tubing. The airside fins are 100mm (4 inches) deep.

The evaporator circuitry is diagrammed in Figure 1.6. There are twelve circuits, in four groups of three. The pattern amongst each trio repeats with minor variations four times in the whole evaporator. The topmost circuit of each trio makes six loops while the second and third circuits make five loops.

Figure 1.5: Overview of the evaporator, TXV, and distributor in the wind tunnel which has been opened showing the airflow nozzles downstream

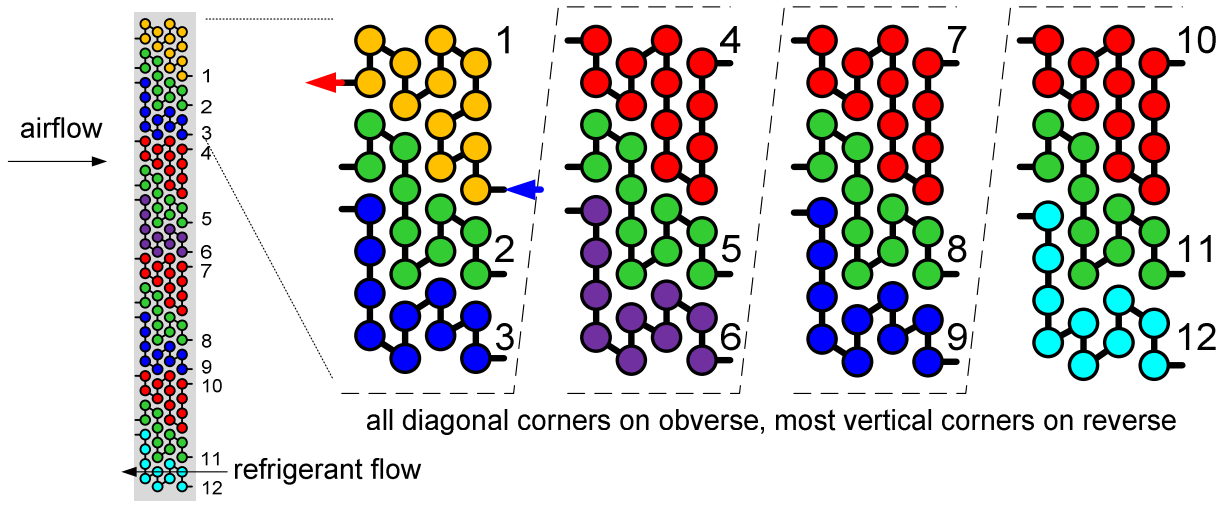

Figure 1.6: Diagram of the evaporator circuitry from the refrigerant inlet/outlet side. Identical circuits have the same color. Airflow is to the right whereas the refrigerant enters the evaporator on the right and exits at the left. The first circuit of each group, circuits 1, 4, 7, and 10, are the long circuits with four passes in the third and fourth layer. In comparison, the second circuit has four passes in the third layer and the third circuit has four passes in the first layer

The evaporator designer attempted to compensate for the lengths in the design of the evaporator. Each circuit has at least one pass in each of the four slabs. The two shorter circuits of the pattern have a second pass in either the first slab or the second slab. The long circuit has two second passes in each of the third and fourth slabs. The additional length is located on the air outlet side so the additional tube length is balanced by being located where it is less effective due to smaller temperature difference.

The capacity the evaporator is based on two independent balances: 1. Air side, 2. Refrigerants side. These two balances were within ±3%.

The air side balance is calculated by combining the air mass flow rate, Eq. 1.3, determined from the static pressure difference across a set of three nozzles as in Equations 1.1 and 1.2.

$$Q_{noz} = 1.414Y\sqrt{P_{noz}/\rho_{aeo,ave}}\sum(CA_{noz}) \tag{1.1}$$

$$Q_{aei} = Q_{noz}\frac{\rho}{\rho_{reference}} \tag{1.2}$$

$$\dot{m}_{air} = Q_{aei}\rho_{aei,ave} \tag{1.3}$$

Y is the expansion factor. It is very close to 1 at conditions encountered. In each run it is calculated to be larger than 0.995, which agrees with a table supplied in the standard.

The mass flow rate is combined with the change in air enthalpy, Eq. 1.4, as measured by the two airside thermocouple grids to determine the air capacity.

$$Q_{evap,air} = \dot{m}_{air}\left(h_{air,in} - h_{air,out}\right) \tag{1.4}$$

The enthalpies are calculated with EES' wet air fluid data:

$$h_{air,in} = f(P_{atm}, T_{aei}, T_{dew}) \quad (1.5)$$

$$h_{air,out} = f\left(P_{atm}, T_{aeo}, T_{dew,out}\right) \quad (1.6)$$

Where $T_{dew,out}$ is calculated from $\dot{m}_{air}$ and $\dot{m}_{w,out}$ as calculated in Equation 1.7.

$$\dot{m}_{w,out} = \dot{m}_{air}\omega_{air,in} - Drip \quad (1.7)$$

The thermocouple array on the inlet T_{eai} (3 by 3) and outlet T_{eao} (5 by 5) sides of the evaporator provide inlet and outlet temperatures. A chilled mirror dew point sensor (General Eastern model D2-SR, accuracy ±0.2 C) measures the dew point (T_{dew}) in the chamber.

The refrigerant side balance is calculated in Equation 1.8 using refrigerant mass flow rate, m_r, measured by 0.1% accurate liquid mass flow meter Micromotion DS025, and enthalpy change of refrigerant from the outlet of the condenser to the outlet of the evaporator.

$$Q_{evap,r} = M_r(h_{ero} - h_{cro}) \quad (1.8)$$

Where h_{ero} and h_{cro} are both calculated from T_{ero} and P_{ero} and P_{cro} and T_{cro}, respectively.

The superheat of each circuit is measured by a thermocouple taped down to a drop of thermal paste at the center top of the exterior of the tube wall, $T_{ers[1\text{-}12]}$. There is about 75 mm (3 inches) of tube between the evaporator side wall and the suction header. One meter down the suction line the pressure is sampled, P_{ero}, and the temperature measured with a probe, T_{ero}.

In running the system, there was no large discrepancy found in the superheats between the longer circuits and the shorter ones.

COP is calculated as in Equation 1.9, the evaporator capacity or load, since runs are conducted in steady state, is divided by the compressor power. The power usage of the blowers is not taken into consideration.

$$COP = {Q_{evap}}/{W_{comp}} \tag{1.9}$$

The uncertainties of the pressure gages and mass flow meters are known, none are larger than 1% full scale. The accuracy of thermocouples is taken as ±0.3 C. Using the uncertainty propagation feature of EES, based on Taylor et al., these measurements yield uncertainties in capacity of 0.53%, in COP of 0.66%, and superheat standard deviation, or sigma, of 2.05%. UA, LMTD, and NTU are between 1.0% and 1.8%.

1.3 Results

The condensation temperature of 47 C was selected as representative of the actual unit and kept over the entire range of conditions.

Once it was confirmed that the system, facility, and instrumentation worked correctly and matched the commercial system performance several initial non-intrusive tests were conducted.

1.3.1 Exploring Condition Effects on the Superheat Profile

Figures 1.7 and 1.8 present the effect on superheat at the exit of the evaporator circuits from variations in the distributor inlet conditions. The differences among 12 superheats at the exits of each circuit are between 0 and 11 C for average 5 C. The shape of the superheat curve in the range explored does not change as a function of quality (Figure 1.7) or mass flux (Figure 1.8).

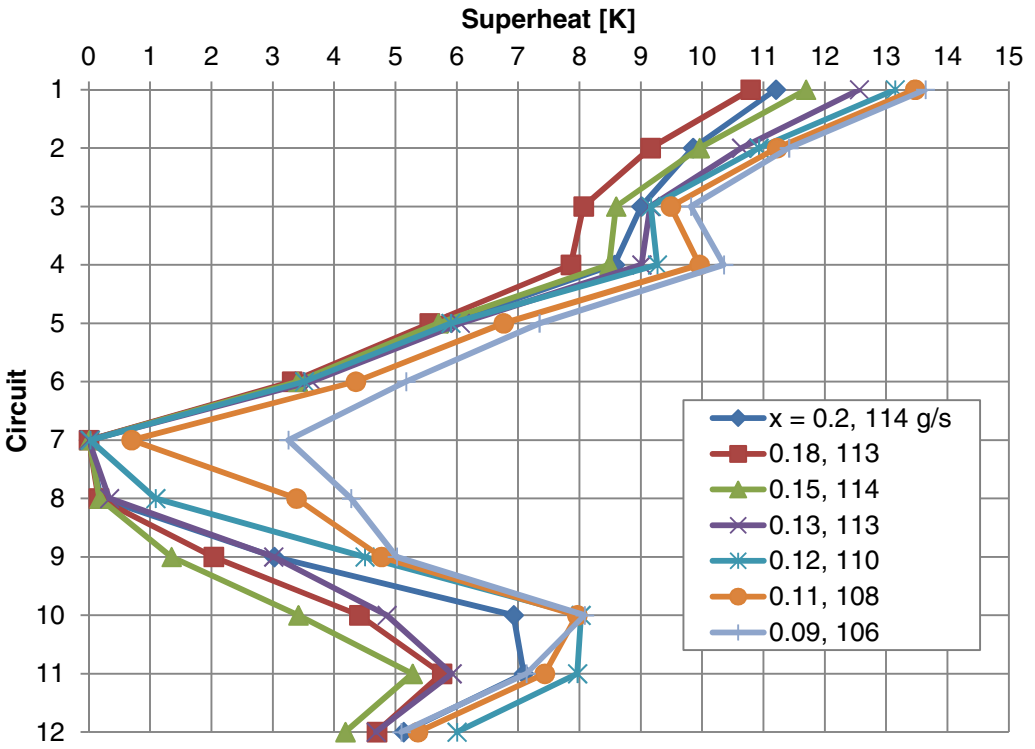

Figure 1.7: Circuit superheats as a function of inlet quality. Only the condensation temperature was decreased by increasing the cooling medium (water) flow rate to achieve lower qualities. Circuit 1 is the topmost circuit

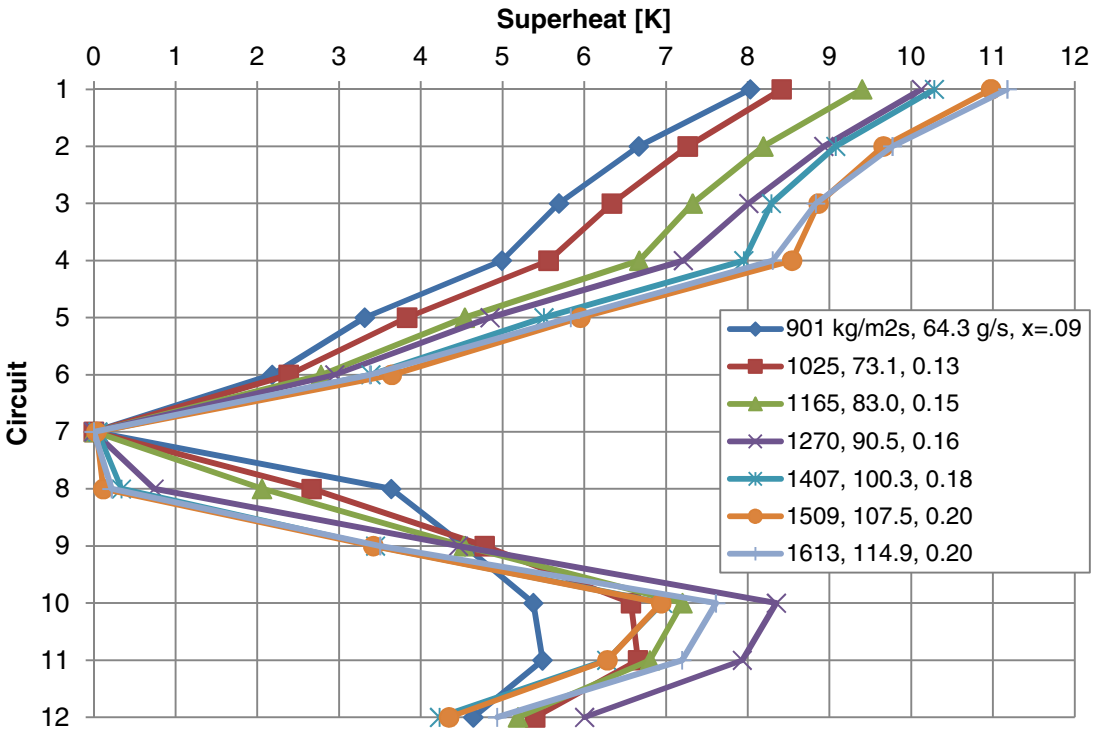

Figure 1.8: Circuit superheats as a function of mass flux in kg/m^{2}s at the distributor inlet, mass flow, and distributor inlet quality. Circuit 7 had two-phase flow at the outlet in all runs

These two plots show the same general superheat pattern over a range of conditions with variations of inlet quality and mass flow rate indicating robust, but imperfect system behavior.

There are several possible hypotheses for imperfect distribution. A suspect issue is flow separation in the distributor (inbound flow regime to the orifice, Figure 1.1). There is about 150mm (6") between the TXV and distributor. However, according to the Bowers [2009] map, the mass flux in the system is far away from any flow regime boundaries. Checking vertical flows via momentum flux, the Hewitt and Roberts [1969] map for upward flow indicates the flow would be in the annular regime, not far from the transition from churn flow.

The same issue may exist on the other side of the orifice, which the distributor uses to rehomogonize the flow in a mixing space before splitting it up. Li [2004] found dramatic differences on uniformity with different shaped spaces and orifice positions with simulations. If there is a separated region inside the distributor, that is a region of one phase next to the orifice outlet, it would be expected that gravity would have an influence, and subsequently distributor angle.

One way to check this hypothesis is to change the angle of, or tilt, the distributor. Figure 1.9 shows the distribution while tilting the distributor up to 45˚ from vertical.

There is very little difference in the superheat profile going from vertical to 45˚ which indicates that angle does not play a role in this case and there is no significant separation at the outlet or inlet. In fact, the superheat of the circuit lowered by the tilt increases slightly, meaning that it may be receiving less liquid.

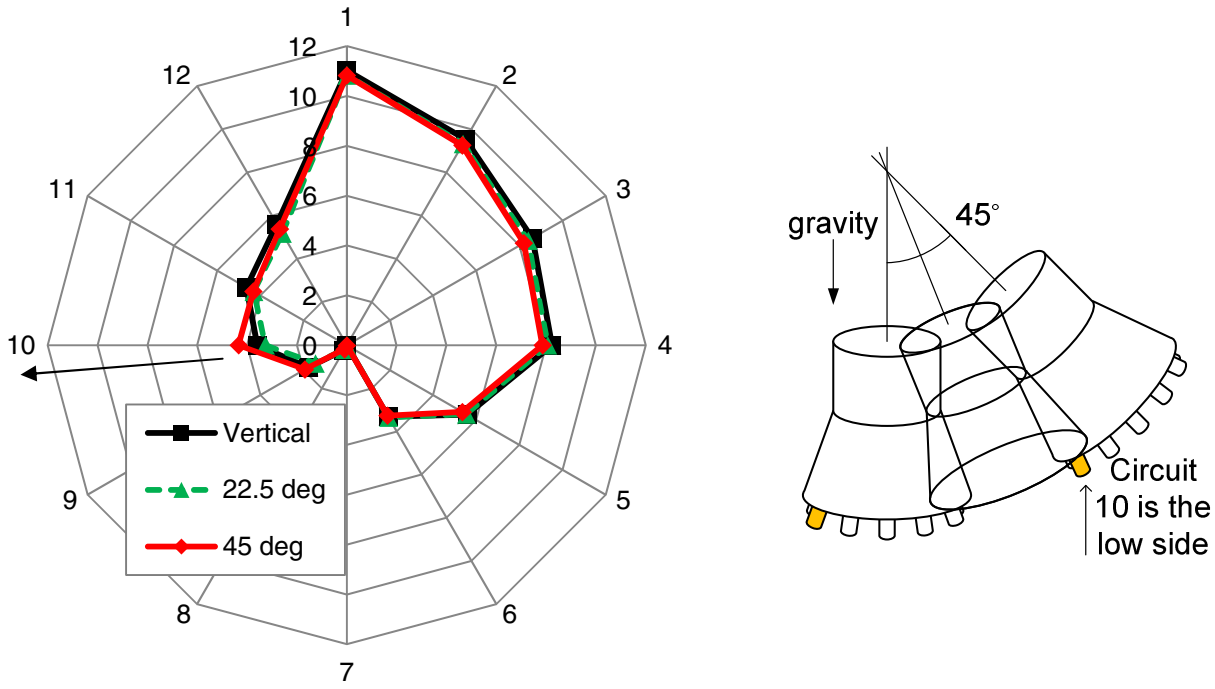

Figure 1.9: Circuit superheats are graphed as radius length in K with circuits as the circumferential points. The distributor was tilted toward circuit 10 due to space available. There was little change in the distribution of superheat. The data of circuits 11 and 12 are switched to reflect their position on the distributor instead of on the evaporator.

1.3.2 Swapping Circuits

The next set of tests involved cutting the feeder lines. Pairs of feeder lines were exchanged one at a time. One of the circuits with no superheat was swapped with a circuit of identical geometry in the high superheat region. The first pair was 7 and 4, followed by the circuits 8 and 2, then 9 and 3 to finally 10 and 4.

If the imbalance were due to the evaporator, like a heat load or tube issue, switching the circuits should have little effect because the source would not be due to the distributor supplying different amounts of liquid to different circuits. If the imbalance were due to the distributor, the switch should exchange the superheat values. This hypothesis is illustrated in Figure 1.10.

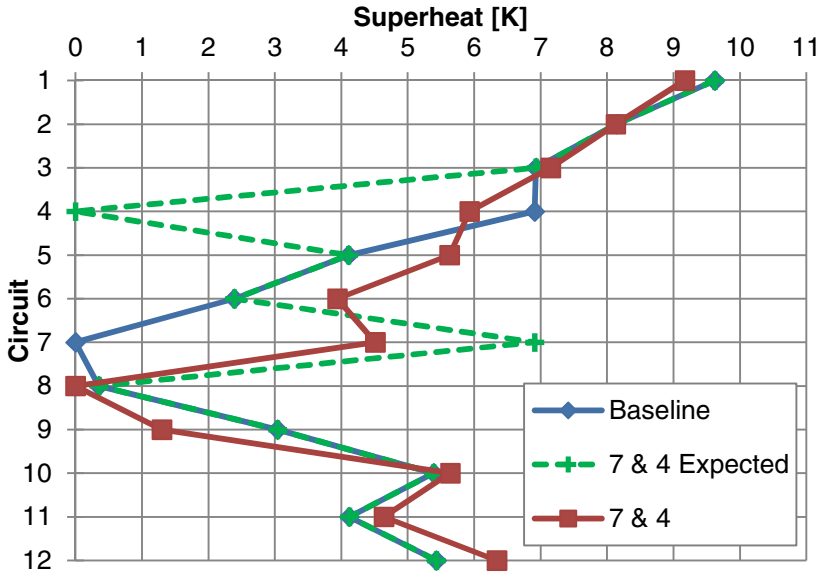

Figure 1.10: A plot of the expected superheat profile with circuits 7 and 4 flipped if the distributor is not performing well. The red line is the actual result.

As plotted in Figure 1.11, the pattern did change, but not in a way that points strongly to either component. The superheat profile is a result of a complex relationship between the distributor and the evaporator.

A feature is that the superheat minimum is pushed from circuits 7 and 8 to 8 and 9 before splitting to 7 and 10 when 9 is exchanged. When 10 is exchanged, the minimum returns to its original position. 10 is beyond the other side of the cause of the particular imbalance.

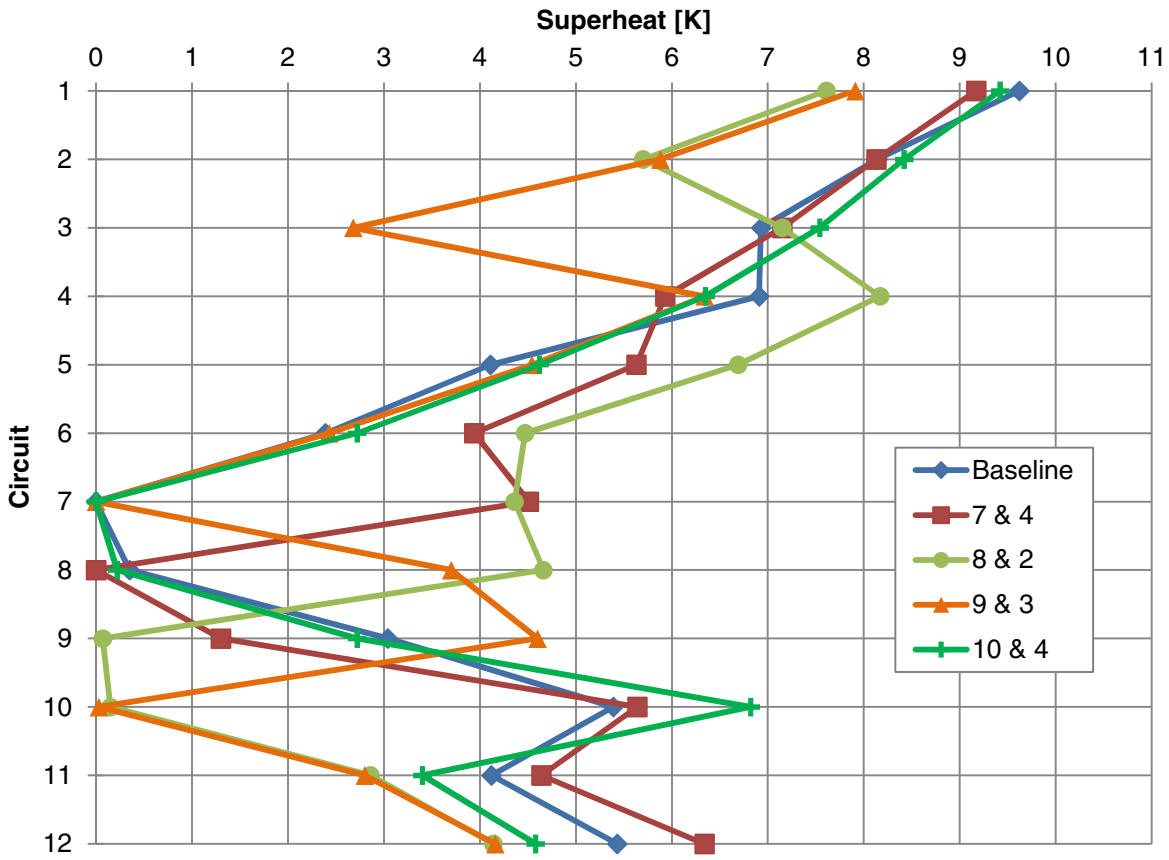

Figure 1.11: Superheat profiles with pairs of circuits switched. The circuit flips pushed the trough from 7 and 8 to 9 and 10 before the trough split with 9 flipped and then reappeared in the original position when 10 was switched with 4.

1.3.3 Potential for Improvement

The difference in superheats among the twelve circuits has been documented. The logical question is: is that difference significant, or even better, what is the cost of such maldistribution in terms of capacity (Q) and efficiency (COP)? Addressing that issue is important to gauge the magnitude of the problem and the need for an improved component. To establish the maximum capacity and efficiency, as a goal, an attempt was made to generate "ideal" distribution.

1.3.3.1 Ideal Distribution

"Ideal" distribution is defined as uniform superheat at the exit from each circuit. Superheat is defined as difference between actual refrigerant temperature and saturation temperature. It this case it is specifically $SH = T_{ero} - T_{sat}$ where T_{sat} is determined as a function of the refrigerant pressure in the suction line.

The standard deviation of the superheats, referred to as σ, is calculated to quantify the departure from uniformity as in Equation 1.10.

$$\sigma = \sqrt{\frac{1}{n}\sum_{i=1}^{n}(SH_i - SH_{ave})^2} \tag{1.10}$$

The smaller the standard deviation, the more uniform the distribution. The lower limit, the best distribution with no variation from the average, is when sigma is zero. The maximum value of superheat is a function of operating conditions ($SH_{max} = T_{aei} - T_{sat,evap}$) so the worst sigma is also a function of conditions. The largest sigma, representing the most uneven distribution, is when half of the superheats have the maximum value and the other half have zero superheat.

The advantage of this method of seeking to minimize variation in outlet superheats is that it is a simple and quick measurement to make and parameter to calculate. However there are some shortcomings. Superheat is meaningful only when greater than zero, the temperature measurement is above the refrigerant saturation temperature, and less than the value that corresponds to the inlet air temperature. Measuring outlet superheats alone does not capture the entire distribution picture since the temperature measured downstream in the suction line is the amalgamation of the enthalpies and mass flows of all the circuits. As the mass flow of all circuits approaches the average mass flow, the averaged outlet superheat temperature will approach the measured suction line superheat.

Although mass flow issues are outside measuring the uniformity of superheat, seeking to make uniform the superheats does mitigate negative effects of mass imbalances. To make uniform the superheat of all circuits, liquid refrigerant is distributed around the evaporator to match the capacity of the circuit. In this way airside imbalances are taken into consideration and accounted for so performance lost to airside degradation from being in the field is automatically recovered.

In addition, this measure, superheat uniformity, alone does not tell the entire picture of performance. In principle the existence of superheat is not beneficial for the function of the evaporator or the system as a whole. Heat transfer in the superheated region is poor and the temperature difference between air and refrigerant is small. Refrigerant superheat is used for the simplicity of flow control. Superheat should be maintained as low as possible from the performance point of view and as high as needed to provide a sufficient and stable control signal in order to avoid fluctuations described first by Wedekind [1965] and afterwards elaborated by few others. In the case of the maldistribution some exits are superheated and some at some quality and their mixture is typically superheated in the location of the TXV bulb, or sensor. To achieve that condition superheats at superheated streams must be significant to provide sufficient energy to evaporate liquid droplets and liquid absorbed in oil coming from the non-superheated exits. That causes reduction in performance of the superheated circuits. So, more uniformity of superheat provides improvement of overall heat transfer.

1.3.3.2 Adjustment for Maximizing COP and Capacity

Small valves were installed on all twelve, 3/16 inch feeder lines. Adjusting the resistance, that is opening, in each adjusts the flow rates to provide equal superheats and to make uniform distribution while the system runs.

The system was started and brought up to full compressor speed with all valves an equal number of turns nearly fully open. The typical σ the system settled on at full speed was around 1.1. The valves were gradually tightened to restrict some circuits and produce a high variation in SH. At

60 Hz supplied to the compressor with σ about 4, the capacity at that point, or the air temperature difference across the evaporator, was the target for the remainder of the run. The dew point in the chamber was below the saturation temperature so the evaporator was dry, condensation was not an issue.

After achieving steady state and collecting data at that point, valves were gradually opened, reducing the maldistribution in steps back to the original pattern. The constant speed point was recorded then the compressor speed was reduced, letting the suction line pressure and temperature rise, reducing the load until the air temperature difference returned to the target for constant capacity.

Improving the distribution, that is reducing σ, took longer. After every circuit was mostly closed, tweaking took many adjustments since it took time for the temperature to settle and the system to come to steady state. Moreover, adjusting one circuit affected all the others as well. It was found that the valve setting that unified the superheat was repeatable on following days, indicating that the maldistribution was not significantly a result of starting conditions and two-phase flow issues in the evaporator.

The data in Figures 1.12 and 1.13 were collected under the same conditions. The condensation saturation temperature and air flow, air inlet temperature, and dew point were maintained at 47.35 ± 0.08 C, 2005 ± 3 SCFM or 1.084 kg/s, 29.6 ± 0.1 C, and 12.8 ± 2 C, respectively. One set of data was taken with a constant compressor speed and the other set was taken with variable compressor speed to maintain the load over different refrigerant distributions.

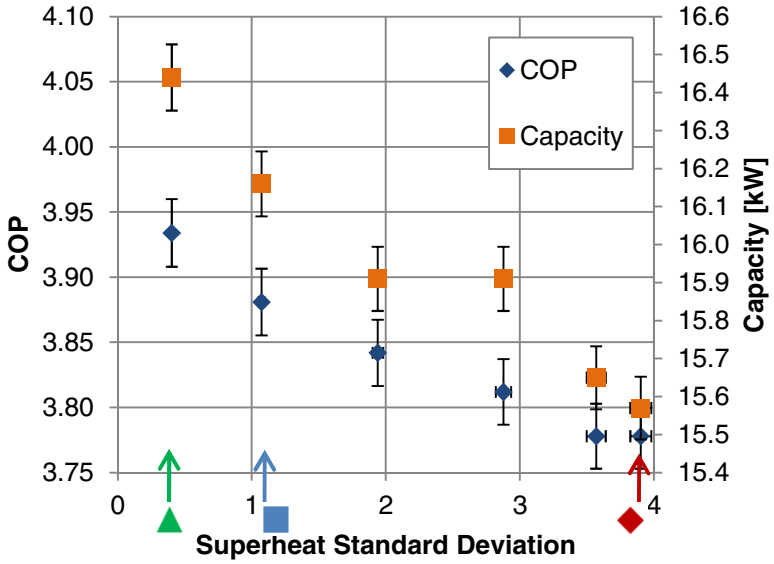

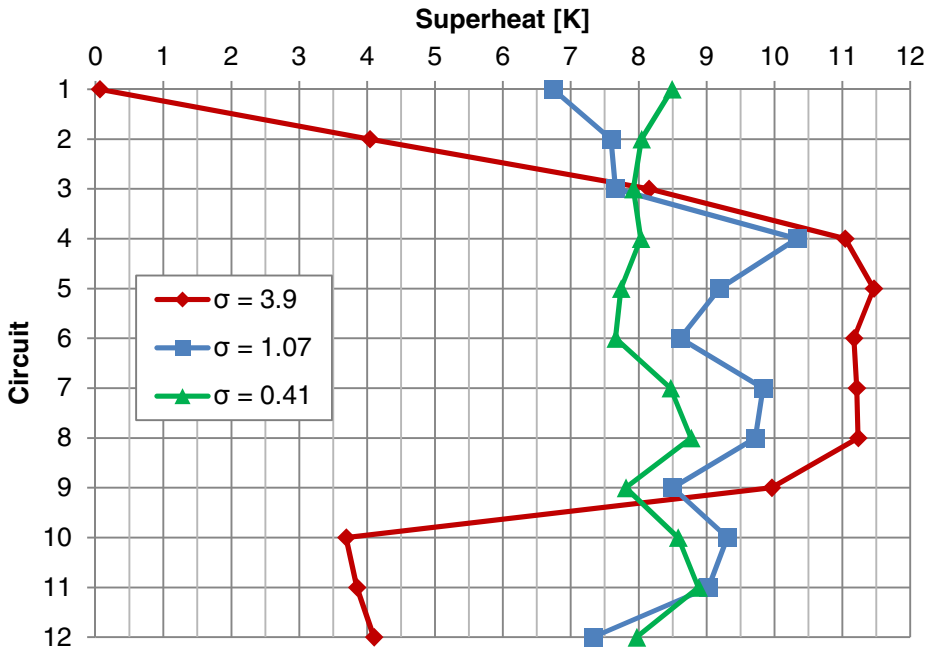

Figure 1.12: Effect of distribution on capacity and COP over a range of superheat distributions by adjusting pressure drop of feeder lines at all other conditions unchanged. Below, the superheats of the individual circuits at unmodified, worst, and improved conditions.

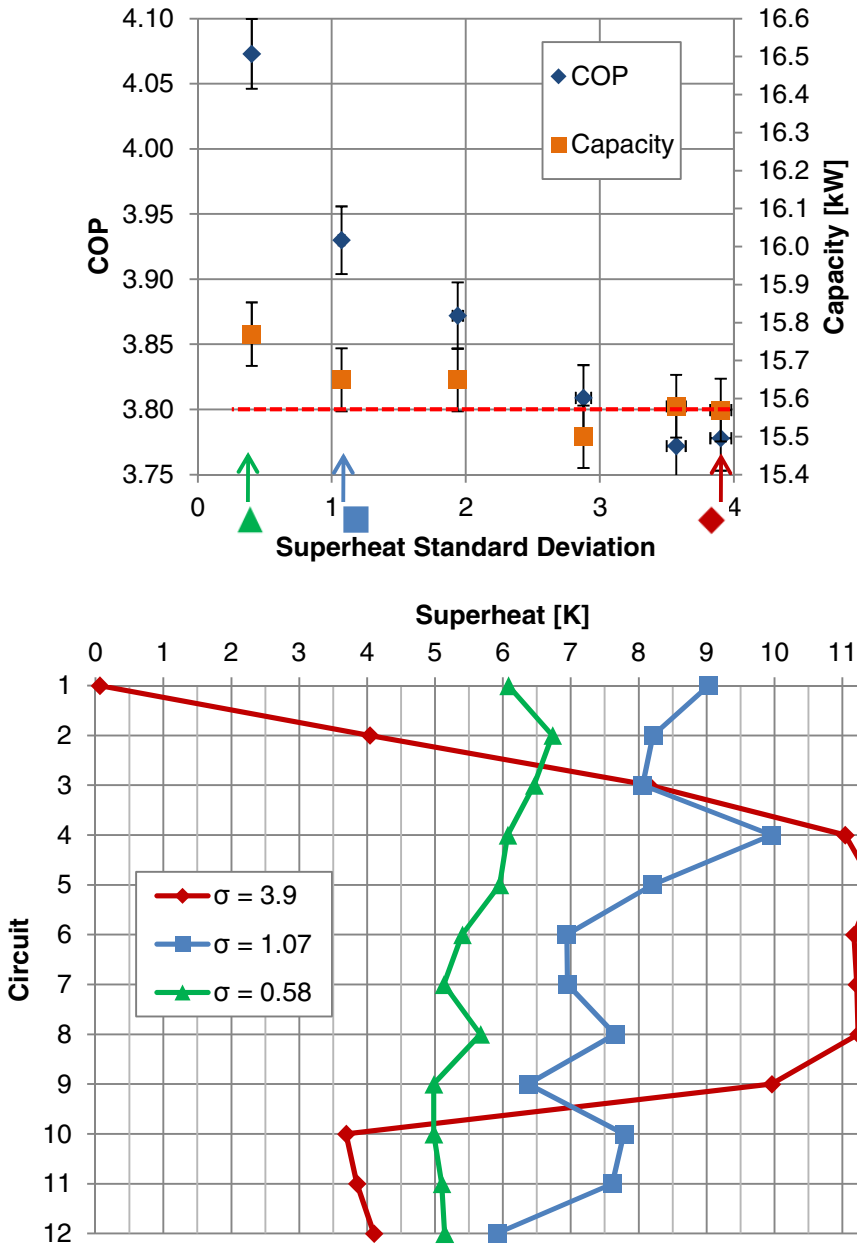

Figure 1.13: The improvement in COP at a constant capacity over a range of superheat distributions by slowing compressor speed. The red dashed line is the target load. Below, the superheats of the individual circuits at unmodified, worst, and improved conditions.

Table 1.1: The compressor speed data corresponding to Figure 1.13. The speed decreased as the distribution improved.

σ	Hz
3.90	60.0
3.46	59.7
2.92	58.5
1.64	58.2
1.07	57.3
0.58	55.8

In one series, Figure 1.12, the compressor remained at 60 Hz while the distribution varied. Both the capacity and the COP increased from the most maldistributed condition.

In the second series, Figure 1.13, the compressor speed is reduced from 60 Hz at the poorest distribution to keep the load approximately the same as at the most maldistributed condition. There is a much larger gain in COP than the previous run, 7.8% was measured. Despite aiming to keep the capacity constant, the capacity at the most uniform distribution was larger than at the least uniform by approximately 1.3% which means that the compressor was not slowed enough. As listed in Table 1.1, the lowest speed at the best distribution is 55.8 Hz. From the data, it is expected that further slowing the compressor to match the initial capacity would further increase the gain in COP to 8-10%.

Table 1.2: Comparison of the changes in capacity and COP from unmodified, with all valves open (σ = 1.1), to improved (σ = 0.5) and worsened (σ = 3.9) distributions.

Constant		Distribution			Gain from Unmodified	Gain from Worsened
		Unmodified	Improved	Worsened		
Speed	COP	3.88	3.93	3.78	1.37%	4.13%
	Capacity (kW)	16.16	16.44	15.57	1.73%	5.59%
Capacity	COP	3.93	4.07	3.78	3.64%	7.81%
	Capacity (kW)	15.65	15.77	15.57	0.77%	1.28%

Table 1.2 summarizes the performance of these series. At the worsened condition, σ = 3.9, two of the circuits had no superheat while the other circuits had 10 to 15 K superheat. The usual unmodified distribution was about σ = 1.1, the distribution the system had with the valves open. Improved achieved around σ = 0.5. In the improved cases, the range of variations in superheats was within 1.5 K.

The numbers in the table show that the gains in COP in both conditions are double for constant load than at constant speed. For a constant load, even the more modest improvement,

from the unmodified distribution, yields a significant 3.6% gain in COP. If the evaporator runs with a flooded circuit or two, the potential improvement is in the neighborhood of 8%.

Simply improving the distribution of an unmodified existing system with everything else being equal, for the system explored, one could expect a 1.4% increase in COP and a 1.7% increase in load simultaneously. Again, if the system is distributing poorly and has two flooded circuits there are potential gains of 4.1% and 5.6% in COP and load, respectively.

1.3.3.3 Distributor Pressure Drop

The feeder line valves had a range of five and a quarter turns but adjustments had little impact in pressure or distribution until the final turn. Figure 1.14 is a plot of the pressure difference from the tube between the TXV and the distributor and in a feeder line two inches beyond the distributor, well upstream from the feeder line valve.

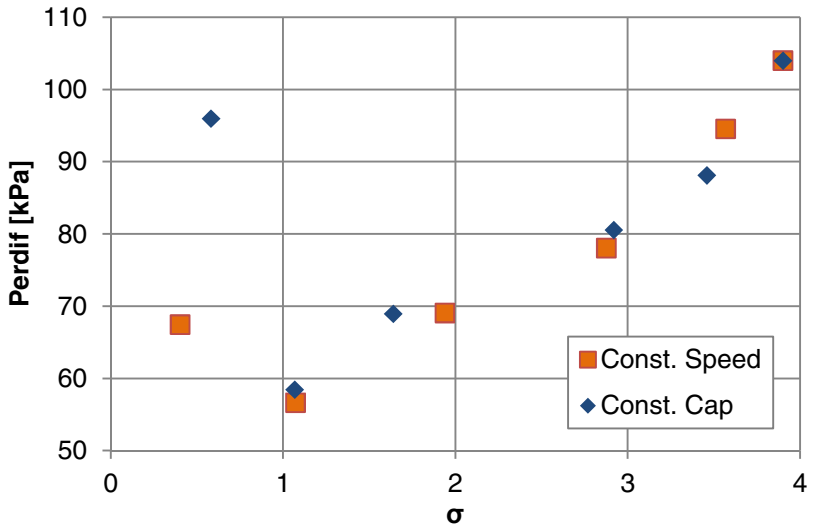

Figure 1.14: The pressure difference across the distributor, P_{erdif}, photographed in Figure 1.4 and in schematic Figure 1.2, for runs that resulted in various σ for the two series.

The minimum pressure difference occurred with the unmodified condition, all valves open. This is a function of the orifice size. On either side of that point, the difference increases—it takes pressure increases to disturb or steer the flow. The left side of the chart climbs toward an

asymptote. As the SH is made uniform, additional pressure drop is transferred from the TXV to the valves. To get to the extreme case of σ = 0, the distributor would be on the liquid line and each feeder line would have a TXV sampling from its outlet on the evaporator.

In both high and low σ cases, decreasing the compressor speed to decrease the capacity pushed the σ towards the unmodified case by large enough amounts that the valves needed to be adjusted to keep the system at a particular σ. In improved runs, decreasing the compressor slowed the refrigerant through the orifice, decreasing the pressure drop and the distribution worsened toward the unmodified distribution.

1.3.3.4 Heat Exchanger Performance

In addition to system performance and capacity, distribution affects the performance of the evaporator. Figure 1.15 is a plot of the suction line saturation temperatures with the measured temperature. For constant speed, T_{sat} rises from 11.4 to 12.4 C and the T_{sl} increases from 15.4 to 20.7 C. For constant capacity, T_{sat} increases more dramatically from 11.4 to 13.7 C. T_{sl}, however, starts off at 15.4 C, peaks at 21.1 C, then declines to 19.7 C at the improved distribution. The smaller superheat at a higher T_{sat} conserves compressor work, boosting the COP.

Looking at heat exchanger performance parameters in Figure 1.16, the LMTD decreases from 8 to 5 C. UA increases linearly with σ from 1.9 kW/K to over 3.25 kW/K.

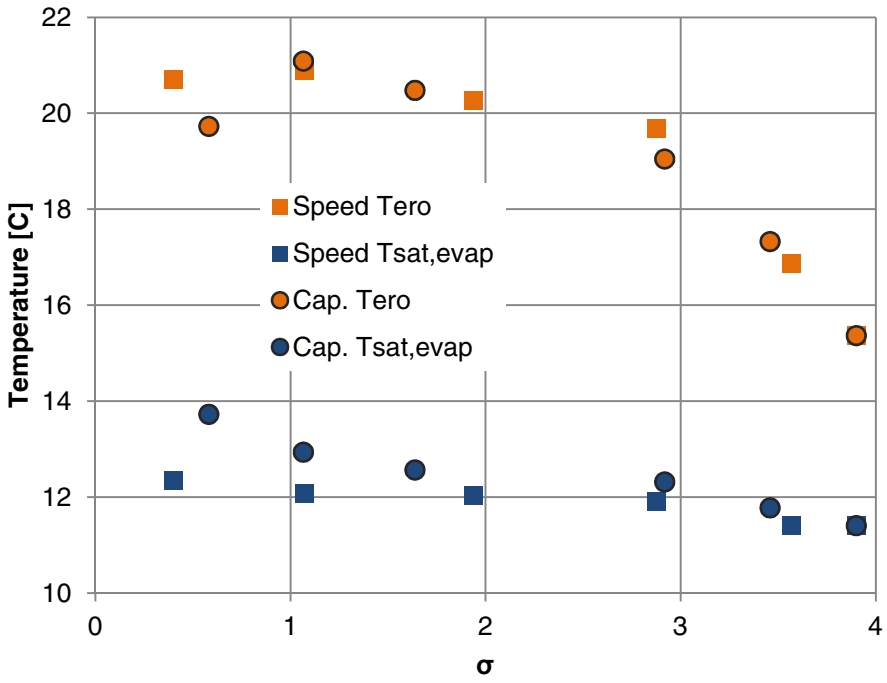

Figure 1.15: Saturation temperature, $T_{sat,evap}$, and measured temperature in the suction line, T_{ero}, for the constant speed run and constant capacity run.

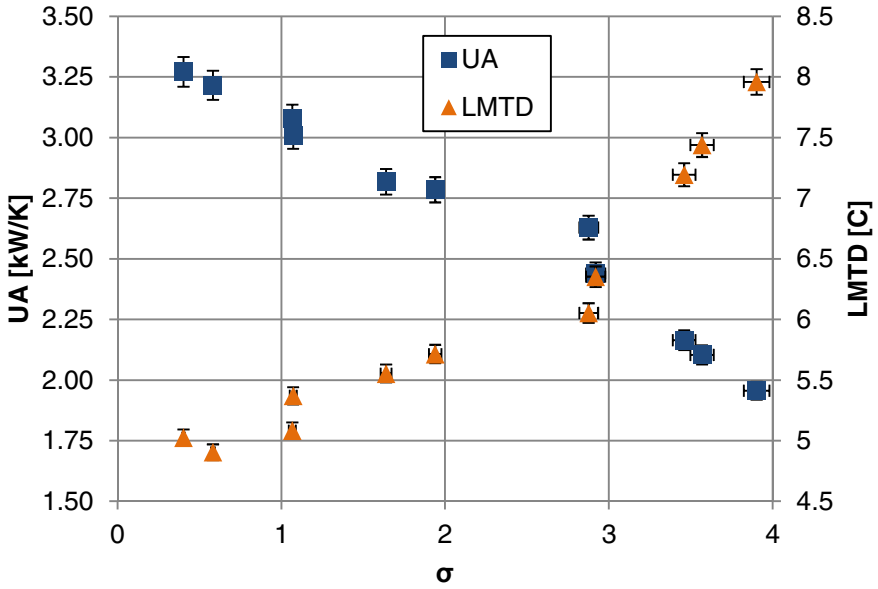

Figure 1.16: Effect of distribution on evaporator performance (UA, LMTD). The superheat distribution was altered by valves adjusting flow resistance conditions on the feeder lines. Airside conditions were unchanged.

Figure 1.17 is a plot of heat exchanger effectiveness in terms of epsilon and NTU. Epsilon is calculated in Equation 1.11. $Q_{max,r}$, the largest amount of heat transferable, is determined in Equation 1.12 as the largest possible enthalpy change for the refrigerant, dh_r, which is the enthalpy of the refrigerant at the suction line pressure and temperature of the incoming air subtracted by the enthalpy of the refrigerant exiting the condenser.

$$Epsilon_r = {Q_{evap,r}}\Big/{Q_{max,r}} \tag{1.11}$$

$$Q_{max,r} = m_r \cdot dh_r \tag{1.12}$$

For NTU, the heat capacity of air is used because it is not changing phase. In Equation 1.13, the mass flow of air is combined with the specific heat to calculate the heat capacity. Then the UA of the evaporator is divided by that to calculate the NTU, Equation 1.14.

$$C_{min} = \dot{m}_{air} \cdot cp_{air} \tag{1.13}$$

$$NTU = UA/C_{min} \tag{1.14}$$

UA was calculated from the log mean temperature difference, LMTD, Eq. 1.15. LMTD is defined as in Equation 1.16.

$$Q_{evap,air} = UA \cdot LMTD \tag{1.15}$$

$$LMTD = \frac{\left(\mathrm{T_{aeo,ave}} - \mathrm{T_{erin}}\right) - \left(\mathrm{T_{aei}} - \mathrm{T_{ero}}\right)}{\ln\left(\frac{\mathrm{T_{aeo,ave}} - \mathrm{T_{erin}}}{\mathrm{T_{aei}} - \mathrm{T_{ero}}}\right)} \tag{1.16}$$

In the very maldistributed case, σ = 3.9, epsilon is just above 0.9. It rises to a knee at about σ = 2.5 where it levels out at about 0.94.

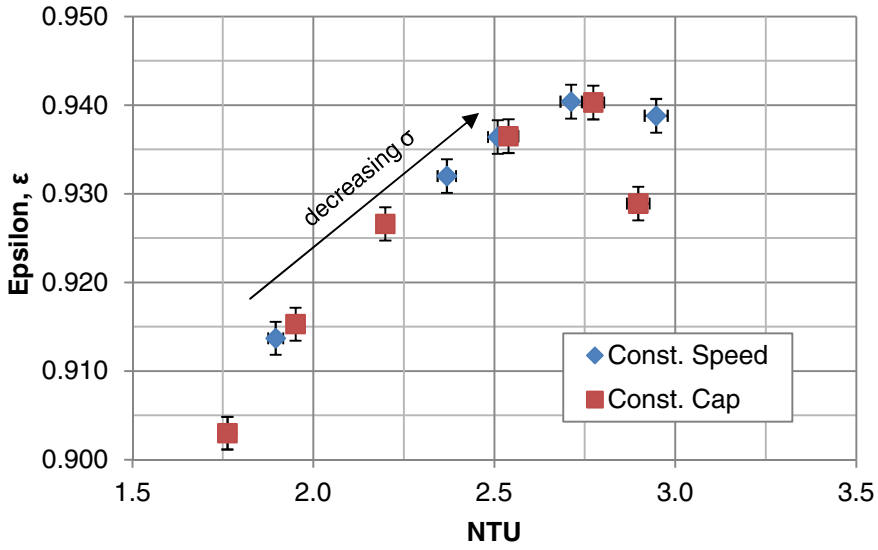

Figure 1.17: Evaporator performance for both constant load and constant speed runs.

There is not much gain in evaporator performance as a heat exchanger from the undisturbed distribution, but there is a large gain from the very maldistributed case with flooded circuits.

1.4 Conclusion

A 5 ton commercial air conditioning system with a modified water cooled condenser was used to explore the effects of maldistribution of a conical distributor on a real system. Maldistribution, or inadequate flow rates to the circuits, was defined and quantified as the standard deviation of the superheats of each evaporator circuit.

Tests were conducted to probe the maldistribution. The two phase flow did not appear to separate in the distributor so inadequate size of the orifice did not appear to be an issue. Variation of inlet quality, mass flow rate, and distributor angle did not produce effects that changed the superheat pattern. Neither did switching pairs of circuits between the distributor and the

evaporator change the pattern suggesting that both the distributor and evaporator have imbalance issues.

It was found that simultaneous gains of 1% to 4% can be made in capacity and COP from a typical distributor, used as a baseline in this experiment. From the system running with two-phase flow observed at some circuit outlets, the measured gain in COP was at least 8% for a constant load, while at constant speed the simultaneous gains were 4% in COP and 5% in capacity. Undisturbed the system ran with pressure drop minimized across the distributor and either improving or worsening the distribution required increasing the pressure drop. Improving the distribution also showed significant gains in evaporator performance of LMTD, from 8 to 5 C, UA, from 3.25 to less than 2 kW/K, and effectiveness, from 0.90 to 0.94.

1.5 References

Bowers, C. D., P. S. Hrnjak, 2009. Developing Adiabatic Two-Phase Flow. Ph.D. thesis, Air Conditioning and Refrigeration Center, University of Illinois Urbana-Champaign.

Hewitt, G.F., D.N. Roberts, 1969. Studies of two-phase flow patterns by simultaneous x-ray and flash photography. AERE-M 2159, Her Majesty's Stationary Office, London.

Hrnjak, P., 2004. Developing Adiabatic Two Phase Flow in Headers—Distribution Issue in Parallel Flow Microchannel Heat Exchangers, Heat Transfer Engineering. 25(3), 1–8.

Kim, J., J.E. Braun, E. A. Groll, 2009. Evaluation of a hybrid method for refrigerant flow balancing in multi-circuit evaporators. International Journal of Refrigeration. 32, 1283-1292.

Lee, J., Y.C. Kwon, M.H. Kim, 2003. An improved method for analyzing a find and tube evaporator containing a zeotropic mixture refrigerant with air mal-distribution. International Journal of Refrigeration. 26, 707-720.

Liang, S.Y., T.N. Wong, G.K. Nathan, 2001. Numerical and experimental studies of refrigerant circuitry of evaporator coils. International Journal of Refrigeration. 24, 823-833.

Li, G., S. Frankel, J.E. Braun, E.A. Groll, 2004. Application of CFD models to two-phase flow in refrigerant distributors. HVAC&R Research. 11, 45-62.

Mueller, A.C., 1987. Effects of some types of maldistribution on the performance of heat exchangers. Heat Transfer Engineering. 8, 75-86.

Mueller, A.C., J.P. Chiou, 1988. Review of various types of flow maldistribution in heat exchangers. Heat Transfer Engineering. 9, 36-50.

Shen, B., J.E. Braun, E.A.Groll, 2009. Improved methodologies for simulating unitary air conditioners at off-design conditions. International Journal of Refrigeration. 32, 1837-1849.

Taylor B.N., C.E. Kuyatt, 1994. Guidelines for Evaluating and Expressing the Uncertainty of NIST Measurement Results, National Institute of Standards and Technology Technical Note 1297.

Wedekind, G.L., Transient Response of the Mixture-Vapor Transition Point in Two-Phase Horizontal Evaporating Flow, Ph.D. Thesis, University of Illinois at Urbana-Champaign, 1965.

Wen, M.Y., C.H. Lee, J.C. Tasi, 2008. Improving two-phase refrigerant distribution in the manifold of the refrigeration system. Applied Thermal Engineering. 28, 2126-2135.

2 Airside Maldistribution

2.1 Introduction

To achieve maximum performance, an evaporator depends on both the air and the refrigerant being evenly supplied and distributed. Imbalances in loads on the air side and cooling effect on the refrigerant side cause parts of the evaporator to be underutilized, costing COP and either capacity or necessitating a larger evaporator to allow variation in airflow speeds without losing capacity.

Mueller [1987], surveying sources of steady flow imbalances, suggests that maldistribution generally reduces performance by 5 to 15% and that bypasses and leakages are more significant on performance than velocity-type imbalances. In another survey, Mueller et al. [1988] states that that "the most important factor affecting heat transfer performance is the effect of flow maldistribution on the average effective temperature difference".

Solar et al. [1983] found a small performance reduction, less than 5%, compared to uniform flow because of non-severe flow non-uniformity and low NTU. McDonald and Eng [1963] investigated several flow patterns in a cross-flow heat exchanger with NTU smaller than 4 and found less than 4% reduction in heat transfer. Chiou [1978] studying different combinations and configurations of cross flow exchangers found that performance losses become significant at high NTU. Liang et al. [2001] found that optimal coil design decreases the required heat transfer area by about 5%. Lee et al. [2003] found that different patterns of air maldistribution impact the heat transfer rate by up to 6%. Kaga [2009] studied a two-circuit residential wall AC evaporator and found an airside imbalance of 40% would degrade performance by 6%. Kim [2009] studied the optimization of evaporators with individual circuit control with a computer simulation. The study calculated that improving refrigerant distribution would recover much of the loss in load and COP due to air side imbalances.

It is apparent that for an evaporator which has a small NTU due to operating with air at low temperature differences, the effects air side imbalances create will not be huge. That has been measured. When considering both air and refrigerant flow imbalances occurring concurrently, with the resulting interplay it is not as simple to know which side is a better place towards which to put investments in order to recover performance.

2.2 Equipment/Method

2.2.1 Lab System

The refrigeration system was taken from a commercial rooftop air conditioning system running a vapor-compression cycle with a scroll compressor. The unit used refrigerant R410A. The evaporator design nominal capacity is 5 Ton or about 17.5 kW at air flow rate through evaporator 1.8 kg/s (2000 SCFM). The AC system was comprised of only a compressor, condenser, TXV, distributor, and evaporator. There were also high and low pressure safety switches.

The environmental chamber facility, interior dimensions 14' x 7' x 7', was not large enough to accommodate the rooftop unit so parts were removed from the system and reconstructed as a new facility, diagramed in Figures 1.2 and 1.3.

The compressor was a scroll type, Copeland Scroll ZP49K5E-TFE-130, with electronics compatible with the lab, 220 V/60 Hz. For experimental simplicity and with no effect on the evaporator distribution it was decided to use a water cooled a flat plate heat condenser.

The evaporator was removed from the unit by cutting the liquid line and suction line, keeping the Thermal Expansion Valve (TXV) and conical distributor, flowing down, with gravity, as well as the suction header and some of the suction line undisturbed as one piece with the evaporator. It was installed at the inlet of a wind tunnel, constructed to standard of the same cross section.

A drip pan emptying to a bucket on a load cell was built into the wind tunnel underneath the evaporator to collect condensation. Nozzles, one each of 3, 5, and 6 inches throat diameter, downstream were installed for airflow measurement. There were no gaps at the evaporator at the drip pan which allowed air to flow around the evaporator.

2.2.2 Wind Tunnel

Figure 1.3 is an overview of the air side of the facility. The wind tunnel was constructed to standard ASHRAE 41.2-1987. The inlet is 8 inches long and has the same cross section as the evaporator, 32" tall and 33.75" wide. There is a 3x3 fishing line grid 6" before the evaporator with nine thermocouples averaged together. Six inches downstream from the evaporator is a screen in a window screen frame of the same cross section as the tunnel. There is a differential pressure sensor measuring the pressure across the evaporator from points in the center of each of the four walls two inches from the evaporator both up and down stream. There are 25 thermocouples arrayed on the screen as prescribed by the ASHRAE standard.

Further downstream there are three calibrated nozzles, 6", 5", and 3" in diameter, visible in Figure 1.5. The pressure difference across the nozzles correlates to a volumetric flow rate of air. There is a thermocouple in the outlet stream of each nozzle.

From that point, the wind tunnel turns downward into an electric heater of 3 tons, 10.5 kW. As it rounds another corner, there is a steam injection tube. There are two identical blowers, Dayton model 4C329 with 3.5 kW motors model Dayton Wattrimmer 3KW33A drawing air from the end of the tunnel. With radially straight blades, the fan curve is stiff. The blowers exhaust laterally. There are three 1500 W electrical heaters arrayed around the blowers to further heat the air.

A chilled dew point sensor is mounted below the evaporator drawing air from just below the inlet. The low pressure side of the sensor is attached to the end of the wind tunnel to draw air through. A drip pan emptying to a bucket on a load cell was built into the wind tunnel underneath the evaporator to collect condensation.

2.2.3 TXV and Distributor

Both the TXV and distributor are mass produced commercial units, Figure 1.4. The TXV, Sporlan model BBIZE-4-GA, has a non-adjustable spring and is externally equalized. The sensing bulb is mounted in an 8-4 position (following clock hour sign locations) on the suction line.

The inlet of the distributor (Sporlan distributor Type 1115) is 13mm (1/2 inch) diameter tube. The orifice is 5mm (0.199 inch)in diameter and 6mm (0.250 inch) long. The orifice points toward a triangular cone. The feeder lines are recessed in a ring around the base of the cone. The twelve feeder lines are 4.75 mm (3/16 inch) OD, 3.34 mm (0.1315 inch) ID, and about 500 mm in length.

2.2.4 Evaporator

The round tube plate fin evaporator is approximately 32" tall and 33.75" wide. There are four slabs of refrigerant tubing. The airside fins are 4" deep.

The evaporator circuitry is complicated, Figure 1.6. There are twelve circuits, in four groups of three. The pattern amongst each trio repeats with minor variations four times in the whole evaporator. The topmost circuit of each trio makes six loops while the second and third circuits make five loops.

The evaporator designer compensated for the extra lengths in the design of the evaporator. Each circuit has at least one pass in each of the four slabs. The two shorter circuits of the pattern have a second pass in either the first slab or the second slab. The long circuit has two second passes in each of the third and fourth slabs. The additional length is located on the air outlet side so the additional tube length is balanced by being located where it is less effective due to smaller temperature difference.

The air side balance is calculated by combining the air mass flow rate, Equation 2.3, determined from the static pressure difference across a set of three nozzles as in Equations 2.1 and 2.2.

$$Q_{noz} = 1.414Y\sqrt{P_{noz}/\rho_{aeo,ave}}\sum(CA_{noz}) \tag{2.1}$$

$$Q_{aei} = Q_{noz}\frac{\rho}{\rho_{reference}} \tag{2.2}$$

$$\dot{m}_{air} = Q_{aei}\rho_{aei,ave} \tag{2.3}$$

Y is the expansion factor. It is very close to 1 at conditions encountered. In each run it is larger than 0.995, which agrees with a table supplied in the standard.

The mass flow rate is combined with the change in air enthalpy, Eq. 2.4, as measured by the two airside thermocouple grids to determine the air capacity.

$$Q_{evap,air} = \dot{m}_{air}\left(h_{air,in} - h_{air,out}\right) \tag{2.4}$$

The enthalpies are calculated with EES' wet air fluid data:

$$h_{air,in} = f(P_{atm}, T_{aei}, T_{dew}) \tag{2.5}$$

$$h_{air,out} = f\left(P_{atm}, T_{aeo}, T_{dew,out}\right) \tag{2.6}$$

Where $T_{dew,out}$ is calculated from $\dot{m}_{air}$ and $\dot{m}_{w,out}$ as calculated in Equation 2.7.

$$\dot{m}_{w,out} = \dot{m}_{air}\omega_{air,in} - Drip \tag{2.7}$$

The thermocouple array on the inlet T_{eai} (3 by 3) and outlet T_{eao} (5 by 5) sides of the evaporator provide inlet and outlet temperatures. A chilled mirror dew point sensor (General Eastern model D2-SR, accuracy ±0.2 C) measures the dew point (T_{dew}) in the chamber.

The refrigerant side balance is calculated in Equation 2.8 using refrigerant mass flow rate, m_r, measured by 0.1% accurate liquid mass flow meter Micromotion DS025, (±0.1% reading), and enthalpy change of refrigerant from the outlet of the condenser to the outlet of the evaporator.

$$Q_{evap,r} = M_r(h_{ero} - h_{cro}) \tag{2.8}$$

Where h_{ero} and h_{cro} are both calculated from T_{ero} and P_{ero} and P_{cro} and T_{cro}, respectively.

The superheat of each circuit is measured by a thermocouple taped down to a drop of thermal paste at the center top of the exterior of the tube wall, $T_{ers[1-12]}$. There is about 75 mm (3 inches) of tube between the evaporator side wall and the suction header. One meter down the suction line the pressure is sampled, P_{ero}, and the temperature measured with a probe, T_{ero}.

In running the system, there was no large discrepancy found in the superheats between the longer circuits and the shorter ones.

COP is calculated as in Equation 2.9, the evaporator capacity or load, since runs are conducted in steady state, is divided by the compressor power. The power usage of the blowers is not taken into consideration.

$$COP = {Q_{evap}}/{W_{comp}} \tag{2.9}$$

The uncertainties of the pressure gages are 0.25% FS and mass flow meters are 0.1% reading. The accuracy of thermocouples is taken as ±0.3 C. Using the uncertainty propagation feature of EES, based on Taylor et al., these measurements yield uncertainties in capacity of 0.53%, in COP of 0.66%, and superheat standard deviation, or sigma, of 2.05%. UA, LMTD, and NTU are between 1.0% and 1.8%.

2.3 Results

2.3.1 Ideal Airflow

The system was run several times to establish normal conditions before checking the airflow with a hot-wire anemometer. It was discovered that there were significant differences in air velocities. Some parts of the evaporator experienced three times the average airspeed. It was discovered that the exhaust from one of the blowers was blowing onto a chamber wall, rolling down the wall, and past the inlet of the wind tunnel pushing airflow away from that side of the evaporator.

Various measures were used to mitigate the problem: a barrier across the back third of the chamber to diffuse drafts, placed under the wind tunnel around the blowers. Above, plastic sheets were put across drafty areas.

Figure 2.1 is the resulting airflow speeds across the face of the evaporator. Nearly all the evaporator faces speeds within 35% of the average. The anemometer measured temperature as well. It was uniform across the face.

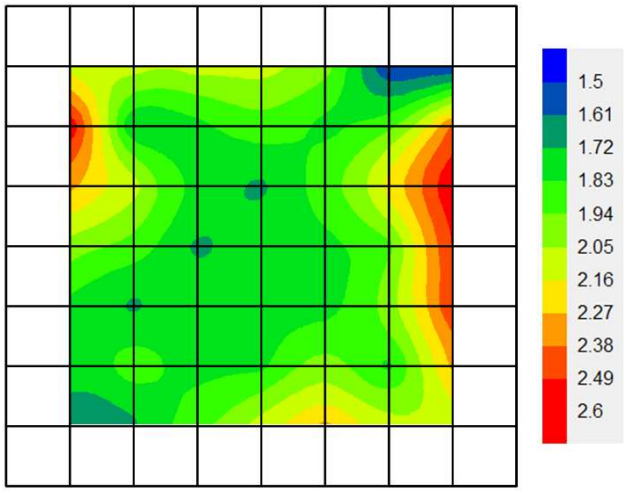

Figure 2.1: A map of the air speed at the face of the evaporator measured with a hot wire anemometer. The speeds were measured at the center of each rectangle, one-eighth the length of a side.

2.3.2 Ideal Refrigerant Distribution

To examine effect of air maldistribution refrigerant distribution had to be improved, or made "ideal". Valves were installed on the evaporator feeder lines so that the profile of evaporator circuit outlet superheats was adjustable. The standard deviation of the superheats, referred to as σ, is calculated, Equation 2.10, to quantify the departure from uniformity. The smaller the standard deviation, the more uniform the distribution.

$$\sigma = \sqrt{\frac{1}{11}\sum_{i=1}^{12}(SH_i - SH_{ave})^2} \tag{2.10}$$

The baseline conditions of the system were established at condensation saturation temperature of 47.55 ± 0.06 C, the air flow as 2000 SCFM or 0.9485 m^3/s or 1.85 m/s at unblocked conditions, air inlet temperature of 29.6 ± 0.1 C, and dew point at 13.6 ± 0.3 C. The tests were conducted dry without humidification.

While the system was running, the distribution was adjusted to minimize σ, at about 0.57, as low as it is practical to achieve with the system, establishing the ideal refrigerant distribution. The valve settings were marked and it was found that the valve settings reproduced σ on different days.

2.3.3 Non-ideal Airflow

Obstructions were used to block airflow to the evaporator. The barrier was pressed against the front of the evaporator fins by air pressure. Obstructing airflow completely to parts of the evaporator represents the limit of the effects of a more realistic imbalance which would not be as dramatic. Three ways of blocking were explored:

1. Vertical, covering equally all 12 circuits,

2. Horizontal, covering just one circuit, and
3. Circular, mimicking air flow with axial fan.

2.3.3.1 Vertical Blockages

In the first series of tests, a plastic sheet was used as the blockage. The blockage was vertical, as diagrammed in Figure 2.2, which is perpendicular to the refrigerant circuits, meaning that the heat transfer area of all circuits was reduced equally. The sheet was larger than the evaporator so there were no gaps at the edges. The blockage was also parallel to the evaporator fins. They blocked the air from flowing behind the barrier within the evaporator. Tests were conducted with up to half of the evaporator covered in steps of 10% of the evaporator face area. Since the blowers had a stiff curve, the volumetric airflow remained nearly constant even with large blockages. At 50% blockage, the volumetric airflow was only 1.9% smaller than when unblocked. Air speed increased from an average of 1.87 m/s to 3.65 m/s at 50% blocked.

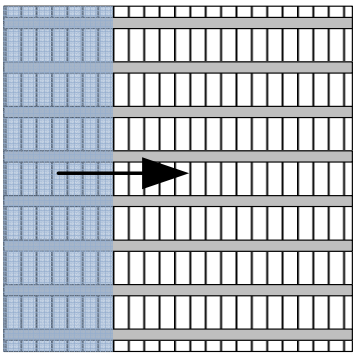

Figure 2.2: Vertical blockage of the evaporator affects all circuits equally and is parallel to the fins preventing air from flowing through the space behind the blockage.

From Figure 2.3, it is apparent that this pattern of airflow maldistribution impacts COP more than capacity. At 50% blockage, the capacity is reduced by almost 5% and COP by almost 7%. Both COP and capacity decreased linearly up to 40% before dropping off at 50%.

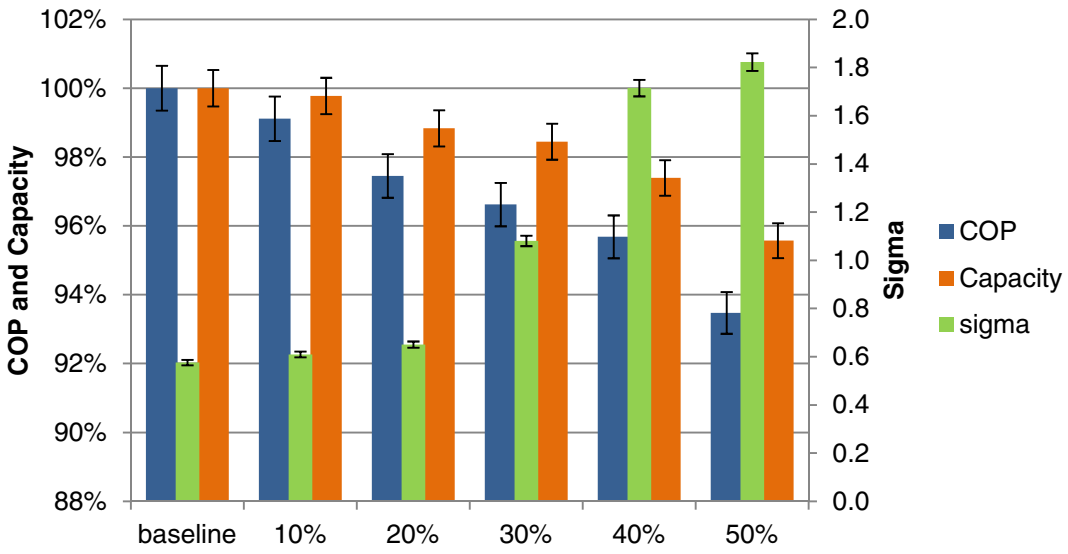

Figure 2.3: The performance and COP effects of blocking the listed percentage of the face area all the way across the evaporator face vertically from the side. Sigma, the superheat distribution, is included. The baseline run had a capacity of 15.81 kW and a COP of 3.85.

In looking at heat exchanger performance parameters, ε, NTU, LMTD, and UA, graphed in Figure 2.4, the LMTD, NTU, and UA decreased nearly as much as the fraction of open area decreased.

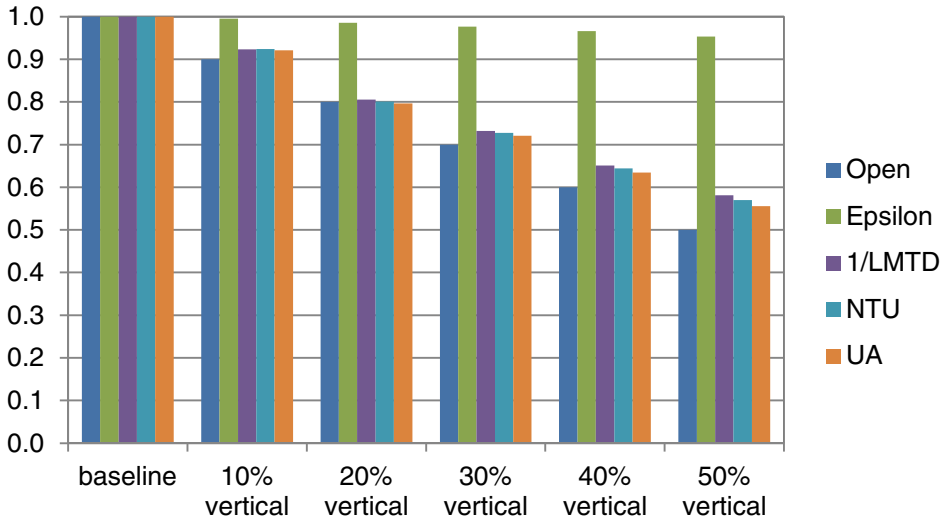

Figure 2.4: Heat exchanger performance, in terms of epsilon, LMTD, NTU, and UA, compared to baseline as the unobstructed vertical face area decreases.

In blocking the airflow evenly across the evaporator circuits, it was expected that distribution would stay the same from the baseline situation. That it does change, specifically, worsen, indicates that the heat transferred in each circuit is changing relative to the other circuits. Although unifying the superheat profile by minimizing sigma does cover up airflow imbalances by shifting liquid refrigerant to match the not necessarily uniform airflow across different circuits, that sigma changes is not necessarily an indication that the baseline reference does not have even airflow. Because the valves were not altered during this series, the imposed flow restrictions, an analogy of the mass flows, of the circuits remain the same relative of each other. From the circuit geometry, some circuits have particularly favorable arrangements with extra length in the first layer, with high temperature differences facilitating larger capacities and mass flows which may be impacted higher than average, with less airflow across the entire face of the evaporator.

The change in sigma compared to the change in performance seems to indicate that in this case, sigma is an effect of the deterioration in performance. Performance greatly declined between 40% and 50% blockage whereas sigma gets worse between 20% and 40% and is relatively level elsewhere.

2.3.3.2 Horizontal Blockages

In the second series, the plastic sheet covered the evaporator from side to side and was advanced up from the bottom, Figure 2.5. The 10% blockage completely cut off the bottom-most circuit. Next 20% was attempted, cutting off two circuits and affecting a third. The system did not remain stable. The saturation temperature steadily decreased and the compressor began to rapidly cool, indicating liquid flowing into the compressor. The sheet was lowered back to 10% and then slowly raised to 15% which did maintain a superheat. The blockage was perpendicular to fins so there was some air reaching the volume behind blockage.

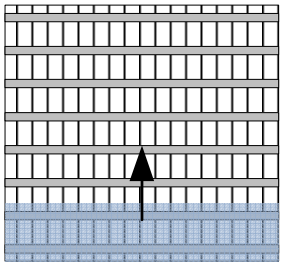

Figure 2.5: Vertical blockage of the evaporator effects all circuits equally and is parallel to the fins preventing air from flowing through the space behind the blockage.

With the sheet replaced to 10%, the valves were adjusted to improve the distribution, minimizing σ, which included fully closing the blocked circuit. Then the sheet was raised to 15% and the valves were adjusted again to improve the distribution.

Figure 2.6 represents graphically what using the valves to improve the superheat profile is expected to accomplish. Imposing bad airflow reduces the COP, represented by the red arrow. Liquid refrigerant flow is not matched well to where air is being supplied. With the valves, the flow resistances of different circuits are adjusted to redirect liquid to better match the airflow. With liquid refrigerant better matched to the airflow of circuits, part of the loss of COP may be recovered.

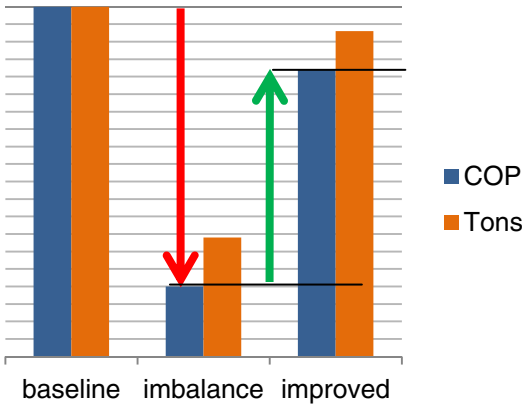

Figure 2.6: The loss and recovery of performance of an imposed airside imbalance and then improving the superheat distribution back to uniformity where most of the performance is recovered.

The results for the horizontal obstruction as well as σ are plotted in Figure 2.7 normalized to the initial run. The initial run was at a capacity of 4.51 tons, or 15.85 kW, and had a COP of 3.85. As the airflow area was reduced the velocity increased, maintaining the volumetric airflow. The system COP declined faster than the capacity, but even at 50% blocked, neither is reduced by more than 7%.

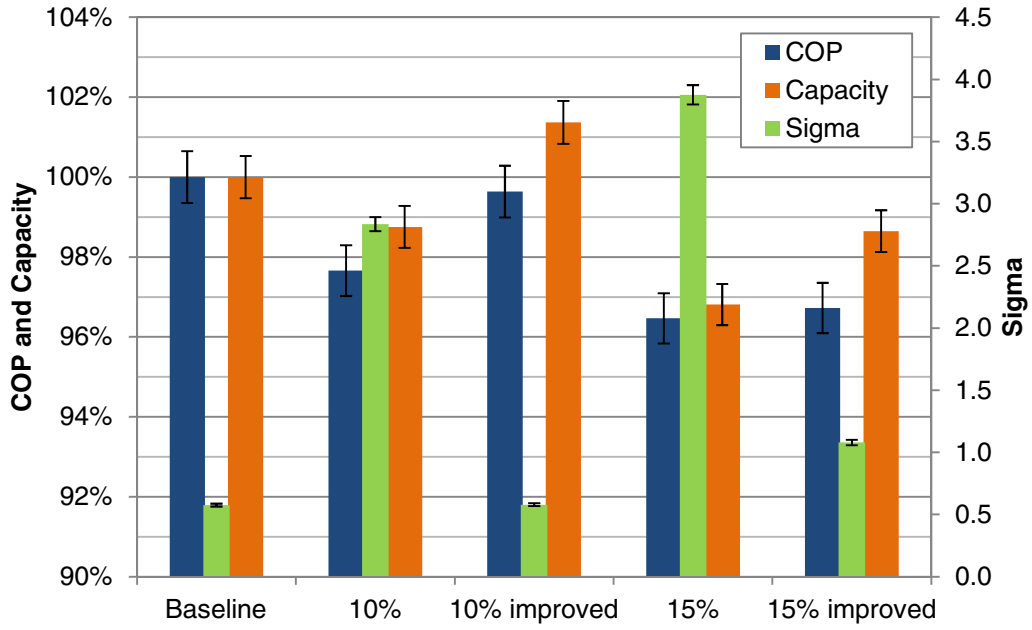

Figure 2.7: The performance and COP effects of blocking the listed percentage of the face area vertically from top to bottom. The baseline run had a capacity of 15.81 kW and a COP of 3.85. The runs were improved (imp) by adjusting the valves to change the flow resistances to make the evaporator circuit superheat profile more uniform.

The 10% run was with one circuit starved of air. One circuit of twelve is 8.3% however capacity and COP were reduced by approximately 1.3% and 2.4%, as listed in Table 2.1. With superheat of one circuit gone and additional circuits affected, σ greatly increased up to 3. The system adjusted to absorb the impact, indicated by COP being decreasing more than capacity. Also the evaporator fins, running vertically, were perpendicular to the sheet, making it possible for air to

flow past the barrier and descend behind it within the evaporator where it could still maintain some temperature difference.

Improving the refrigerant superheat profile recovered nearly all of the COP lost and even increased the capacity of the evaporator. The capacity in this series, about 15.8 kW, is smaller than the nominal rating of 17.5 kW. The higher air velocity and supplying the same refrigerant into a 'smaller' evaporator increased the capacity.

With the valves returned to their baseline configuration and the sheet advanced to 15%, σ is much larger, nearly 4, and the performance is further reduced by at least 3%. Again, air was free to flow through the fins, behind barrier so there was some heat transfer, but it was reduced enough that the two bottom-most circuits had no superheat.

After adjusting the valves to unify the flow, a majority of the capacity lost was recovered but only 7% of the COP lost was.

For the same obstruction area, the horizontal blockage parallel to circuit tubing has a larger impact on performance. The reduction at 10% horizontal is greater than 10% vertical and the reduction at 15% horizontal is greater than 20% vertical. Improving the distribution recovers much of the capacity lost at low blockages as listed in Table 2.1, but not as much of the COP.

Table 2.1: Summary of the lost performance of the horizontal runs. Sigma is the standard deviation of the outlet superheats. The ideal sigma is 0.58. Adjusting the flow recovered the lost performance when only one circuit was blocked. There is little recovery at 15%, when a second circuit was being blocked as well.

	Sigma	COP loss	Recovered	Capacity loss	Recovered
10%	2.836	2.34%		1.25%	
10% improved	0.579	0.36%	84%	-1.37%	210%
15%	3.877	3.54%		3.19%	
15% improved	1.079	3.28%	7%	1.35%	58%

The effects on heat exchanger performance are more dramatic, Figure 2.8. The 10% blockage knocks performance down by 30% and a 15% blockage reduces performance by more than 50%. Unifying superheats with one circuit completely blocked, the 10% case, recovers all of

the lost performance, but at 15% blocked, with the airflow to more than one circuit shut off, reunifying superheats recovers 15% of heat exchanger performance.

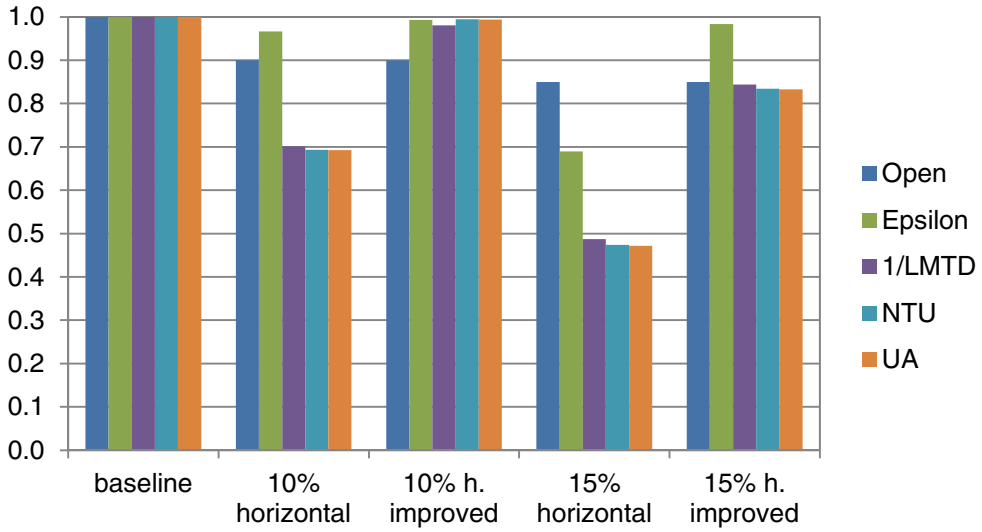

Figure 2.8: Heat exchanger performance, in terms of epsilon, LMTD, NTU, and UA, for horizontal blockages compared to baseline.

2.3.3.3 Simulated Fan

An extreme airflow pattern resulting from an axial fan sitting right behind the evaporator was simulated. The evaporator is roughly square and a fan would produce airflow within the circle swept by the blades. The corners would not have airflow. Additionally there would be little airflow in the center where the blades attach to the shaft and do not move fast enough to move significant amounts of air. Therefore shapes were made to block the evaporator to make an annulus shaped airflow pattern. The outer radius of the fan was chosen to be 15" so that there would be at least a 1" gap all the way around. No circuit spans less than 4" vertically. The inner circle, representing the center of the fan, has a diameter of 7". Figure 2.9 is a photograph of the evaporator with these blockages. The corners cover 32.3% of the evaporator and the center covers a further 14.7% leaving 67.7% of the evaporator open.

Figure 2.9: The evaporator with poster board used to create a poorly positioned axial fan. The "corners" are with the four corner pieces. The "center" condition is with the yellow circle in the center in addition to the four corners.

The conditions of this series were the same as the previous two. The initial ideal case had a capacity of 4.48 tons, or 15.77 kW, and a COP of 3.78. The results are graphed in Figure 2.10, normalized to the baseline.

From the baseline, adding the four corners produced a much larger drop than the decrease in system performance of the four corners and the center. With the four corners added, sigma shot up to 4 with very little superheat in the top and bottom circuits, as can be seen in Figure 2.12, yet the loss in system performance was only about 1%. Adding the center further decreased performance by about 0.25% from the baseline while sigma stayed high but decreased. The superheat of the middle circuits was reduced bringing them closer to the average, reducing the standard deviation, σ.

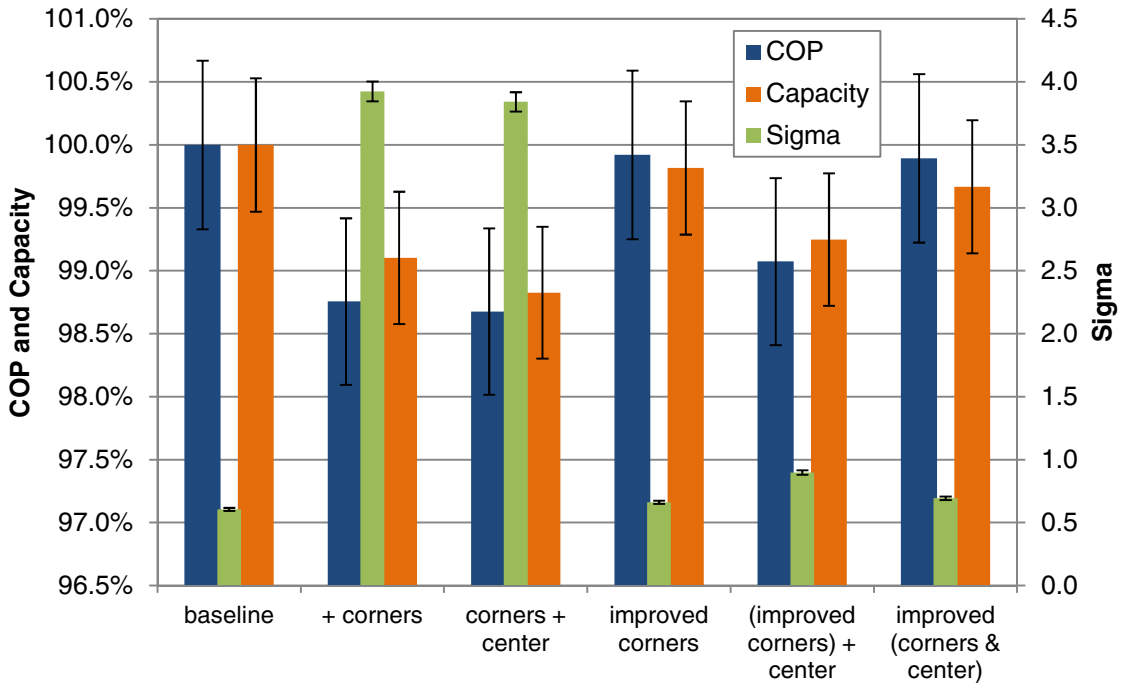

Figure 2.10: The simulated fan series, conducted in order from left to right. The ideal run had a capacity of 15.71 kW at a COP of 3.78. After the baseline run, the corners were added then the center. The center was removed and the refrigerant flow in the evaporator circuits was improved to return the superheats to uniformity by adjusting the valves. The center was added to that then improved again.

From that point, the center was removed, and the corners were improved. As seen in prior runs, most of the system performance lost was recovered. In this case, as listed in Table 2.2, 94% of the COP was recovered and 80% of the capacity. Then the center was added, which increased sigma to 0.9 but brought performance down by 1%.

The valves were used to improve the distribution again back to uniformity. Again most of the losses were recovered, 92% of COP and 72% of capacity.

In the big picture, the greatest reduction in performance is not larger than 2% for this case, despite 1/3 of the evaporator face being blocked. From Figure 2.3, a 30% blockage produced losses between 2% and 4%. The obstruction was circular so very few of the fin channels were blocked completely, meaning air was likely blowing around the obstruction and getting into the supposed

dead area. Moreover, there was a small gap, not larger than 5mm at the edges of the evaporator between the blockage and the walls.

Table 2.2: Summary of the effects of adding the corners and the corners and center as well as the performance adjusting the refrigerant distribution recovers.

	Sigma	COP Loss	Recovered	COP Loss	Recovered
+corners	3.925	1.24%		0.90%	
improved corners	0.6625	0.08%	94%	0.18%	80%
corners + center	3.842	1.32%		1.17%	
improved (corners & center)	0.695	0.11%	92%	0.33%	72%
(improved corners) + center	0.8981	0.93%		0.75%	

Figure 2.11 shows the losses in heat exchanger performance parameters. Again, before the flow is adjusted with valves, the performance decreases in proportion to the amount of face area open as with the vertical blockage case. Adjusting the refrigeration distribution to unify the outlet superheats recovers most of the performance and only 10% is lost. As in the previous sets, the magnitude of performance lost is much larger on just the evaporator than the whole system performance. The whole system absorbs changes in performance, mitigating effects from one component.

The air blockages are evident in the outlet superheat patterns. They are graphed in Figure 2.12. The airflow lost with the corners added impacts the top and bottom circuits the most and spills over to the neighboring circuit at the bottom, circuit 11. Adding the center decreases the superheat of circuits 6 and 7. The valve adjustment returns the profile to close to uniform and re-adding the center takes another bite out of the superheat in the center, before unifying it again with the valves.

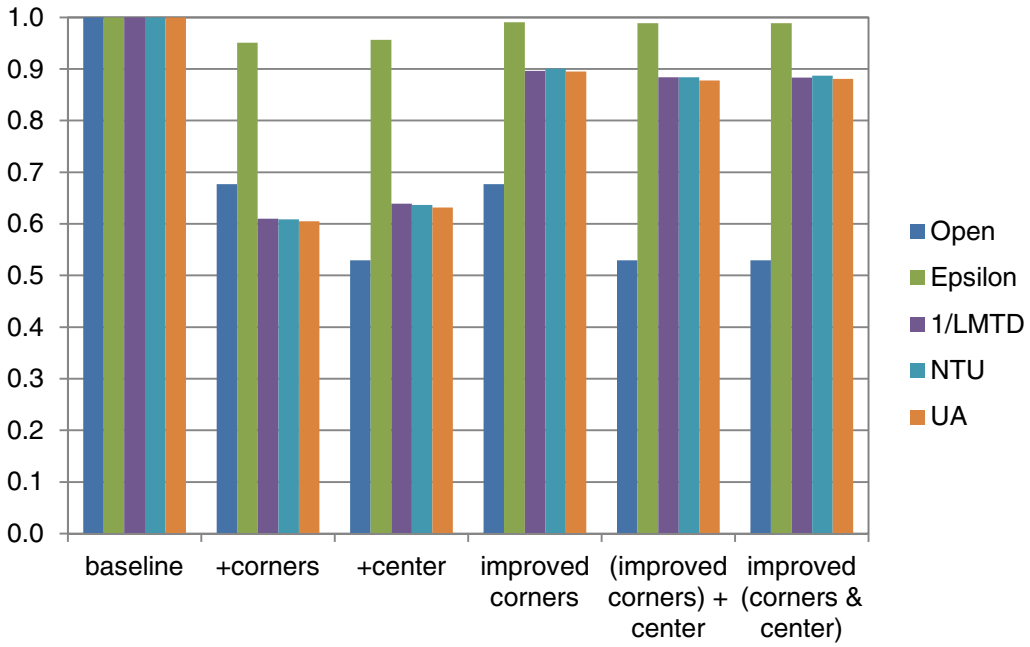

Figure 2.11: Heat exchanger performance, in terms of epsilon, LMTD, NTU, and UA, for simulated fan airflow imbalances compared to baseline.

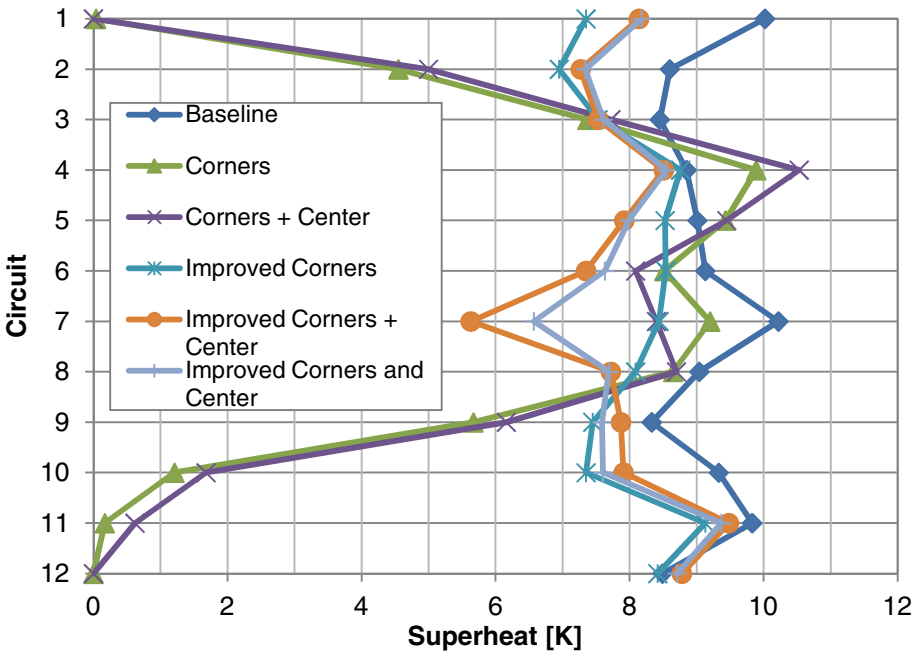

Figure 2.12: The superheat profiles of the axial fan series. The airside blockages are clearly reflected in the refrigerant superheat profiles.

For these runs, the airflow was blocked but the volumetric flow rate remained the same. Heat transfer should increase at a higher velocity as seen in the dimensionless correlation relationship in Equation 2.11.

$$h \sim Nu = f\left(Re^{4/5}, Pr^{1/3}\right) \tag{2.11}$$

where

$$Re \sim U \tag{2.12}$$

Unfortunately it is not possible to correlate the data to heat transfer correlations. The range of air velocities is a narrow range between 1.5 and 3.5 m/s so $U^{4/5}$ is virtually linear due to the exponent being close to 1 and also due to being in a small range that does not span orders of magnitude. The heat transfer coefficients for all horizontal, vertical, and fan tests correlate to both $U^{4/5}$ and U above the 0.9997 level.

2.3.4 Comparison to Refrigerant Distribution

As a function of sigma, airside imbalances have a smaller impact on performance. In both refrigerant side and airflow side imbalance cases, there were situations with at least one two-phase exit and a sigma around 4. The magnitude of the change in performance was larger with refrigerant distribution.

When the airflow was made to be imbalanced, the air was free to move around behind much of the obstruction. The flow was greatly reduced compared to the ideal, uniform situation explored in the refrigerant maldistribution case, but there was still airflow which created a temperature

difference on the circuits. This changed the heat profile of circuits. With a smaller temperature difference, refrigerant was still boiled, but there was not enough of a temperature difference to achieve superheat.

Using the superheats at evaporator circuit outlets as an analogy for mass flow through the evaporator circuits works well for minor differences in airflow to circuits. When there are significant differences in airflow from one area of the evaporator to another, effects other than the amount of liquid entering a circuit start to matter and superheats no longer convey the full picture and the analogy starts to break down.

Regardless of how well superheat indicates mass flow, making superheats uniform works well as a method to increase performance of any evaporator because to do that, the imbalances in airflow are taken into account and exploited.

2.4 Conclusion

The components from a 5 ton commercial air conditioning system were used to explore the performance effects of air imbalances on the evaporator of a real system. Air was blocked vertically, horizontally, and in an inverted annulus shape. Valves on the refrigerant feeder lines were used to adjust the refrigerant flows. The volumetric rate of airflow was approximately the same in all tests.

- The performance impact from airside imbalances is bigger on COP than capacity.
- Blocking airflow parallel to circuits, that is impacting one or two circuits greatly instead of a small amount on all circuits, has a much greater effect on the system. 50% of the evaporator blocked evenly on all evaporator circuits resulted in less than a 7% decrease in performance and COP whereas 15% blocked horizontally makes a 5% decrease.

- The simulated axial fan, produced a much smaller impact, less than 2%, on system performance than a much larger rectangular block.
- Using valves on the refrigerant feeder lines enables nearly all of the capacity and most of the COP to be recovered for the simulated fan. Unifying superheats is a simple way to ensure that airside losses are minimized. Refrigerant imbalances due to the presence of air side imbalances account for much of the performance loss.

2.5 References

Chiou, J.P., 1978. Thermal performance deterioration in crossflow heat exchanger due to flow nonuniformity. J. Heat Transfer Trans. ASME. 100, 580-587.

Kim, J.H., J.E. Braun, E.A. Groll, 2009. Evaluation of a hybrid method for refrigerant flow balancing in multi-circuit evaporators. International Journal of Refrigeration. 32, 1283-1292.

Kaga, Kunihiko, S. Kotoh, T. Ogushi, H. Yoshia, 2009. Influence of air-flow imbalance and refrigerant flow path pattern on an evaporator's performance. Trans. JSME Ser B. 75, 117-124.

Lee, J., Y.C. Kwon, M.H. Kim, 2003. An improved method for analyzing a fin and tube evaporator containing a zeotropic mixture refrigerant with air mal-distribution. International Journal of Refrigeration. 26, 707-720.

Liang, S.Y., T.N. Wong, G.K. Nathan, 2001. Numerical and experimental studies of refrigerant circuitry of evaporator coils. International Journal of Refrigeration. 24, 823-833.

McDonald, J.S., K.Y. Eng, 1963. Tube side flow distribution effects on heat exchanger performance. Chem. Eng. Prog. Sym. Ser. 59, 11-17.

Mueller, A.C., 1987. Effects of some types of maldistribution on the performance of heat exchangers. Heat Transfer Engineering. 8, 75-86.

Mueller, A.C., J.P. Chiou, 1988. Review of various types of flow maldistribution in heat exchangers. Heat Transfer Engineering. 9, 36-50.

Solar, A.I., K.P. Singh, and T.L. Ng, 1983. Effect of nonuniform air flow on air cooler heat exchanger performance. Proc. ASME-JSME Thermal Eng. Joint Conf., 1, 537-542.

Taylor B.N., C.E. Kuyatt, 1994. Guidelines for Evaluating and Expressing the Uncertainty of NIST Measurement Results, National Institute of Standards and Technology Technical Note 1297.

Appendix A: Laboratory System

The refrigeration system has a nominal capacity of 5 Ton or 17.5 kW. With R410A, the typical mass flow rate was 110 g/s.

The cooling water conditions drove the heat transfer in the condenser. From the building chilled water system, water arrived at between 4 and 7 C. The sink supplied water of about 15 to 17 C. Both systems were at about the same pressure in that with all the valves open, both arrangements produced flows at about 250 to 260 g/s. In this configuration, the system condensed in the upper 20's or low 30's C, which is not realistic for a rooftop AC unit. The water flow was reduced to something like 120-160 g/s depending on temperature to achieve a condensation temperature around 47 C.

Nearly all the runs were done dry, partially for simplicity and partially due to the inability to get the dew point temperature above 14 C. A bigger steam pipe would need to be installed to be able to deliver more steam.

There was about 3 Ton of electric heating in the wind tunnel duct from previous experiments. About 1 ton of additional electric heat was added to the chamber as off the shelf utility electric heaters. They were scattered around the chamber and positioned to be in gusty spots for mixing. Barriers had to be put up in the chamber to diffuse air against the back wall of the chamber otherwise the airflow was disturbing the air evenness on the face of the evaporator.

The fan power made up the difference to 5 Ton.

The least fortunate decision made in designing and building the system was putting most of the components outside the environmental chamber. Only the evaporator was in the environmental chamber, while the condenser and compressor sit outside, next to the experiment operation station. This made it rather noisy. There was also unaccountable heat transfer to the room from the compressor. (The condenser was insulated which should have taken care of most of that.) If it had been located under the evaporator in the environmental chamber, heat from the compressor would have helped heat the chamber and been accounted for within the insulated chamber walls.

Input to the DAQ

Phys Ch	TC Ch	PP	Variable		Comp Ch
1	1	1	Taeo1	E 1 (bottom, door side)	300
2	2	2	Taeo2	Air exit array	301
3	3	3	Taeo3		302
4	4	4	Taeo4		303
5	5	5	Taeo5	E 5	304
6	6	6	Taeo6	D 1	305
7	7	7	Taeo7		306
8	8	8	Taeo8		307
9	9	9	Taeo9		308
10	10	10	Taeo10	D 5	309
11	11	11	Taeo11	C 1	310
12	12	12	Taeo12		311
13	13	13	Taeo13		312
14	14	14	Taeo14		313
15	15	15	Taeo15	C 5	314
16	16	16	Taeo16	B 1	315
17	17	17	Taeo17		400
18	18	18	Taeo18		401
19	19	19	Taeo19		402
20	20	20	Taeo20	B 5	403
21	21	21	Taeo21	A 1	404
22	22	22	Taeo22		405
23	23	23	Taeo23		406
24	24	24	Taeo24		407
25	25	25	Taeo25	A 5	408
26	26	26	Tcwi	Chamber inside wall	409
27	27	27	Tero	evaporator out	410
28	28		Twi	cooling water	411
29	29		Two	cooling water	412
30	30		Tcri	R loop condensor in	413
31	31		Tcro	R loop condensor out	414
32	32		Tcwo	Chamber outside wall	415
1	33	1	Taei	Air inlet 1	500
2	34	2	Tnoz1	Air nozzle 6"	501
3	35	3	Tnoz2	Air nozzle 5"	502
4	36	4	Tnoz3	Air nozzle 3"	503
5	37	5	Ters1	R outlet superheat	504
6	38	6	Ters2	R outlet superheat	505
7	39	7	Ters3	R outlet superheat	506
8	40	8	Ters4	R outlet superheat	507
9	41	9	Ters5	R outlet superheat	508
10	42	10	Ters6	R outlet superheat	509
11	43	11	Ters7	R outlet superheat	510
12	44	12	Ters8	R outlet superheat	511
13	45	13	Ters9	R outlet superheat	512
14	46	14	Ters10	R outlet superheat	513
15	47	15	Ters11	R outlet superheat	514
16	48	16	Ters12	R outlet superheat	515
17	not connected to comp				
18	not connected to comp				

Phys Ch	Data Ch	Variable		Comp Ch.
1	1	Tdew	Dew Temp	100
2	2	Pcro	R P conds exit	101
3	3	Perdi	R P txv-dist	102
4	4	Perdif	R P diff evp	103
5	5	Pcri	R P conds exit	104
6	6			
7	7			
8	8	Wfan	Power blowers	107
9	9	Wh1	Power 3 ton HTR	108
10	10	Wh2	Aux. HTR	109
11	11	Wcomp		110
12	12	Pnoz	A dP nozzle	111
13	13	Ptun	A dP wind tunnel	112
14	14			
15	15	Mw	W mass flow	114
16	16			
17	17			
18	18			
19	19			
20	20			
21	21			
22	22			
23	23			
24	24			
25	25			
26	26	Pero	R P evap outlet	209
27	27	Mr	R mass flow	210
28	28	Dr	D density	211
29	29			
30	30			
31	31			
32	32			

Pressure gauges and uncertainties

Parameters	Brand	Model	Range	Accuracy
Pcri	Sensotec	TJE/713-18	0~500PSIA	±0.1% F.S.
Pcro	Sensotec	TJE/713-18	0~500PSIA	±0.1% F.S.
Perdi	Omega	PX176-200A5V	0~200PSIA	±1% F.S.
Perdo	Setra	206	0~250PSIG	±0.13% F.S.
Pers	Setra	C206	0~250PSIG	±0.13% F.S.
DPena	Setra	264	0~5 in.WC	±1% F.S.
Null (DP)	Setra	261-1	0~5 in.WC	±1% F.S.

Refrigerant mass flow rate:
Remote Flow Transmitter
Model: RFT9712 1PNU

Mass Flow sensor
Model: DS025S119SU
S/N: 219690

Water mass flow rate:
Elite Remote flow transmitter
Model: RFT9739 E4SUJ
S/N: 2055574

Mass Flow sensor
Model: CMF 010M324MU
S/N: 386047

Appendix B: Uncertainty Propagation

Uncertainty in measurements:

Variable	Range	Uncertainty
Pcri	500 psi	±0.1% FS
Pcro	500 psi	±0.1% FS
Perdi	200 psi	±1% FS
Perdo	250 psi	±0.13% FS
Pero	250 psi	±0.13% FS
Ptun	5 in H2O	±1% FS
Pnoz	5 in H2O	±1% FS
Mw	2000 g/s	±0.1% FS
Mr	300 g/s	±0.2% FS
thermocouples		±0.3 C
Tdew	-80 C to 85 C	±0.2 C
Wauxhtr	8kW	±0.4% FS
Wcomp	6kW	±0.4% FS
Wfan	6kW	±0.4% FS
Wh1	12kW	±0.4% FS

Uncertainties were propagated in EES. The accuracies of calculated measurements were determined to be:

Variable	Uncertainty
Capacity	0.53%
Sigma	2.05%
COP	0.66%
UA	1.87%
LMTD	1.33%
Epsilon	0.20%
NTU	1.08%

Appendix C: Data

Data for Figure 1.7, varying quality

alpha[i]	dP_dist[i] [kPa]	Drip[i] [g/s]	eta[i]	h_airin[i] [kJ/kg]	h_airout[i] [kJ/kg]	h_cri[i] [kJ/kg]	h_cro[i] [kJ/kg]	h_eamax[i] [kJ/kg]
0.9955	113.4	1.345	0.769	59.98	42.53	321.5	115.4	37.29
0.9955	115.6	1.234	0.7499	60.35	43.1	320.1	114.8	37.34
0.9955	111.5	1.336	0.7646	60.13	42.44	319	113.6	36.99
0.9955	106.7	1.232	0.7557	59.58	42.04	317.7	111.8	36.37
0.9955	97.04	1.276	0.755	58.62	40.57	317	106.4	34.72
0.9955	83.1	1.347	0.7577	58	39.67	317.9	102.7	33.81
0.9955	74.42	1.252	0.7364	56.76	38.55	318.3	98.18	32.03
0.9955	109.3	1.194	0.7541	59.43	42.09	319.6	114.9	36.44
0.9955	117.7	1.173	0.7599	59.93	42.66	320.2	116.9	37.2

h_ero[i] [kJ/kg]	h_ers1[i] [kJ/kg]	h_ers10[i] [kJ/kg]	h_ers11[i] [kJ/kg]	h_ers12[i] [kJ/kg]	h_ers2[i] [kJ/kg]	h_ers3[i] [kJ/kg]	h_ers4[i] [kJ/kg]	h_ers5[i] [kJ/kg]
288.3	296.9	287.8	289.7	288.4	294.8	293.2	293.3	289.7
288.4	297.1	287.2	289.5	288.2	295.1	293.5	293.4	290
288.6	297.4	287.3	289.4	288.1	295.4	293.8	293.5	290.1
289.1	297.5	287.5	289.5	288.3	295.4	293.8	293.7	290.3
290.8	298.5	292.6	292.5	290.2	295.9	293.9	294	290
292.7	299.8	293.5	292.9	290.4	297.2	295.2	295.8	292
293.5	300	293.7	292.6	290.2	297.5	295.7	296.3	292.8
288.8	297.2	287.4	289.9	288.5	295.4	294.2	293.9	291.1
288.7	297.2	287	289.7	288.2	295.2	294	293.6	290.9

h_ers6[i] [kJ/kg]	h_ers7[i] [kJ/kg]	h_ers8[i] [kJ/kg]	h_ers9[i] [kJ/kg]	mu_aeo_ave[i] [kg/m-s]	m_dot_air[i] [kg/s]	m_dot_win[i] [kg/s]	m_dot_wout[i] [kg/s]	M_r[i] [g/s]
287	76.07	76.42	285.2	0.00001801	1.137	0.01347	0.01213	113.2
287.2	76.18	76.45	284.7	0.00001802	1.137	0.01357	0.01234	113.7
287.3	75.87	76.18	285.2	0.00001801	1.138	0.01346	0.01212	113.4
287.5	75.54	75.89	285.7	0.000018	1.139	0.01326	0.01203	112.9
287.1	74.58	109.1	288.4	0.00001798	1.139	0.01289	0.01161	110.3
289.2	284.7	288	289.7	0.00001796	1.141	0.0127	0.01135	108.2
290.3	288	289.2	290.1	0.00001794	1.143	0.01234	0.01109	105.7
288.1	76.16	76.33	285	0.000018	1.137	0.0132	0.012	111.9
288	76.69	76.85	284.6	0.00001801	1.136	0.01335	0.01218	112.8

M_w[i] [g/s]	omega_ai[i]	omega_ao[i]	P_cri[i] [kPa]	P_cro[i] [kPa]	P_erdi[i] [kPa]	P_erdif[i] [kPa]	P_erdo[i] [kPa]	P_ero[i] [kPa]
132.5	0.01185	0.01066	2701	2710	1304	31.45	1190	1159
140.8	0.01193	0.01085	2582	2587	1307	31.62	1191	1159
149.6	0.01183	0.01065	2467	2469	1298	32.01	1186	1154
167.4	0.01164	0.01056	2299	2298	1285	32.19	1178	1146
207.6	0.01131	0.01019	2027	2022	1253	30.94	1156	1125
228.7	0.01114	0.009955	1931	1926	1227	40.86	1144	1103
264.4	0.0108	0.009703	1825	1818	1195	31.69	1120	1089
214.1	0.01161	0.01056	2528	2484	1288	32.38	1179	1147
199.9	0.01175	0.01072	2621	2576	1307	33	1189	1156

Data for Figure 1.7, varying quality

P_noz[i] [kPa]	P_tun[i] [kPa]	Q_eai[i] [m^3/s]	Q_evap_air[i] [kW]	Q_evap_r[i] [kW]	Q_evap_rs[i] [kW]	Q_evap_rsg[i] [kW]	Q_max[i] [kW]	Q_noz[i] [m^3/s]
0.4438	0.06193	0.9969	19.85	19.58	15.8	19.84	25.81	0.9488
0.4442	0.06241	0.9976	19.62	19.73	15.92	19.98	26.16	0.9495
0.4442	0.06249	0.9981	20.14	19.85	16.03	20.09	26.33	0.9492
0.4444	0.06257	0.9981	19.97	20.01	16.17	20.22	26.43	0.949
0.4438	0.06281	0.9977	20.55	20.33	16.81	20.5	27.23	0.9473
0.4443	0.06262	0.9982	20.91	20.55	20.51	20.64	27.6	0.9471
0.4453	0.06263	0.9987	20.82	20.64	20.59	20.69	28.27	0.9473
0.443	0.0628	0.9961	19.71	19.47	15.72	19.72	26.13	0.9476
0.4429	0.06225	0.9963	19.62	19.38	15.6	19.63	25.82	0.9479

Re1[i]	Re2[i]	Re3[i]	rho_aei_ave[i] [kg/m^3]	rho_aeo_ave[i] [kg/m^3]	SCFM[i] [ft^3/min]	T_aei[i] [C]	T_aeo1[i] [C]	T_aeo10[i] [C]
271312	226093	135656	1.141	1.199	2112	29.51	14.96	13.77
271267	226056	135634	1.14	1.198	2114	29.65	15.11	13.76
271516	226263	135758	1.14	1.199	2115	29.7	14.89	13.57
271782	226485	135891	1.141	1.2	2115	29.62	14.79	13.44
272279	226899	136140	1.142	1.203	2114	29.51	14.15	13.18
272828	227357	136414	1.143	1.204	2115	29.36	13.84	13.12
273773	228144	136887	1.145	1.207	2116	28.98	13.25	12.47
271281	226068	135641	1.141	1.2	2111	29.56	14.53	13.32
271025	225854	135512	1.14	1.199	2111	29.7	14.79	13.61

T_aeo11[i] [C]	T_aeo12[i] [C]	T_aeo13[i] [C]	T_aeo14[i] [C]	T_aeo15[i] [C]	T_aeo16[i] [C]	T_aeo17[i] [C]	T_aeo18[i] [C]	T_aeo19[i] [C]
14.03	14.18	13.95	14.1	14.07	16.68	16.72	16.43	16.27
14.03	14.25	13.94	14.02	14.07	16.7	16.9	16.59	16.35
13.83	14.06	13.77	13.79	13.88	16.65	16.78	16.4	16.17
13.63	13.8	13.59	13.64	13.72	16.45	16.69	16.32	16.09
13.06	13.27	12.98	13.1	13.11	15.5	15.96	15.65	15.48
12.72	12.9	12.61	12.75	12.79	15.55	15.85	15.48	15.19
12.31	12.56	12.19	12.25	12.28	15.12	15.42	15.13	14.93
13.66	13.71	13.42	13.45	13.58	16.45	16.76	16.61	16.71
13.95	14.05	13.78	13.79	13.84	16.68	17.05	16.73	16.51

T_aeo2[i] [C]	T_aeo20[i] [C]	T_aeo21[i] [C]	T_aeo22[i] [C]	T_aeo23[i] [C]	T_aeo24[i] [C]	T_aeo25[i] [C]	T_aeo3[i] [C]	T_aeo4[i] [C]
14.72	15.97	16.8	17.12	16.82	16.62	15.09	15.21	16.93
14.76	16.19	16.89	17.73	16.91	17.08	15.1	15.16	17
14.62	16	16.85	17.4	16.66	16.74	14.87	15.03	16.93
14.44	15.81	16.56	17.44	16.3	16.66	14.99	14.91	16.83
13.86	15.22	16.15	17.24	16.24	16.19	14.61	14.37	16.4
13.49	14.86	16.32	16.84	15.8	15.72	14.29	14.01	15.71
13.04	14.99	15.94	16.46	15.38	15.17	13.58	13.33	15.39
14.33	16.9	17.59	17.55	16.76	17.14	15.63	14.71	15.66
14.57	16.29	17.32	17.68	16.84	16.87	15.85	15	15.94

Data for Figure 1.7, varying quality

T_aeo5[i] [C]	T_aeo6[i] [C]	T_aeo7[i] [C]	T_aeo8[i] [C]	T_aeo9[i] [C]	T_aeo_ave[i] [C]	T_chwallin[i] [C]	T_chwallout[i] [C]	T_cri[i] [C]
17.66	14.89	14.85	14.9	13.69	15.46	30.04	23.61	67.78
17.8	14.85	14.9	14.91	13.76	15.55	30.38	23.7	65.15
17.78	14.81	14.92	14.88	13.49	15.39	30.27	23.54	62.72
17.54	14.57	14.62	14.58	13.32	15.23	30.3	23.62	59.41
17.13	13.99	14.06	14.08	12.88	14.71	30.2	23.76	54.81
16.83	13.65	13.71	13.78	12.62	14.42	30.07	23.76	54.16
16.22	12.99	13.14	13.08	11.96	13.94	29.67	23.79	52.85
17.52	14.32	14.28	14.24	13.23	15.28	29.88	23.94	64
17.7	14.55	14.56	14.6	13.61	15.45	30.01	24.16	65.72

T_cro[i] [C]	T_dew[i] [C]	T_dew_o[i] [C]	T_erin[i] [C]	T_ero[i] [C]	T_ers1[i] [C]	T_ers10[i] [C]	T_ers11[i] [C]	T_ers12[i] [C]
33.94	16.59	14.97	13.22	15.49	22.71	15.09	16.67	15.58
33.68	16.7	15.24	13.24	15.58	22.92	14.64	16.51	15.41
33.07	16.56	14.96	13.1	15.63	23.06	14.57	16.27	15.22
32.14	16.32	14.83	12.86	15.81	22.96	14.55	16.19	15.18
29.17	15.87	14.28	12.22	16.73	23.38	18.27	18.22	16.26
27.07	15.63	13.93	11.85	17.85	24.04	18.53	18.01	15.94
24.41	15.16	13.54	11.13	18.18	23.92	18.36	17.41	15.37
33.79	16.28	14.82	12.89	15.59	22.73	14.46	16.55	15.35
34.87	16.46	15.05	13.18	15.72	22.88	14.34	16.55	15.33

T_ers2[i] [C]	T_ers3[i] [C]	T_ers4[i] [C]	T_ers5[i] [C]	T_ers6[i] [C]	T_ers7[i] [C]	T_ers8[i] [C]	T_ers9[i] [C]	T_noz1[i] [C]
20.96	19.57	19.6	16.68	14.44	11.17	11.39	12.98	15.18
21.18	19.82	19.72	16.93	14.63	11.24	11.41	12.55	15.26
21.31	19.93	19.75	16.85	14.54	11.04	11.24	12.9	15.21
21.18	19.8	19.67	16.84	14.51	10.84	11.06	13.04	14.96
21.15	19.4	19.5	16.12	13.74	10.24	11.29	14.73	14.49
21.79	20.06	20.52	17.31	14.91	11.22	13.93	15.34	14.35
21.69	20.09	20.63	17.62	15.45	13.52	14.55	15.3	14.06
21.13	20.15	19.86	17.51	15.04	11.23	11.34	12.53	15.46
21.22	20.16	19.88	17.54	15.14	11.56	11.66	12.46	15.71

T_noz2[i] [C]	T_noz3[i] [C]	T_shellbot[i] [C]	T_shelltop[i] [C]	T_steam[i] [C]	T_wi[i] [C]	T_wo[i] [C]	V_eai[i] [m/s]	V_noz[i] [m/s]
15.22	14.01	41.91	65.1	114.3	4.261	46.52	1.662	26.75
15.3	14.02	40.54	62.37	113.9	4.281	43.97	1.663	26.77
15.36	13.93	40.22	60.96	113.8	4.144	41.34	1.663	26.76
15.07	13.65	38.84	57.27	113.1	4.446	37.55	1.664	26.76
14.48	13.17	37.8	52.89	112.8	4.348	31.03	1.663	26.71
14.22	12.84	37.84	52.2	112.8	4.29	28.55	1.664	26.7
13.93	12.31	38.25	50.98	112.6	4.557	25.47	1.664	26.71
15.76	13.6	39.28	61.04	111.9	14.37	40.01	1.66	26.72
15.67	13.99	39.91	62.59	111.7	14.52	42.07	1.66	26.72

Data for Figure 1.7, varying quality

W_auxhtr[i] [kW]	W_comp[i] [kW]	W_fan[i] [kW]	W_h1[i] [kW]	W_outlet[i] [kW]	x_din[i]	x_dout[i]	Y[i]
6.346	3.876	4.15	6.37	0.02434	0.1534	0.1753	0.9955
6.374	3.703	4.146	6	0.02443	0.15	0.1724	0.9955
6.378	3.535	4.149	5.951	0.02451	0.1457	0.1675	0.9955
6.369	3.316	4.146	6.149	0.0245	0.1393	0.1604	0.9955
6.388	2.985	4.152	6.42	0.02447	0.119	0.1387	0.9955
6.387	2.859	4.156	6.438	0.0245	0.1062	0.1235	0.9955
6.368	2.715	4.158	6.417	0.0244	0.09071	0.1065	0.9955
6.281	3.605	4.145	6.311	0.02401	0.1539	0.1751	0.9955
6.267	3.723	4.141	5.962	0.02393	0.1603	0.1829	0.9955

Data for Figure 1.8, varying mass flux

alpha[i]	DELTAP[i] [kPa]	dP_dist[i] [kPa]	dP_distm[i] [psi]	Drip[i] [g/s]	eta[i]	G_erdf[i] [kg/s-m^2]	G_erdi[i] [kg/m^2-s]	h_airin[i] [kJ/kg]
0.9956	0.02753	24.05	3.488	0.01598	0.7412	1203	901.9	64.9
0.9956	0.0527	38.63	5.602	0.02186	0.7163	1367	1025	62.98
0.9956	0.08201	57.3	8.311	0.3617	0.6522	1554	1165	64.54
0.9956	0.1182	75.57	10.96	0.5706	0.6731	1693	1270	62.81
0.9956	0.1747	103.9	15.06	0.9315	0.654	1877	1407	64.26
0.9956	0.2308	128.6	18.66	1.166	0.6847	2011	1509	62.89
0.9957	0.2782	148.5	21.54	1.228	0.7283	2151	1613	61.54

h_airout[i] [kJ/kg]	h_cri[i] [kJ/kg]	h_cro[i] [kJ/kg]	h_eamax[i] [kJ/kg]	h_ero[i] [kJ/kg]	h_ers1[i] [kJ/kg]	h_ers10[i] [kJ/kg]	h_ers11[i] [kJ/kg]	h_ers12[i] [kJ/kg]
54.35	309	106.6	50.66	291.2	295.1	291.8	291.9	290.9
51.56	312.4	112	47.03	290.8	295	292.8	292.9	291.3
52.23	314.3	115.5	45.66	291	296.1	293.4	293	291
49.15	316.1	118.4	42.52	290.8	296.3	294.2	293.7	291.4
49.93	318.7	123.7	42.35	291.6	297.2	293.3	292.4	289.9
47.44	320.8	126.6	40.33	291.3	297.5	292.8	292	289.6
45.11	321.3	127.5	38.98	290.1	297.3	293.1	292.6	289.9

h_ers2[i] [kJ/kg]	h_ers3[i] [kJ/kg]	h_ers4[i] [kJ/kg]	h_ers5[i] [kJ/kg]	h_ers6[i] [kJ/kg]	h_ers7[i] [kJ/kg]	h_ers8[i] [kJ/kg]	h_ers9[i] [kJ/kg]	mu_aeo_ave[i] [kg/m-s]
293.4	292.2	291.3	289.2	287.7	85.77	289.6	290.7	0.0000182
293.6	292.5	291.5	289.3	287.5	83.4	287.8	290.5	0.00001816
294.6	293.6	292.8	290.1	287.9	82.56	287	290.1	0.00001815
294.9	293.8	292.8	289.9	287.6	80.3	101.4	289.5	0.00001811
295.8	294.9	294.5	291.5	288.9	81.15	285	289	0.00001812
296	295.1	294.7	291.6	288.8	79.3	79.44	288.5	0.00001808
295.7	294.5	293.9	291	288	77.7	78.05	288.1	0.00001804

m_dot_air[i] [kg/s]	m_dot_win[i] [kg/s]	m_dot_ wout[i] [kg/s]	M_r[i] [g/s]	M_r2[i] [g/s]	M_w[i] [g/s]	omega_ai[i]	omega_ao[i]	P_cri[i] [kPa]
1.115	0.01526	0.01525	-18.9	64.27	131.1	0.01368	0.01367	1887
1.118	0.01449	0.01447	-18.91	73.06	131.2	0.01296	0.01294	2044
1.117	0.01518	0.01482	82.63	83.02	130.2	0.01359	0.01327	2161
1.118	0.01447	0.0139	89.37	90.49	130	0.01294	0.01243	2256
1.116	0.01506	0.01413	99.2	100.3	129.9	0.0135	0.01266	2420
1.117	0.01453	0.01336	106.7	107.5	130.4	0.013	0.01196	2547
1.117	0.01397	0.01274	114.6	114.9	130.3	0.0125	0.0114	2629

P_cro[i] [kPa]	P_erdi[i] [kPa]	P_erdif[i] [kPa]	P_erdo[i] [kPa]	P_ero[i] [kPa]	P_noz[i] [kPa]	P_tun[i] [kPa]	Q_dot_cond[i] [kW]	Q_dot_water[i] [kW]
1866	1383	17.21	1359	1342	0.4353	0.04942	13.01	13.01
2016	1353	19.14	1315	1295	0.4354	0.05013	14.64	14.64
2126	1355	21.67	1298	1276	0.4346	0.05515	16.5	16.5
2216	1333	21.96	1258	1236	0.4334	0.0579	17.89	17.89
2376	1359	25.05	1256	1231	0.4323	0.05964	19.56	19.56
2500	1358	31.39	1230	1198	0.4318	0.06009	20.88	20.88
2578	1361	39.22	1212	1173	0.4297	0.06134	22.28	22.28

Data for Figure 1.8, varying mass flux

Q_eai[i] [m^3/s]	Q_evap_air[i] [kW]	Q_evap_r[i] [kW]	Q_evap_rs[i] [kW]	Q_evap_rsg[i] [kW]	Q_max[i] [kW]	Q_noz[i] [m^3/s]	Re1[i]	Re2[i]
0.9812	11.77	-3.489	-3.166	-3.493	15.88	0.9482	263353	219461
0.9822	12.77	-3.382	-3.064	-3.398	17.83	0.9464	264584	220486
0.9821	13.75	14.5	13.12	14.6	21.08	0.9455	264443	220369
0.9818	15.26	15.41	12.55	15.55	22.68	0.9422	265322	221101
0.981	15.99	16.65	14.96	16.77	24.45	0.9414	264726	220605
0.9812	17.26	17.58	13.93	17.72	25.21	0.9393	265498	221248
0.9797	18.35	18.63	14.8	18.9	25.2	0.9352	266001	221668

Re3[i]	rho_aei_ave[i] [kg/m^3]	rho_aeo_ave[i] [kg/m^3]	rho_erdi[i] [kg/m^3]	SCFM[i] [ft^3/min]	T_aei[i] [C]	T_aeo1[i] [C]	T_aeo10[i] [C]	T_aeo11[i] [C]
131677	1.137	1.176	391.8	2079	29.73	19.2	18.44	18.4
132292	1.138	1.181	314.5	2081	29.65	18.19	17.3	17.28
132222	1.137	1.181	286.3	2081	29.61	18.08	17.23	17.02
132661	1.139	1.187	258.1	2080	29.54	17.03	16.29	15.98
132363	1.138	1.186	238.2	2079	29.56	16.95	16.57	16.15
132749	1.139	1.19	224	2079	29.47	16.16	15.65	15.43
133001	1.14	1.194	220.8	2076	29.4	15.49	14.74	14.67

T_aeo12[i] [C]	T_aeo13[i] [C]	T_aeo14[i] [C]	T_aeo15[i] [C]	T_aeo16[i] [C]	T_aeo17[i] [C]	T_aeo18[i] [C]	T_aeo19[i] [C]	T_aeo2[i] [C]
18.5	18.44	18.49	18.48	19.73	20.03	20.12	20.14	19.18
17.4	17.31	17.34	17.35	18.94	19.33	19.41	19.45	18.16
17.17	16.98	17.03	17.06	19.26	19.53	19.35	19.25	18.05
16.12	15.9	15.91	15.95	18.36	18.58	18.29	18.17	16.77
16.09	15.99	16.02	16.14	19.08	19.22	19.01	19.34	16.52
15.43	15.25	15.29	15.35	18.58	18.97	18.79	18.81	15.78
14.67	14.48	14.54	14.58	17.27	17.4	17.17	17.14	15.15

T_aeo20[i] [C]	T_aeo21[i] [C]	T_aeo22[i] [C]	T_aeo23[i] [C]	T_aeo24[i] [C]	T_aeo25[i] [C]	T_aeo3[i] [C]	T_aeo4[i] [C]	T_aeo5[i] [C]
19.72	20.9	21.3	21.07	20.97	19.94	19.39	19.62	21.25
19.19	19.96	20.66	20.35	20.22	19.31	18.31	18.71	20.39
19.06	20.02	20.63	20.18	20.06	19.36	17.99	18.72	20.03
18	19.2	20.1	19.46	19.6	19.16	17.01	17.84	19.17
18.99	19.29	19.92	19.59	19.81	19.07	16.89	17.91	18.95
18.21	18.47	19.43	19.18	18.87	17.97	16.07	17.26	18.43
16.94	17.39	18.73	18.25	17.88	16.88	15.36	16.71	18.14

T_aeo6[i] [C]	T_aeo7[i] [C]	T_aeo8[i] [C]	T_aeo9[i] [C]	T_aeo_ave[i] [C]	T_chwallin[i] [C]	T_chwallout[i] [C]	T_cri[i] [C]	T_cro[i] [C]
18.99	18.98	18.97	18.29	19.54	30.23	23.66	46.36	29.38
17.96	17.92	17.84	17.19	18.62	30.21	23.71	51.49	32.39
17.71	17.68	17.59	16.83	18.47	29.58	23.76	54.74	34.38
16.71	16.65	16.65	15.81	17.55	29.57	23.83	57.55	35.95
16.69	16.64	16.59	15.88	17.73	29.73	24.14	61.9	38.8
15.94	15.93	15.95	15.11	17.05	29.65	24.16	65.22	40.31
15.27	15.25	15.19	14.39	16.15	29.47	24.12	66.64	40.74

Data for Figure 1.8, varying mass flux

T_dew[i] [C]	T_dew_o[i] [C]	T_erin[i] [C]	T_ero[i] [C]	T_ers1[i] [C]	T_ers10[i] [C]	T_ers11[i] [C]	T_ers12[i] [C]	T_ers2[i] [C]
18.83	18.81	17.89	22.05	25.16	22.5	22.62	21.77	23.79
17.98	17.96	16.7	20.7	24.1	22.26	22.34	21.08	22.95
18.72	18.34	16.24	20.39	24.57	22.37	21.97	20.36	23.36
17.96	17.33	15.15	19.37	23.91	22.13	21.72	19.79	22.71
18.61	17.62	15.09	19.84	24.55	21.23	20.54	18.5	23.34
18.03	16.73	14.36	18.86	24.12	20.09	19.43	17.49	22.81
17.42	16	13.86	17.27	23.36	19.8	19.38	17.12	21.96

T_ers3[i] [C]	T_ers4[i] [C]	T_ers5[i] [C]	T_ers6[i] [C]	T_ers7[i] [C]	T_ers8[i] [C]	T_ers9[i] [C]	T_noz1[i] [C]	T_noz2[i] [C]
22.82	22.12	20.44	19.31	17.13	20.77	21.67	19.34	19.16
22.02	21.25	19.52	18.07	15.69	18.35	20.47	18.25	18.27
22.5	21.84	19.71	17.95	15.17	17.23	19.7	18.2	18.27
21.8	20.99	18.63	16.73	13.78	14.52	18.24	17.05	17.6
22.56	22.22	19.77	17.66	14.32	14.61	17.71	17.97	18.05
22.01	21.69	19.1	16.79	13.18	13.26	16.57	17.32	17.25
21.02	20.49	18.02	15.56	12.19	12.41	15.69	16.16	16.36

T_noz3[i] [C]	T_shellbot[i] [C]	T_shelltop[i] [C]	T_steam[i] [C]	T_wi[i] [C]	T_wo[i] [C]	V_eai[i] [m/s]	V_noz[i] [m/s]	W_auxhtr[i] [kW]
18.64	36.43	43.92	74.31	5.836	29.55	1.635	26.73	6.297
17.38	38.95	48.76	98.48	6.388	33.08	1.637	26.68	6.301
17.03	40.06	51.8	103.4	5.397	35.68	1.637	26.66	6.298
15.92	40.71	54.62	104.1	4.929	37.84	1.636	26.56	6.308
15.99	41.87	58.72	113.4	5.579	41.6	1.635	26.54	6.286
15.18	42.33	62.01	113.3	6.006	44.3	1.635	26.48	6.305
14.41	41.57	63.47	114.3	5.081	45.95	1.633	26.37	6.3

W_comp[i] [kW]	W_fan[i] [kW]	W_h1[i] [kW]	W_outlet[i] [kW]	x_din[i]	x_dout[i]	Y[i]
1.26	3.931	2.151	0.02394	0.0939	0.09871	0.9956
1.65	3.942	2.755	0.02397	0.1268	0.1344	0.9956
2.008	3.941	2.7	0.02395	0.1445	0.1555	0.9956
2.359	3.944	3.696	0.024	0.163	0.1774	0.9956
2.83	3.954	3.557	0.02393	0.1847	0.2038	0.9956
3.291	3.956	3.996	0.024	0.1995	0.2228	0.9956
3.729	3.957	5.049	0.02386	0.2034	0.2302	0.9957

Data for Figure 1.9, 45 deg tilt

	alpha[i]	DELTAP[i] [kPa]	dP_dist[i] [kPa]	dP_distm[i] [psi]	Drip[i] [g/s]	eta[i]	G_erdf[i] [kg/s-m^2]	G_erdi[i] [kg/m^2-s]
45 deg	0.9977	52.83	113.8	16.51	819.8	1.411	2031	1523
22.5 deg	0.9976	52.24	112.1	16.26	747.7	1.409	2022	1517
0 deg	0.9973	51.68	110.9	16.09	580	1.395	2015	1511

h_airin[i] [kJ/kg]	h_airout[i] [kJ/kg]	h_cri[i] [kJ/kg]	h_cro[i] [kJ/kg]	h_eamax[i] [kJ/kg]	h_ero[i] [kJ/kg]	h_ers1[i] [kJ/kg]	h_ers10[i] [kJ/kg]	h_ers11[i] [kJ/kg]
54.9	25.11	321.9	117.5	33.8	287.7	295.9	288.3	289.6
54.7	24.96	321.8	117.2	33.59	287.6	295.8	286.9	289.2
54.37	24.86	321.4	116.6	33.22	287.6	295.9	287.2	289.6

h_ers12[i] [kJ/kg]	h_ers2[i] [kJ/kg]	h_ers3[i] [kJ/kg]	h_ers4[i] [kJ/kg]	h_ers5[i] [kJ/kg]	h_ers6[i] [kJ/kg]	h_ers7[i] [kJ/kg]	h_ers8[i] [kJ/kg]	h_ers9[i] [kJ/kg]
288.3	294.1	292.9	292.5	289.5	287	73.88	74.15	285.4
288.2	294.1	293	292.6	289.6	287	73.55	73.86	284.7
288.4	294.2	293.1	292.7	289.5	286.8	73.17	73.53	285

mu_aeo _ave[i] [kg/m-s]	m_dot _air[i] [kg/s]	m_dot _win[i] [kg/s]	m_dot _wout[i] [kg/s]	M_r[i] [g/s]	M_r2[i] [g/s]	M_w[i] [g/s]	omega_ai[i]	omega_ao[i]
0.00001921	1.542	0.01652	-0.8033	108.2	108.6	131.5	0.01071	0.001
0.00001911	1.517	0.01616	-0.7315	107.8	108.1	131.3	0.01065	0.001
0.00001889	1.451	0.01528	-0.5647	107.3	107.7	131.4	0.01053	0.001

P_cri[i] [kPa]	P_cro[i] [kPa]	P_erdi[i] [kPa]	P_erdif[i] [kPa]	P_erdo[i] [kPa]	P_ero[i] [kPa]	P_noz[i] [kPa]	P_tun[i] [kPa]	Q_dot_cond[i] [kW]
2620	2600	1258	39.03	1144	1105	0.4326	0.06425	22.18
2618	2595	1253	39.81	1141	1101	0.4328	0.0636	22.11
2633	2587	1247	40.21	1136	1096	0.433	0.06331	22.06

Q_dot _water[i] [kW]	Q_eai[i] [m^3/s]	Q_evap _air[i] [kW]	Q_evap _r[i] [kW]	Q_evap _rs[i] [kW]	Q_evap _rsg[i] [kW]	Q_max[i] [kW]	Q_noz[i] [m^3/s]	Re1[i]
22.18	1.34	45.94	18.42	14.8	18.7	32.55	0.6892	344867
22.11	1.317	45.1	18.38	14.76	18.65	32.01	0.7009	340905
22.06	1.26	42.82	18.35	14.75	18.63	30.69	0.7317	330146

Re2[i]	Re3[i]	rho_aei _ave[i] [kg/m^3]	rho_aeo _ave[i] [kg/m^3]	rho_erdi[i] [kg/m^3]	SCFM[i] [ft^3/min]	T_aei[i] [C]	T_aeo1[i] [C]	T_aeo10[i] [C]
287389	172434	1.151	2.238	234.6	2839	27.39	13.42	12.33
284087	170452	1.151	2.164	235	2791	27.33	13.25	12
275121	165073	1.152	1.983	235.9	2670	27.32	13.13	11.79

T_aeo11[i] [C]	T_aeo12[i] [C]	T_aeo13[i] [C]	T_aeo14[i] [C]	T_aeo15[i] [C]	T_aeo16[i] [C]	T_aeo17[i] [C]	T_aeo18[i] [C]	T_aeo19[i] [C]
12.56	12.61	12.3	12.45	12.49	15.12	15.15	14.93	14.7
12.43	12.48	12.23	12.28	12.36	15.03	15.17	14.89	14.7
12.26	12.32	11.96	12.06	12.15	14.93	15.13	14.86	14.71

T_aeo2[i] [C]	T_aeo20[i] [C]	T_aeo21[i] [C]	T_aeo22[i] [C]	T_aeo23[i] [C]	T_aeo24[i] [C]	T_aeo25[i] [C]	T_aeo3[i] [C]	T_aeo4[i] [C]
13.08	14.45	16.03	16	15.65	15.49	14.61	13.33	15.14
12.88	14.65	15.54	15.88	15.22	15.26	14.08	13.13	14.98
12.81	14.55	15.34	16	15.44	15.15	13.97	13.12	14.97

Data for Figure 1.9, 45 deg tilt

T_aeo5[i] [C]	T_aeo6[i] [C]	T_aeo7[i] [C]	T_aeo8[i] [C]	T_aeo9[i] [C]	T_aeo_ave[i] [C]	T_chwallin[i] [C]	T_chwallout[i] [C]	T_cri[i] [C]
15.88	13.14	13.12	13.04	12.05	13.96	26.81	22.55	67
15.78	13.1	13.06	13	11.86	13.81	26.56	22.55	66.86
15.83	12.97	12.91	12.88	11.69	13.72	26.45	22.57	66.82

T_cro[i] [C]	T_dew[i] [C]	T_dew_o[i] [C]	T_erin[i] [C]	T_ero[i] [C]	T_ers1[i] [C]	T_ers10[i] [C]	T_ers11[i] [C]	T_ers12[i] [C]
35.36	15.04	2	11.85	13.7	20.69	14.21	15.25	14.19
35.15	14.96	2	11.76	13.52	20.5	12.94	14.85	13.98
34.81	14.78	2	11.62	13.39	20.46	13.02	15.05	14.07

T_ers2[i] [C]	T_ers3[i] [C]	T_ers4[i] [C]	T_ers5[i] [C]	T_ers6[i] [C]	T_ers7[i] [C]	T_ers8[i] [C]	T_ers9[i] [C]	T_noz1[i] [C]
19.13	18.07	17.72	15.22	13.12	9.878	10.05	11.81	13.97
19	18.07	17.73	15.21	13.01	9.67	9.867	11.12	14.18
18.97	18.04	17.66	15	12.73	9.429	9.655	11.2	13.75

T_noz2[i] [C]	T_noz3[i] [C]	T_shellbot[i] [C]	T_shelltop[i] [C]	T_steam[i] [C]	T_wi[i] [C]	T_wo[i] [C]	V_eai[i] [m/s]	V_noz[i] [m/s]
14.09	12.34	39.87	63.64	111.4	5.204	45.55	2.233	19.43
13.98	12.19	39.98	63.56	110.8	5.028	45.31	2.195	19.76
13.98	12.01	40.12	63.73	110.2	4.991	45.13	2.1	20.63

W_auxhtr[i] [kW]	W_comp[i] [kW]	W_fan[i] [kW]	W_h1[i] [kW]	W_outlet[i] [kW]	x_din[i]	x_dout[i]	Y[i]
6.346	3.799	3.97	5.028	0.02441	0.1731	0.195	0.9977
6.357	3.782	3.976	5.186	0.0244	0.172	0.1936	0.9976
6.368	3.776	3.976	5.178	0.02447	0.1702	0.1917	0.9973

Data for Figure 1.11, flipping pairs of circuits

circuits flipped	air in temp	alpha[i]	DELTAP[i] [kPa]	dP_dist[i] [kPa]	dP_distm[i] [psi]	Drip[i] [g/s]	eta[i]	G_erdf[i] [kg/s-m^2]
baseline	27	0.9955	59.04	136.3	19.77	1.425	0.7405	2041
7&4	27	0.9956	65.49	149.4	21.66	1.055	0.7586	2028
7&4	30	0.9957	68.08	157.5	22.85	1.3	0.7498	2142
8&2	27	0.9956	64.97	148.3	21.52	1.04	0.7409	2020
8&2	30	0.9956	66.23	152.9	22.17	1.086	0.7239	2124
8&2	33	0.9956	66.62	154.9	22.46	1.098	0.7164	2165
9&3	27	0.9957	64.66	146.2	21.21	1.054	0.8043	2051
9&3	30	0.9957	66.44	150.7	21.86	1.178	0.7937	2168
9&3	32	0.9957	67.46	153.7	22.29	1.236	0.7856	2225
10&4	27	0.9957	66.39	145.3	21.07	1.127	0.8181	2059
10&4	30	0.9958	69.11	152.3	22.09	1.14	0.815	2160
10&4	34	0.9959	70.55	158.4	22.98	1.097	0.7796	2295

G_erdi[i] [kg/m^2-s]	h_airin[i] [kJ/kg]	h_airout[i] [kJ/kg]	h_cri[i] [kJ/kg]	h_cro[i] [kJ/kg]	h_eamax[i] [kJ/kg]	h_ero[i] [kJ/kg]	h_ers1[i] [kJ/kg]	h_ers10[i] [kJ/kg]
1531	56.49	41.14	323.7	125.1	35.76	287.6	294.9	289.9
1521	55.2	40.11	323.9	131.3	35.31	289	294.9	290.7
1607	62.63	46.21	324.3	133.7	40.73	290.8	296.9	288.1
1515	54.8	40.05	323.6	130.7	34.88	289.5	293.4	284.4
1593	62.13	46.4	325.3	132.7	40.4	292.2	296.2	285.9
1623	65.1	49.1	326.3	133.5	42.76	293.3	297.2	288.6
1539	54.99	40.06	323.4	130.5	36.43	288.3	293.5	76.8
1626	62.34	46.25	324.2	132.5	42.07	290.7	295.7	80.26
1669	66.46	49.81	325.3	133.9	45.26	292.2	297.1	285.6
1545	55.4	40.27	323.4	132.3	36.9	287.8	294.1	291
1620	62.12	45.71	324.1	135.1	41.98	289.5	296.3	293
1721	72.2	54.54	326.4	137.4	49.54	293.3	299.9	295

h_ers11[i] [kJ/kg]	h_ers12[i] [kJ/kg]	h_ers2[i] [kJ/kg]	h_ers3[i] [kJ/kg]	h_ers4[i] [kJ/kg]	h_ers5[i] [kJ/kg]	h_ers6[i] [kJ/kg]	h_ers7[i] [kJ/kg]	h_ers8[i] [kJ/kg]
289.9	288.4	293.1	291.7	291.7	288.3	286.2	75.14	75.69
291.6	289.5	293.7	292.5	291.1	290.7	288.7	289.4	76.09
290.6	288.7	295.7	294.7	294.2	293	290.8	290.9	79.37
289.3	287.8	291.2	292.9	294.1	292.3	289.7	289.6	289.9
290.5	288.6	293.7	294.9	296.7	294.8	291.8	291.4	291.5
291.4	289.3	294.4	295.6	297.7	295.4	292.4	292.7	292.9
289	287.3	291.1	287.2	291.6	289.5	286.9	76.76	288.4
290.1	288.7	293.2	289.6	294.1	292.3	289.4	287	290.3
291.1	289.4	294.6	290.9	295.5	293.9	291	289.1	291.8
288.3	286.9	293	291.9	290.5	288.4	286.1	75.37	75.71
290.1	287.5	295	293.5	291.5	289.6	286.9	78.2	78.81
292	288.9	298.4	296.9	295.5	293.2	290	83.81	288.7

Data for Figure 1.11, flipping pairs of circuits

h_ers9[i] [kJ/kg]	mu_aeo_ave[i] [kg/m-s]	m_dot_air[i] [kg/s]	m_dot_win[i] [kg/s]	m_dot_wout[i] [kg/s]	M_r[i] [g/s]	M_r2[i] [g/s]	M_w[i] [g/s]	omega_ai[i]
287	0.00001797	1.138	0.01339	0.01196	110.4	109.1	163.4	0.01176
285.5	0.00001796	1.13	0.01256	0.0115	109.5	108.4	168.9	0.01111
284.8	0.00001807	1.114	0.01419	0.01289	115.8	114.5	167.5	0.01273
284.3	0.00001797	1.135	0.01249	0.01145	109.5	107.9	168.1	0.011
284.8	0.00001808	1.119	0.01407	0.01298	115.4	113.5	167.8	0.01257
286.2	0.00001812	1.114	0.01482	0.01372	117.8	115.7	168.2	0.0133
289.5	0.00001796	1.125	0.01248	0.01142	110	109.6	160.3	0.01109
291	0.00001807	1.111	0.01407	0.0129	116.5	115.8	160.2	0.01266
292.7	0.00001813	1.101	0.015	0.01377	119.7	118.9	159.7	0.01363
286.1	0.00001796	1.117	0.01256	0.01143	110.1	110.1	150.2	0.01124
287.5	0.00001805	1.101	0.01386	0.01272	115.8	115.4	149.3	0.01259
290.5	0.0000182	1.081	0.01597	0.01487	123.2	122.6	149.7	0.01478

omega_ao[i]	P_cri[i] [kPa]	P_cro[i] [kPa]	P_erdi[i] [kPa]	P_erdif[i] [kPa]	P_erdo[i] [kPa]	P_ero[i] [kPa]	P_noz[i] [kPa]	P_tun[i] [kPa]
0.01051	2814	2824	1306	42.23	1170	1128	0.4428	0.06317
0.01018	2689	2673	1313	30.92	1164	1133	0.4363	0.06071
0.01157	2790	2749	1392	26.98	1235	1208	0.4284	0.06214
0.01008	2669	2641	1307	33.65	1158	1125	0.4403	0.062
0.0116	2734	2709	1383	31.63	1230	1199	0.4326	0.06239
0.01232	2772	2748	1415	31.32	1261	1229	0.4308	0.06239
0.01015	2723	2701	1325	29.05	1179	1150	0.432	0.06327
0.0116	2775	2756	1403	36.1	1252	1216	0.4265	0.06365
0.0125	2831	2812	1446	37.68	1292	1254	0.421	0.06341
0.01023	2788	2752	1330	32.44	1185	1152	0.4264	0.06121
0.01155	2862	2829	1403	32.32	1251	1218	0.418	0.0623
0.01376	2956	2915	1503	32.1	1345	1313	0.4086	0.06214

Q_dot_cond[i] [kW]	Q_dot_water[i] [kW]	Q_eai[i] [m^3/s]	Q_evap_air[i] [kW]	Q_evap_r[i] [kW]	Q_evap_rs[i] [kW]	Q_evap_rsg[i] [kW]	Q_max[i] [kW]	Q_noz[i] [m^3/s]
21.66	21.66	0.987	17.47	17.94	14.27	18.22	23.6	0.946
20.87	20.87	0.9804	17.06	17.26	15.5	17.48	22.48	0.9385
21.81	21.81	0.9789	18.29	18.18	16.24	18.29	24.4	0.9349
20.81	20.81	0.9842	16.76	17.38	17.43	17.44	22.62	0.9431
21.86	21.86	0.983	17.6	18.4	18.35	18.35	24.31	0.9397
22.3	22.3	0.9834	17.84	18.82	18.76	18.76	24.9	0.9396
21.14	21.14	0.9751	16.79	17.36	13.58	15.15	20.88	0.9339
22.21	22.21	0.9762	17.88	18.44	16.43	16.08	22.52	0.9327
22.77	22.77	0.9737	18.34	18.95	18.92	18.95	23.34	0.9293
21.03	21.03	0.9689	16.91	17.12	13.39	17.32	20.67	0.9278
21.82	21.82	0.967	18.07	17.88	13.96	18.06	22.17	0.9227
23.18	23.18	0.9659	19.09	19.2	17.08	19.29	24.49	0.9186

Data for Figure 1.11, flipping pairs of circuits

Re1[i]	Re2[i]	Re3[i]	rho_aei_ave[i] [kg/m^3]	rho_aeo_ave[i] [kg/m^3]	rho_erdi[i] [kg/m^3]	SCFM[i] [ft^3/min]	T_aei[i] [C]	T_aeo1[i] [C]
272200	226834	136100	1.153	1.203	214.8	2091	26.32	14.17
270452	225377	135226	1.153	1.204	193	2077	26.69	13.49
264794	220662	132397	1.138	1.191	204.4	2074	29.88	15.68
271537	226281	135769	1.154	1.204	193.2	2085	26.57	13.5
265964	221637	132982	1.139	1.191	206.1	2083	29.8	15.65
264275	220229	132137	1.133	1.186	211.4	2084	30.87	16.45
269128	224274	134564	1.154	1.204	198.6	2066	26.53	13.8
264232	220194	132116	1.138	1.192	212	2068	29.77	15.95
260948	217456	130474	1.131	1.185	218.1	2063	31.38	17.05
267331	222775	133665	1.153	1.204	193.9	2053	26.56	13.84
262060	218383	131030	1.139	1.193	202.2	2049	29.75	15.79
255169	212641	127585	1.119	1.176	219.1	2047	34.08	18.47

T_aeo10[i] [C]	T_aeo11[i] [C]	T_aeo12[i] [C]	T_aeo13[i] [C]	T_aeo14[i] [C]	T_aeo15[i] [C]	T_aeo16[i] [C]	T_aeo17[i] [C]	T_aeo18[i] [C]
13.32	13.28	13.43	13.63	13.22	13.34	15	15.32	15.13
12.97	13.42	13.56	14.21	13.68	13.73	14.57	14.66	14.59
14.79	15.72	16.11	17.87	16.07	16.13	17.84	17.53	17.38
12.51	13.35	13.51	14.91	13.54	13.46	18.26	18	17.72
14.74	15.5	15.59	19.9	15.64	15.65	20.77	20.49	20.3
15.54	16.38	16.59	21.89	16.51	16.45	21.58	21.21	21.05
12.77	13.23	13.35	15.1	13.21	13.17	15.59	15.61	15.27
14.89	15.58	15.64	18.89	15.25	15.26	18.18	18.4	18.55
16.02	16.75	16.86	21.35	16.58	16.5	19.35	19.54	19.75
13.82	13.33	13.41	14.21	13.36	13.41	14.57	14.65	14.58
15.95	15.2	15.3	17.19	15.16	15.11	16.52	16.46	16.35
18.65	17.8	17.93	23.67	17.69	17.72	19.39	19.64	19.41

T_aeo19[i] [C]	T_aeo2[i] [C]	T_aeo20[i] [C]	T_aeo21[i] [C]	T_aeo22[i] [C]	T_aeo23[i] [C]	T_aeo24[i] [C]	T_aeo25[i] [C]	T_aeo3[i] [C]
15.08	13.78	14.86	15.6	15.97	15.7	15.52	14.39	14.25
14.45	13.21	14.14	16.22	16.34	15.88	15.89	14.86	13.64
17.09	15.45	16.87	18.68	19.09	18.8	18.67	17.53	15.74
17.42	13.19	16.79	13.6	13.99	14.07	13.63	13.51	13.35
20.34	15.4	19.43	16.2	16.48	16.5	16.16	16.06	15.62
20.97	16.23	19.84	17.24	17.21	17.34	16.89	17.04	16.51
15.24	13.55	14.98	14.84	14.87	14.3	14.41	13.86	13.86
18.64	15.91	18.09	17.09	17.15	16.79	16.41	15.96	16.09
19.82	17	19.3	18.34	18.52	18.13	17.74	17.5	17.25
14.56	13.72	14.35	15.16	15.48	15.42	15.36	14.27	13.76
16.28	15.59	16.02	17.85	18.18	17.98	17.46	16.27	15.8
19.49	18.22	19.24	22.09	22.24	21.41	20.95	20.05	18.56

Data for Figure 1.11, flipping pairs of circuits

T_aeo4[i] [C]	T_aeo5[i] [C]	T_aeo6[i] [C]	T_aeo7[i] [C]	T_aeo8[i] [C]	T_aeo9[i] [C]	T_aeo_ave[i] [C]	T_chwallin[i] [C]	T_chwallout[i] [C]
15.45	16.41	13.94	13.98	14	13.06	14.47	25.36	22.43
15.15	16.24	13.27	13.32	13.33	12.69	14.3	26.19	22.84
17.36	18.51	15.51	15.54	15.48	14.79	16.81	29.26	22.88
15.03	15.99	13.23	13.23	13.2	12.51	14.46	26.07	23.5
17.37	18.26	15.44	15.39	15.36	14.64	16.92	29.16	23.52
18.02	19.04	16.28	16.3	16.23	15.53	17.77	30.19	23.6
15.46	16.43	14.1	14.08	13.72	12.77	14.3	26.04	21.27
18.26	18.62	16.27	16.29	15.97	14.9	16.76	29.12	21.08
19.23	19.73	17.32	17.36	17.08	16.02	18	30.61	21.19
15.94	16.34	13.68	13.66	13.69	13.19	14.31	25.6	20.34
18.04	18.4	15.6	15.66	15.62	15.24	16.36	28.67	20.38
20.86	21.06	18.22	18.29	18.32	17.92	19.49	32.96	20.56

T_cri[i] [C]	T_cro[i] [C]	T_dew[i] [C]	T_dew_o[i] [C]	T_erin[i] [C]	T_ero[i] [C]	T_ers1[i] [C]	T_ers10[i] [C]	T_ers11[i] [C]
70.81	39.43	16.48	14.75	12.63	14.18	20.28	16.05	16.09
69.37	42.87	15.6	14.26	12.45	15.42	20.43	16.9	17.6
70.94	44.14	17.71	16.22	14.5	18.67	23.81	16.46	18.48
68.86	42.59	15.45	14.12	12.28	15.63	18.96	11.5	15.49
70.98	43.59	17.51	16.26	14.38	19.63	23.01	14.5	18.22
72.2	44.01	18.38	17.19	15.23	21.23	24.46	17.43	19.69
69.42	42.45	15.57	14.23	12.89	15.29	19.59	11.71	15.84
70.71	43.45	17.62	16.27	14.98	18.78	22.9	13.85	18.26
72.24	44.16	18.76	17.42	16.1	20.89	24.91	15.65	20
70.26	43.35	15.78	14.35	13.07	14.91	20.21	17.61	15.37
71.77	44.81	17.53	16.2	14.95	17.89	23.52	20.74	18.34
74.59	45.96	20.04	18.92	17.53	23.04	28.55	24.44	22.04

T_ers12[i] [C]	T_ers2[i] [C]	T_ers3[i] [C]	T_ers4[i] [C]	T_ers5[i] [C]	T_ers6[i] [C]	T_ers7[i] [C]	T_ers8[i] [C]	T_ers9[i] [C]
14.78	18.8	17.59	17.57	14.77	13.05	10.66	11.01	13.7
15.9	19.39	18.41	17.19	16.89	15.2	15.77	11.26	12.56
16.94	22.76	21.94	21.47	20.49	18.71	18.74	13.29	13.84
14.21	17.05	18.5	19.52	18.04	15.82	15.71	16.01	11.42
16.65	20.85	21.87	23.38	21.79	19.31	18.94	19.09	13.65
17.98	22.15	23.15	24.88	22.98	20.45	20.71	20.87	15.53
14.48	17.56	14.36	18.02	16.22	14.11	11.68	15.38	16.28
17.15	20.87	17.88	21.55	20.11	17.73	15.81	18.48	19
18.61	22.86	19.86	23.63	22.3	19.95	18.37	20.58	21.27
14.19	19.21	18.33	17.14	15.41	13.51	10.79	11.01	13.51
16.29	22.38	21.18	19.47	17.94	15.82	12.55	12.94	16.26
19.59	27.25	26.02	24.88	22.95	20.44	16.01	19.4	20.81

Data for Figure 1.11, flipping pairs of circuits

T_noz1[i] [C]	T_noz2[i] [C]	T_noz3[i] [C]	T_shellbot[i] [C]	T_shelltop[i] [C]	T_steam[i] [C]	T_wi[i] [C]	T_wo[i] [C]	V_eai[i] [m/s]
14	14.38	13.24	42.47	67.96	119.7	15.85	47.54	1.645
14.26	14.49	13.02	42.27	66.21	113.1	16.26	45.82	1.634
16.38	17.22	15.58	44.09	67.89	113.6	16.25	47.39	1.631
15.41	14.09	13.22	42.34	65.69	111.1	15.74	45.35	1.64
18.65	16.47	15.51	44.62	67.82	112.2	15.72	46.87	1.638
19.04	17.07	16.54	46.04	68.9	113.4	15.93	47.64	1.639
13.87	13.68	13.32	41.83	65.92	112.7	14.78	46.3	1.625
16.09	16.58	15.62	43.18	67.08	114.3	14.48	47.63	1.627
17.91	17.85	16.78	44.43	68.56	114.9	14.71	48.8	1.623
14.09	14.13	13.18	42.08	66.68	114.7	14.09	47.57	1.615
16.21	16.07	15.01	43.37	68.25	112.9	14.19	49.14	1.612
19.26	19.56	17.75	46.24	71.14	113.6	14.09	51.12	1.61

V_noz[i] [m/s]	W_auxhtr[i] [kW]	W_comp[i] [kW]	W_fan[i] [kW]	W_h1[i] [kW]	W_outlet[i] [kW]	x_din[i]	x_dout[i]	Y[i]
26.67	6.36	4.113	4.044	3.176	0.02444	0.2013	0.2264	0.9955
26.46	6.39	3.878	3.972	3.466	-0.005595	0.231	0.2575	0.9956
26.36	6.353	3.978	3.921	4.82	-0.005569	0.2297	0.257	0.9957
26.59	6.275	3.826	4.017	3.908	-0.00559	0.2294	0.2559	0.9956
26.49	6.271	3.906	3.972	5.183	-0.005602	0.2258	0.2525	0.9956
26.49	6.321	3.964	3.959	5.254	-0.005616	0.2244	0.2513	0.9956
26.33	6.342	3.925	3.994	3.431	-0.005557	0.2252	0.2513	0.9957
26.3	6.353	3.995	3.947	4.915	-0.005556	0.2213	0.2477	0.9957
26.2	6.33	4.055	3.917	5.607	-0.005546	0.221	0.2476	0.9957
26.16	6.348	3.992	3.972	3.502	-0.005584	0.2329	0.2586	0.9957
26.02	6.331	4.102	3.923	5.024	-0.00557	0.2348	0.261	0.9958
25.9	6.29	4.187	3.872	5.737	1.221	0.2296	0.2563	0.9959

Data for Figures 1.12- 1.17

alpha[i]	Cmin[i] [kW/C]	Cmin_r[i] [kW/C]	COP[i]	COP_th[i]	cp[i] [kJ/kg-K]	cp_a[i] [kJ/kg-K]	Dep[i] [C]	dh_r[i] [kJ/kg]
0.996	1.109	0.1157	3.778	7.92	1.203	1.024	43.48	166.1
0.996	1.109	0.1169	3.778	7.935	1.189	1.024	36.74	166.2
0.996	1.109	0.117	3.772	8.005	1.192	1.024	36.34	165.7
0.996	1.109	0.06234	3.812	8.051	1.175	1.024	27.04	166
0.9959	1.111	0.0969	3.809	8.139	1.188	1.024	29.54	166
0.996	1.111	0.1135	3.842	8.059	1.173	1.024	18.83	166.2
0.996	1.111	0.1134	3.872	8.21	1.18	1.024	17.91	165.9
0.996	1.11	0.1123	3.881	8.079	1.168	1.024	10.97	166.3
0.996	1.11	-0.02235	3.93	8.297	1.182	1.024	9.798	165.7
0.996	1.111	-0.02221	3.934	8.164	1.175	1.023	4.413	166.2
0.9959	1.112	-0.02286	4.073	8.513	1.209	1.022	6.225	165.2

dP_dist[i] [kPa]	dP_distm[i] [psi]	Drip[i] [g/s]	dT_in[i] [C]	eff_r[i]	epsilon_r[i]	eta[i]	E_in[i] [kW]	E_in_w[i] [kW]
155.5	22.55	0	18.02	0.477	0.9032	0.6997	16.04	15.9
154	22.33	0	18.08	0.4762	0.9138	0.7022	16.28	15.88
150.5	21.83	0	17.84	0.4712	0.9154	0.7202	16.11	15.82
148.6	21.56	0	17.72	0.4735	0.9321	0.7541	16.55	15.94
148.4	21.53	0	17.39	0.468	0.9267	0.7565	16.39	15.67
150	21.75	0	17.55	0.4768	0.9365	0.7593	16.16	16
146.5	21.25	0	17.14	0.4717	0.9366	0.8031	15.99	15.65
152.3	22.09	0	17.59	0.4804	0.9405	0.7883	16.21	16.01
144.4	20.94	0	16.79	0.4736	0.9404	0.8623	16.08	15.57
148.8	21.58	0	17.3	0.4818	0.9389	0.9071	16.53	16.15
127.7	18.52	0	16.11	0.4784	0.929	1.114	16.01	15.44

h_airin[i] [kJ/kg]	h_airout[i] [kJ/kg]	h_cri[i] [kJ/kg]	h_cro[i] [kJ/kg]	h_eamax[i] [kJ/kg]	h_ero[i] [kJ/kg]	LMTD[i] [C]	mu_aeo_ave[i] [kg/m-s]	m_dot_air[i] [kg/s]
53.1	38.72	327.1	139.1	32.55	289.1	7.959	0.00001801	1.083
53.12	38.66	328.4	139	32.53	290.9	7.439	0.00001801	1.083
53.43	39.04	328.7	139.4	33.45	291.1	7.194	0.00001802	1.083
53.27	38.58	331.6	139	33.79	293.8	6.054	0.000018	1.083
53.68	39.4	330.4	138.8	34.8	292.6	6.353	0.00001803	1.085
53.4	38.73	332.4	138.7	34.08	294.3	5.715	0.000018	1.085
53.4	38.98	331.6	138.7	35.44	294.1	5.554	0.00001802	1.085
53.08	38.18	333.2	138.7	34.17	295	5.37	0.000018	1.085
53.1	38.67	331.9	138.7	36.37	294.5	5.084	0.00001802	1.085
51.55	36.42	332.6	138.5	34.87	294.6	5.026	0.00001798	1.086
51.46	36.95	328.7	138.7	38.44	292.2	4.905	0.00001802	1.088

M_r[i] [g/s]	M_w[i] [g/s]	NTU[i]	omega_ai[i]	omega_ao[i]	P_cri[i] [kPa]	P_cro[i] [kPa]	P_erdi[i] [kPa]	P_erdif[i] [kPa]
96.15	149.1	1.764	0.009214	0.009214	2920	2878	1386	104
98.29	148.7	1.898	0.009201	0.009201	2915	2873	1375	94.55
98.15	147.3	1.953	0.009269	0.009269	2922	2880	1378	88.11
53.06	146.9	2.37	0.009199	0.009199	2919	2877	1370	78.05
81.6	143.3	2.196	0.009333	0.009333	2922	2882	1386	80.54
96.84	145.5	2.507	0.009273	0.009273	2925	2883	1366	69.07
96.11	141.2	2.537	0.009221	0.009221	2919	2880	1381	68.94
96.16	145	2.711	0.009115	0.009115	2921	2880	1358	56.64
-18.91	140	2.771	0.009095	0.009095	2921	2883	1381	58.45
-18.91	146.8	2.945	0.008525	0.008525	2914	2877	1374	67.46
-18.91	139.9	2.892	0.008412	0.008412	2912	2884	1429	95.97

Data for Figures 1.12- 1.17

P_erdo[i] [kPa]	P_ero[i] [kPa]	P_noz[i] [kPa]	P_tun[i] [kPa]	Q_cond[i] [kW]	Q_e[i] [tons]	Q_eai[i] [m^3/s]	Q_evap_air[i] [kW]	Q_evap_r[i] [kW]
1231	1127	0.4014	0.03187	20.02	4.4265	0.9448	15.57	14.42
1221	1127	0.4013	0.0322	20.03	4.4509	0.9449	15.65	14.93
1227	1139	0.4014	0.03202	19.95	4.4295	0.9451	15.58	14.89
1221	1143	0.4013	0.03206	20.12	4.525	0.9455	15.91	8.211
1237	1157	0.4035	0.03197	19.74	4.4071	0.9475	15.5	12.55
1216	1147	0.4026	0.0317	20.14	4.5253	0.9469	15.91	15.07
1234	1165	0.403	0.03195	19.69	4.4498	0.9472	15.65	14.94
1205	1149	0.4021	0.03207	20.18	4.5961	0.9468	16.16	15.04
1236	1178	0.403	0.03217	19.55	4.4491	0.9471	15.65	-2.946
1225	1158	0.4025	0.03195	20.33	4.6743	0.9471	16.44	-2.951
1301	1205	0.4047	0.032	19.31	4.4851	0.9489	15.77	-2.902

Q_max[i] [kW]	Q_max_r[i] [kW]	Q_noz[i] [m^3/s]	Re1[i]	Re2[i]	Re3[i]	rho_aei_ave[i] [kg/m^3]	rho_aeo_ave[i] [kg/m^3]	rho_ero[i] [kg/m^3]
22.25	15.97	0.9009	258374	215311	129187	1.146	1.202	42.43
22.29	16.34	0.9008	258377	215314	129188	1.146	1.202	41.94
21.63	16.26	0.9012	258159	215132	129079	1.145	1.201	42.38
21.1	8.809	0.9007	258463	215386	129232	1.145	1.202	41.87
20.49	13.55	0.9039	258598	215498	129299	1.145	1.2	42.7
20.96	16.1	0.9021	258891	215743	129446	1.146	1.202	41.88
19.49	15.95	0.9031	258618	215515	129309	1.145	1.201	42.66
20.51	15.99	0.9012	258952	215793	129476	1.146	1.203	41.75
18.15	-3.133	0.9031	258634	215529	129317	1.145	1.201	43.04
18.12	-3.142	0.9008	259464	216220	129732	1.147	1.206	42.24
14.16	-3.124	0.9045	259295	216079	129647	1.146	1.202	44.77

SCFM[i] [ft^3/min]	Sigma[i] [C]	T_aei[i] [C]	T_aeo1[i] [C]	T_aeo10[i] [C]	T_aeo11[i] [C]	T_aeo12[i] [C]	T_aeo13[i] [C]	T_aeo14[i] [C]
2002	3.9	29.36	13.73	13.26	18.38	18.63	12.05	17.34
2002	3.567	29.41	13.76	12.79	18.47	18.77	12.2	17.98
2003	3.458	29.55	14	12.97	18.6	18.85	12.27	18
2003	2.875	29.56	14.23	13.49	17.1	16.98	15.9	16.84
2008	2.918	29.63	14.55	13.47	17.4	17.58	16.12	16.72
2006	1.938	29.51	14.34	13.5	16.89	16.87	20.94	16.24
2007	1.638	29.64	14.84	13.78	16.56	16.8	21.16	16.57
2006	1.071	29.59	14.81	14.73	16.38	16.1	21.52	15.33
2007	1.066	29.66	15.25	14.32	14.68	15.11	21.83	14.91
2007	0.4015	29.57	15.01	14.13	14.96	15.14	21.4	14.65
2011	0.5811	29.76	15.93	14.52	15.17	15.49	20.32	14.88

T_aeo15[i] [C]	T_aeo16[i] [C]	T_aeo17[i] [C]	T_aeo18[i] [C]	T_aeo19[i] [C]	T_aeo2[i] [C]	T_aeo20[i] [C]	T_aeo21[i] [C]	T_aeo22[i] [C]
16.82	17.7	17.72	17.52	17.36	13.68	17.25	13.44	13.31
17.87	18.09	17.92	17.6	17.41	13.7	17.34	13.46	13.38
17.71	18.18	18.3	17.98	17.74	13.94	17.63	13.8	13.71
16.57	17.47	17.19	16.81	16.5	14.17	16.47	14.01	13.95
16.64	18.49	18.58	18.24	18.02	14.47	17.98	14.34	14.29
16.07	17.52	17.28	16.69	16.37	14.34	16.36	14.13	14.04
16.59	17.05	17.38	17.14	16.89	14.78	16.86	15.03	14.82
15.18	15.7	15.98	15.69	15.34	14.54	15.16	14.12	14.18
14.85	17.41	17.56	17.31	16.98	15.15	16.96	15.42	15.32
14.53	15.05	15.05	14.82	14.53	14.86	14.31	14.73	14.58
14.88	15.43	15.95	15.92	15.7	15.82	15.48	15.74	15.64

Data for Figures 1.12- 1.17

T_aeo23[i] [C]	T_aeo24[i] [C]	T_aeo25[i] [C]	T_aeo3[i] [C]	T_aeo4[i] [C]	T_aeo5[i] [C]	T_aeo6[i] [C]	T_aeo7[i] [C]	T_aeo8[i] [C]
13.08	12.94	12.05	13.85	13.92	17.32	14.6	15.11	14.89
13.23	13.12	12.28	13.91	14.08	17.31	13.95	14	13.78
13.56	13.42	12.54	14.12	14.24	17.42	14.07	14.08	13.9
13.86	13.71	12.51	14.46	14.57	17.63	14.37	14.47	14.37
14.16	13.99	12.65	14.67	14.86	17.95	14.71	14.73	14.52
13.84	13.67	12.26	14.62	14.72	17.8	14.52	14.61	14.45
14.53	14.34	12.94	15.08	15.14	18.17	14.73	14.83	14.73
14.04	13.86	12.5	14.89	15.09	17.87	14.75	15.07	15.15
14.95	14.71	13.41	15.4	15.55	18.37	15.36	15.39	15.19
14.3	14.09	12.68	15.1	15.28	18.06	14.87	15.01	14.89
15.43	15.28	13.82	16.01	16.04	18.97	15.8	15.81	15.67

T_aeo9[i] [C]	T_aeo_ave[i] [C]	T_chwallin[i] [C]	T_chwallout[i] [C]	T_cri[i] [C]	T_cro[i] [C]	T_dew[i] [C]	T_erin[i] [C]	T_ero[i] [C]
13.72	15.32	27.62	22.58	74.68	46.85	12.76	11.34	15.37
12.86	15.29	27.62	22.59	75.58	46.79	12.74	11.33	16.88
13.03	15.49	27.81	22.81	75.87	47.02	12.85	11.71	17.33
13.36	15.21	27.49	22.7	77.99	46.8	12.73	11.84	19.68
13.37	15.68	27.26	22.67	77.11	46.69	12.95	12.25	19.05
13.2	15.18	27.14	22.62	78.67	46.62	12.86	11.96	20.26
13.58	15.55	27.31	22.81	78.01	46.64	12.77	12.5	20.48
14.21	15.03	27.34	22.81	79.25	46.63	12.6	12	20.9
14.02	15.57	27.29	22.87	78.23	46.64	12.56	12.86	21.09
13.83	14.77	27.16	22.96	78.66	46.56	11.6	12.27	20.7
14.38	15.57	27.22	23	75.71	46.64	11.4	13.65	19.73

T_ers1[i] [C]	T_ers10[i] [C]	T_ers11[i] [C]	T_ers12[i] [C]	T_ers2[i] [C]	T_ers3[i] [C]	T_ers4[i] [C]	T_ers5[i] [C]	T_ers6[i] [C]
11.47	15.1	15.26	15.51	15.45	19.56	22.45	22.87	22.58
11.6	15.07	17.02	16.64	17.51	20.22	22.61	23.26	23
11.85	14.49	16.63	16.33	17.77	20.36	22.7	22.62	22.43
12.46	18.39	18.67	17.27	19.25	20.98	22.93	22.34	22.27
12.9	16.24	17.58	16.96	19.57	21.11	23.03	22.5	22.14
15.73	19.76	19.67	17.95	19.79	21.19	22.92	22	21.41
18.36	18.85	19.2	17.71	20.64	21.4	22.85	21.8	21.44
18.81	21.38	21.1	19.4	19.66	19.73	22.4	21.26	20.68
21.97	20.72	20.55	18.85	21.15	21	22.9	21.14	19.88
20.84	20.93	21.23	20.32	20.39	20.27	20.38	20.09	20.01
19.81	18.71	18.83	18.87	20.46	20.19	19.8	19.68	19.13

T_ers7[i] [C]	T_ers8[i] [C]	T_ers9[i] [C]	T_ers_ave[i] [C]	T_noz1[i] [C]	T_noz2[i] [C]	T_noz3[i] [C]	T_sat_cond[i] [C]	T_sat_evap[i] [C]
22.62	22.64	21.37	18.91	16.46	14.17	17.03	47.34	11.41
22.76	21.94	19.21	19.24	17.14	14.32	16.21	47.27	11.41
22.32	21.47	18.49	18.95	17.18	14.55	16.41	47.38	11.78
22.55	21.86	19.84	19.9	15.83	14.48	15.41	47.33	11.92
21.78	20.29	18.45	19.38	17.14	15.2	14.93	47.39	12.32
22.32	21.04	19.16	20.25	15.49	14.56	14.91	47.42	12.04
21.59	19.71	17.98	20.13	15.95	15.13	14.94	47.38	12.57
21.9	21.79	20.57	20.72	15.04	13.88	15.07	47.38	12.07
19.89	20.59	19.31	20.66	15.33	15.12	14.97	47.42	12.94
20.82	21.12	20.16	20.55	14.69	13.78	14.69	47.32	12.35
18.86	19.4	18.71	19.37	15.73	14.96	15.15	47.43	13.73

Data for Figures 1.12- 1.17

T_shellbot[i] [C]	T_shelltop[i] [C]	T_sh_sl[i] [C]	T_steam[i] [C]	T_wi[i] [C]	T_wo[i] [C]	UA[i] [kW/C]	UA_r[i] [kW/C]	V_eai[i] [m/s]
45.24	70.98	3.954	24.35	18.05	50.15	1.956	1.812	1.575
44.95	71.9	5.476	24.45	18.07	50.27	2.104	2.007	1.575
45.45	72.2	5.554	24.41	18.14	50.53	2.165	2.069	1.575
47.32	74.02	7.763	24.31	17.92	50.66	2.628	1.356	1.576
48.39	73.52	6.727	24.47	17.7	50.62	2.44	1.976	1.579
48.78	75.22	8.222	24.62	17.61	50.71	2.785	2.638	1.578
49.56	73.9	7.908	24.73	17.49	50.85	2.818	2.689	1.579
49.53	75.59	8.829	24.79	17.57	50.86	3.01	2.8	1.578
50.16	74.43	8.148	24.95	17.58	50.96	3.078	-0.5795	1.579
49.46	74.88	8.352	25.06	17.46	50.59	3.271	-0.5871	1.579
48.41	72.61	6.001	25.25	17.49	50.5	3.216	-0.5917	1.582

V_noz[i] [m/s]	W_auxhtr[i] [kW]	W_comp[i] [kW]	W_fan[i] [kW]	W_h1[i] [kW]	W_outlet[i] [kW]	W_plugin[i] [kW]	x_din[i]	x_dout[i]
25.4	3.241	4.121	3.906	5.022	1.413	2.46	0.2579	0.2841
25.4	3.226	4.143	3.909	5.279	1.409	2.46	0.2591	0.2851
25.41	3.225	4.13	3.902	5.113	1.405	2.46	0.261	0.2863
25.39	3.237	4.175	3.908	5.54	1.409	2.46	0.26	0.2851
25.48	3.232	4.069	3.907	5.386	1.408	2.46	0.2564	0.2814
25.43	3.216	4.142	3.915	5.161	1.405	2.46	0.2589	0.2843
25.46	3.204	4.041	3.901	5.021	1.399	2.46	0.2567	0.2815
25.41	3.195	4.165	3.915	5.238	1.397	2.46	0.2605	0.2863
25.46	3.217	3.982	3.917	5.082	1.403	2.46	0.2567	0.2811
25.4	3.211	4.179	3.911	5.548	1.399	2.46	0.257	0.2822
25.5	3.228	3.873	3.914	5.006	1.406	2.46	0.2487	0.2701

Y[i]
0.996
0.996
0.996
0.996
0.9959
0.996
0.996
0.996
0.996
0.996
0.9959

Data for Figure 2.1

velocities in m/s

2.1	2.1	2.1	2.1	2	1.5	1.5
2.6	1.7	1.8	1.9	1.8	1.9	2.4
2.3	2.1	1.8	1.7	1.9	2.2	2.6
2	1.9	1.7	1.8	1.8	1.9	2.5
1.8	1.7	1.8	1.8	1.8	2	2.5
1.8	1.9	1.8	1.8	2	1.8	2.3
1.6	1.7	1.9	2.1	2.3	2.1	2.1

looking downstream in air at front of evaporator

Data for Figs. 2.3, 2.4, 2.7, 2.8

	alpha[i]	Balance[i]	COP[i]	COP_th[i]	Dep[i] [C]	dh_r[i] [kJ/kg]	dP_dist[i] [kPa]	dP_distm[i] [psi]
baseline	0.9959	0.9701	3.847	8.115	5.842	165.4	298.7	43.32
10% V	0.996	0.9759	3.813	8.054	6.066	165.2	301	43.65
20% V	0.996	0.9734	3.749	8.039	5.747	165.6	305.1	44.25
30% V	0.996	0.9803	3.717	7.987	8.639	165.8	302.4	43.86
40% V	0.9961	0.9812	3.681	7.913	12.46	166.3	312.3	45.3
50% V	0.9961	0.9769	3.596	7.826	13.57	166.6	313.5	45.47
10% H	0.9959	0.9758	3.757	8.014	26.07	165.9	315.4	45.74
10% H imp	0.9959	0.9821	3.833	8.113	6.23	165.2	318.4	46.18
15% H	0.996	-2.283	3.711	7.851	35.42	166.5	327.8	47.55
15% H imp	0.996	0.9581	3.721	8.103	11.82	165.2	326.9	47.42

Drip[i] [g/s]	dT_airside[i] [C]	dT_in[i] [C]	eff_r[i]	epsilon_r[i]	eta[i]	E_in[i] [kW]	E_in_w[i] [kW]	h_airin[i] [kJ/kg]
0	14.24	17.27	0.474	0.9495	0.7564	16.7	16.2	53.97
0	14.25	17.49	0.4734	0.9448	0.7032	16.6	16.07	55.25
0	14.16	17.77	0.4664	0.9354	0.6855	16.44	15.95	55.28
0	14.16	18	0.4654	0.927	0.6732	16.23	15.77	55.3
0	14.09	18.34	0.4652	0.9173	0.6542	16.04	15.6	55
0	13.96	18.55	0.4595	0.905	0.6314	15.51	15.39	54.76
0	14.09	17.68	0.4688	0.9174	0.6863	16.45	15.98	54.91
0	14.45	17.16	0.4725	0.9432	0.7341	16.7	16.17	55.14
0	13.83	18.41	0.4727	-0.3809	0.6546	16.06	15.59	53.74
0	14.08	17.21	0.4592	0.9335	0.7146	16.5	16.18	55.13

h_airout[i] [kJ/kg]	h_cri[i] [kJ/kg]	h_cro[i] [kJ/kg]	h_eamax[i] [kJ/kg]	h_ero[i] [kJ/kg]	LMTD[i] [C]	mu_aeo_ave[i] [kg/m-s]	m_dot_air[i] [kg/s]	M_r[i] [g/s]
39.38	334.6	139.2	34.68	296.3	4.87	0.000018	1.086	104
40.64	334.4	139.7	34.48	295.8	5.274	0.00001801	1.083	103.9
40.77	333.2	139.5	34.11	294.4	6.044	0.00001802	1.079	103.9
40.78	332.4	139.6	33.74	293.2	6.653	0.00001802	1.075	103.6
40.55	331.2	139.3	32.92	291.8	7.479	0.00001803	1.069	103.1
40.46	329.7	139.1	32.1	289.9	8.378	0.00001803	1.059	102.9
40.47	330.2	139.1	33.87	291.3	6.946	0.00001801	1.084	105.4
40.33	333.4	139.4	34.97	295.2	4.966	0.00001799	1.085	105
39.57	325.1	139.1	32.1	75.67	9.989	0.00001803	1.083	106
40.69	332	139.4	34.93	293.6	5.77	0.00001801	1.083	105.8

M_w[i] [g/s]	omega_ai[i]	omega_ao[i]	P_cri[i] [kPa]	P_cro[i] [kPa]	P_erdi[i] [kPa]	P_erdif[i] [kPa]	P_erdo[i] [kPa]	P_ero[i] [kPa]
145	0.009511	0.009511	2912	2885	1379	-75.02	1080	1155
143.1	0.009955	0.009955	2909	2897	1378	-75.3	1077	1153
144	0.009916	0.009916	2903	2890	1376	-76.94	1071	1148
142.8	0.009892	0.009892	2910	2894	1371	-74.63	1068	1143
141	0.009769	0.009769	2905	2892	1362	-81.98	1050	1132
139.8	0.009725	0.009725	2909	2893	1354	-80.41	1040	1121
145	0.009843	0.009843	2906	2890	1371	-88.93	1056	1144
145.1	0.009967	0.009967	2910	2894	1395	-82.81	1076	1159
146.8	0.009382	0.009382	2900	2885	1356	-92.33	1028	1121
145.6	0.009947	0.009947	2911	2896	1416	-69.2	1089	1159

Data for Figs. 2.3, 2.4, 2.7, 2.8

P_noz[i] [kPa]	P_tun[i] [kPa]	Q_cond[i] [kW]	Q_e[i] [tons]	Q_eai[i] [m^3/s]	Q_evap_air[i] [kW]	Q_evap_r[i] [kW]	Q_max[i] [kW]	Q_max_r[i] [kW]
0.4039	0.03172	20.32	4.5068	0.9485	15.85	16.34	20.96	17.21
0.4018	0.03701	20.22	4.4967	0.9465	15.81	16.2	22.49	17.15
0.3995	0.04599	20.12	4.4544	0.9438	15.67	16.09	22.85	17.2
0.3964	0.05864	19.97	4.4368	0.9402	15.6	15.92	23.18	17.17
0.3919	0.07691	19.79	4.3894	0.9346	15.44	15.73	23.6	17.15
0.3848	0.1061	19.6	4.3072	0.9256	15.15	15.51	23.99	17.13
0.4028	0.03674	20.14	4.4506	0.9472	15.65	16.04	22.81	17.48
0.4028	0.03659	20.37	4.5685	0.9478	16.07	16.36	21.89	17.34
0.4023	0.03999	19.73	4.363	0.9459	15.34	-6.722	23.44	17.65
0.4021	0.04063	20.38	4.4459	0.9465	15.64	16.32	21.88	17.48

Q_noz[i] [m^3/s]	Re1[i]	Re2[i]	Re3[i]	rho_aei_ave[i] [kg/m^3]	rho_aeo_ave[i] [kg/m^3]	rho_ero[i] [kg/m^3]	SCFM[i] [ft^3/min]	Sigma[i] [C]
0.9039	259243	216036	129622	1.145	1.202	41.7	2010	0.5759
0.902	258319	215265	129159	1.144	1.2	41.73	2006	0.6096
0.8997	257349	214458	128675	1.144	1.2	41.87	2000	0.6506
0.8963	256251	213543	128126	1.143	1.199	41.98	1992	1.081
0.8911	254709	212258	127355	1.143	1.199	41.91	1980	1.715
0.883	252370	210309	126185	1.144	1.199	41.98	1961	1.823
0.9031	258531	215442	129265	1.144	1.2	42.56	2007	2.836
0.9026	259010	215841	129505	1.144	1.202	42.12	2008	0.579
0.9027	258147	215122	129073	1.145	1.2	1129	2004	3.877
0.9024	258353	215294	129176	1.144	1.2	42.51	2005	1.079

T_aei[i] [C]	T_aeo1[i] [C]	T_aeo10[i] [C]	T_aeo11[i] [C]	T_aeo12[i] [C]	T_aeo13[i] [C]	T_aeo14[i] [C]	T_aeo15[i] [C]	T_aeo16[i] [C]
29.47	14.98	14.97	16.19	16.11	22.82	14.86	14.68	15.55
29.61	15.27	14.5	16.32	16.02	22.16	14.71	15.3	15.67
29.74	15.58	15.62	16.47	16.12	20.76	14.92	15.72	15.73
29.82	15.81	16.03	16.25	16.02	19.62	14.91	15.54	15.96
29.83	16.07	16.06	16.16	16.09	17.48	15.25	15.21	16.14
29.71	16.32	15.79	15.91	16.02	12.64	15.67	15.19	16.71
29.56	14.2	13.66	16.84	17.35	15.15	17.02	16.81	18.18
29.48	15.21	13.91	14.73	15.03	22.07	14.8	14.82	15.63
29.57	14.18	13.3	17.81	17.83	11.74	16.95	16.97	18.62
29.51	15.83	13.94	14.41	14.77	20.74	14.47	14.63	15.48

T_aeo17[i] [C]	T_aeo18[i] [C]	T_aeo19[i] [C]	T_aeo2[i] [C]	T_aeo20[i] [C]	T_aeo21[i] [C]	T_aeo22[i] [C]	T_aeo23[i] [C]	T_aeo24[i] [C]
15.87	15.71	15.46	14.88	15.21	14.84	15.04	15.01	14.85
16.13	15.98	15.75	15.12	15.98	15.17	15.23	15.04	14.87
16.5	16.34	16.13	15.43	16.22	15.36	15.08	14.72	14.53
16.79	16.62	15.91	15.71	16.22	15.31	15.05	14.77	14.98
16.79	16.84	15.38	15.94	15.9	15.04	14.94	14.94	15.31
16.8	16.52	15.38	16.31	15.54	15.12	14.89	14.6	15.34
17.54	16.98	16.59	13.92	16.44	15.21	15.64	15.21	15.02
15.76	15.75	15.53	14.87	15.3	15.03	15.16	14.89	14.55
18.47	18.22	18.08	12.86	17.75	15.21	16.02	15.74	15.51
15.45	15.04	14.62	16.75	14.41	15.18	15.14	14.72	14.46

Data for Figs. 2.3, 2.4, 2.7, 2.8

T_aeo25[i] [C]	T_aeo3[i] [C]	T_aeo4[i] [C]	T_aeo5[i] [C]	T_aeo6[i] [C]	T_aeo7[i] [C]	T_aeo8[i] [C]	T_aeo9[i] [C]	T_aeo_ave[i] [C]
13.67	15.16	15.24	17.8	14.8	15.07	15.12	14.44	15.23
13.95	15.41	15.55	16.84	14.99	15.2	15.23	14.53	15.37
15.39	15.68	15.84	16.43	15.25	15.39	15.32	14.2	15.58
15.26	15.94	15.51	16.55	15.51	15.62	15.41	14.11	15.66
14.75	15.93	16.21	16.76	15.78	15.78	15.26	15.02	15.73
14.62	15.98	16.49	16.75	15.93	15.68	15.31	15.07	15.75
13.89	13.94	14.11	14.59	14.8	14.92	14.76	13.61	15.47
13.31	14.89	14.92	17.36	15.18	15.2	15	13.9	15.03
14.5	13.05	13.09	14.57	15.53	15.21	14.69	13.42	15.73
13.23	17.26	17.82	23.26	15.34	15.26	15.02	13.86	15.43

T_chwallin[i] [C]	T_chwallout[i] [C]	T_cri[i] [C]	T_cro[i] [C]	T_dew[i] [C]	T_erin[i] [C]	T_ero[i] [C]	T_ers1[i] [C]	T_ers10[i] [C]
27.59	23.16	80.16	46.91	13.24	12.2	22.13	22.82	21.93
27.78	23.28	79.99	47.15	13.93	12.12	21.6	22.48	21.31
27.96	23.35	79.04	47.05	13.87	11.97	20.35	18.68	20.44
27.95	23.33	78.46	47.07	13.83	11.82	19.22	16.16	19.64
27.81	23.27	77.52	46.94	13.64	11.49	17.78	12.79	18.86
27.71	23.18	76.44	46.85	13.57	11.16	15.88	11.66	18.04
27.41	23.23	76.82	46.82	13.76	11.87	17.63	21.15	16.89
27.43	23.39	79.21	47	13.94	12.31	21.27	21.63	20.2
27.54	23.41	72.98	46.83	13.03	11.16	11.01	21.36	16.28
27.56	23.46	78.22	46.99	13.91	12.3	19.93	19.15	21.3

T_ers11[i] [C]	T_ers12[i] [C]	T_ers2[i] [C]	T_ers3[i] [C]	T_ers4[i] [C]	T_ers5[i] [C]	T_ers6[i] [C]	T_ers7[i] [C]	T_ers8[i] [C]
22.28	20.95	22.03	21.77	22.44	21.25	21.08	22.05	21.64
21.93	20.75	21.45	21.13	21.84	20.72	20.53	21.38	20.88
21.18	20.31	19.93	20.19	21.11	20.08	19.91	20.66	20.06
20.52	19.94	18.73	19.39	20.41	19.31	19.17	19.66	19.12
19.73	19.31	17.41	18.25	19.32	18.25	18.24	18.61	18.16
18.99	18.85	15.87	16.95	18.2	17.2	17.29	17.2	17.04
14.95	10.81	20.44	20.07	20.91	19.43	18.19	19.54	19.19
21.32	21.37	21.61	21.6	22.06	20.92	20.64	20.47	20.86
9.648	9.679	20.46	19.95	21.21	19.43	18.07	19.66	19.66
21.61	21.83	20.92	20.82	20.43	19.63	19.73	18.57	18.92

T_ers9[i] [C]	T_ers_ave[i] [C]	T_noz1[i] [C]	T_noz2[i] [C]	T_noz3[i] [C]	T_sat_cond[i] [C]	T_sat_evap[i] [C]	T_shellbot[i] [C]	T_shelltop[i] [C]
21.03	21.77	14.88	14.2	14.67	47.45	12.28	49.2	76.2
20.31	21.22	15.22	15.11	15.05	47.62	12.19	48.89	76.24
19.48	20.17	15.6	14.69	15.32	47.52	12.05	49.61	75.55
18.61	19.22	15.87	14.94	15.42	47.58	11.9	49.57	75.19
17.73	18.06	16.07	15.17	15.24	47.55	11.56	49.3	74.16
16.74	17	16.29	15.39	15.58	47.57	11.23	48.71	73.29
17.34	18.24	16.08	15.05	16.45	47.52	11.95	48.11	73.39
20.27	21.08	15.18	14.51	14.87	47.58	12.39	48.54	75.65
17.73	17.76	16.82	15.2	17.18	47.45	11.23	43.5	70.31
19.09	20.17	15.26	14.06	14.36	47.61	12.37	48.55	74.83

Data for Figs. 2.3, 2.4, 2.7, 2.8

T_sh_sl[i] [C]	T_steam[i] [C]	T_wi[i] [C]	T_wo[i] [C]	UA[i] [kW/C]	UA_r[i] [kW/C]	V_eai[i] [m/s]	V_noz[i] [m/s]	W_auxhtr[i] [kW]
9.858	24.69	17.8	51.3	3.254	3.355	1.581	25.48	3.215
9.404	24.95	17.84	51.62	2.998	3.072	1.578	25.43	3.211
8.308	25.31	17.89	51.3	2.592	2.663	1.573	25.37	3.201
7.324	25.49	17.85	51.3	2.345	2.393	1.567	25.27	3.2
6.211	25.64	17.56	51.12	2.064	2.104	1.558	25.12	3.191
4.645	25.5	17.38	50.9	1.808	1.851	1.543	24.89	3.222
5.68	25.39	17.46	50.67	2.254	2.309	1.579	25.46	3.218
8.882	25.27	17.67	51.22	3.235	3.294	1.58	25.45	3.218
-0.2237	25.31	17.75	49.88	1.536	-0.6729	1.576	25.45	3.225
7.555	25.37	17.56	51.04	2.71	2.828	1.577	25.44	3.237

W_comp[i] [kW]	W_fan[i] [kW]	W_h1[i] [kW]	W_outlet[i] [kW]	W_plugin[i] [kW]	x_din[i]	x_dout[i]	Y[i]
4.121	3.925	5.701	1.4	2.46	0.2597	0.3106	0.9959
4.148	3.912	5.619	1.399	2.46	0.2623	0.3134	0.996
4.178	3.906	5.483	1.392	2.46	0.2616	0.3136	0.996
4.198	3.905	5.274	1.39	2.46	0.2627	0.3143	0.996
4.194	3.895	5.108	1.39	2.46	0.2629	0.3163	0.9961
4.212	3.868	4.562	1.399	2.46	0.2634	0.3172	0.9961
4.166	3.924	5.452	1.398	2.46	0.2601	0.3141	0.9959
4.191	3.919	5.704	1.398	2.46	0.258	0.3122	0.9959
4.134	3.925	5.051	1.402	2.46	0.2627	0.319	0.996
4.202	3.926	5.471	1.407	2.46	0.2543	0.3098	0.996

Data for Figs 2.10, 2.11, 2.12

	alpha[i]	Balance[i]	COP[i]	COP_th[i]	Dep[i] [C]	dh_r[i] [kJ/kg]	dP_dist[i] [kPa]	dP_distm[i] [psi]
baseline	0.996	0.9653	3.778	8.058	5.98	164.7	162.5	23.56
w/ corners	0.996	0.9935	3.731	7.829	42.63	165.4	169.8	24.62
+ center	0.996	0.9854	3.728	7.874	41.34	165.4	166.4	24.13
imp corners	0.996	0.9779	3.775	7.998	7.209	164.7	162.3	23.53
imp corners w/cent	0.996	0.9726	3.743	8.013	7.423	164.7	159.6	23.16
imp all	0.996	0.9752	3.774	8.003	6.571	164.8	161.9	23.49

Drip[i] [g/s]	dT_airside[i] [C]	dT_in[i] [C]	eff_r[i]	epsilon_r[i]	eta[i]	E_in[i] [kW]	E_in_w[i] [kW]	h_airin[i] [kJ/kg]
-6.993	14.24	17.1	0.4688	0.9473	0.708	16.58	16.17	54.9
-7.385	14.21	18.06	0.4765	0.9007	0.6695	16.21	15.65	53.86
-7.446	14.18	17.9	0.4734	0.9061	0.6859	16.15	15.7	53.68
-7.343	14.3	17.28	0.472	0.9382	0.7131	16.37	15.97	54.38
-7.104	14.23	17.19	0.4671	0.9363	0.713	16.65	15.97	54.42
-7.315	14.29	17.26	0.4716	0.9366	0.7119	16.16	16	54.42

h_airout[i] [kJ/kg]	h_cri[i] [kJ/kg]	h_cro[i] [kJ/kg]	h_eamax[i] [kJ/kg]	h_ero[i] [kJ/kg]	LMTD[i] [C]	mu_aeo_ave[i] [kg/m-s]	m_dot_air[i] [kg/s]	M_r[i] [g/s]
40.3	334	139.7	34.28	295.7	4.857	1.799E-05	1.08	104.7
39.3	327.7	139.8	32.12	288.7	7.959	1.799E-05	1.073	105.6
39.15	328.1	139.7	32.5	289.5	7.598	0.000018	1.073	105.5
39.72	333.2	139.8	33.82	294.4	5.418	1.798E-05	1.074	104.1
39.83	332.9	139.8	33.96	294	5.495	1.799E-05	1.073	104.3
39.78	332.9	139.7	33.86	294.1	5.497	1.798E-05	1.073	104.4

M_w[i] [g/s]	omega_ai[i]	omega_ao[i]	P_cri[i] [kPa]	P_cro[i] [kPa]	P_erdi[i] [kPa]	P_erdif[i] [kPa]	P_erdo[i] [kPa]	P_ero[i] [kPa]
149.1	0.01001	0.01001	2906	2890	1387	74.91	1225	1150
148.7	0.009568	0.009568	2910	2893	1368	77.12	1198	1121
148.9	0.009495	0.009495	2909	2891	1369	76.56	1203	1126
147.3	0.009803	0.009803	2912	2894	1410	104.1	1248	1144
145.7	0.009833	0.009833	2913	2893	1411	105.2	1251	1146
146.9	0.009823	0.009823	2912	2893	1415	108.6	1253	1144

P_noz[i] [kPa]	P_tun[i] [kPa]	Q_cond[i] [kW]	Q_e[i] [tons]	Q_eai[i] [m^3/s]	Q_evap_air[i] [kW]	Q_evap_r[i] [kW]	Q_max[i] [kW]	Q_max_r[i] [kW]
0.3994	0.03259	20.34	4.4838	0.943	15.77	16.34	22.27	17.24
0.3942	0.05119	19.84	4.4436	0.9366	15.63	15.73	23.34	17.46
0.3939	0.0544	19.89	4.4312	0.9361	15.58	15.81	22.72	17.45
0.3942	0.05096	20.14	4.4756	0.9368	15.74	16.1	22.07	17.16
0.3936	0.05442	20.15	4.4501	0.936	15.65	16.09	21.95	17.18
0.3941	0.0546	20.17	4.4689	0.9367	15.72	16.12	22.08	17.21

Q_noz[i] [m^3/s]	Re1[i]	Re2[i]	Re3[i]	rho_aei_ave[i] [kg/m^3]	rho_aeo_ave[i] [kg/m^3]	rho_ero[i] [kg/m^3]	SCFM[i] [ft^3/min]	Sigma[i] [C]
0.8986	258069	215058	129035	1.146	1.202	41.63	1998	0.6059
0.8926	256335	213613	128168	1.146	1.203	42.29	1985	3.925
0.8922	256192	213493	128096	1.146	1.203	42.3	1983	3.842
0.8925	256495	213746	128248	1.146	1.203	41.73	1985	0.6625
0.8919	256251	213543	128126	1.146	1.203	41.9	1983	0.8981
0.8924	256438	213698	128219	1.146	1.203	41.82	1985	0.695

Data for Figs 2.10, 2.11, 2.12

T_aei[i] [C]	T_aeo1[i] [C]	T_aeo10[i] [C]	T_aeo11[i] [C]	T_aeo12[i] [C]	T_aeo13[i] [C]	T_aeo14[i] [C]	T_aeo15[i] [C]	T_aeo16[i] [C]
29.14	14.77	14.04	16.3	16.3	22.04	15.01	14.66	15.18
29.22	12.41	13.32	19.19	18.99	11.96	17.85	16.38	18
29.22	12.57	13.46	17.98	17.99	12.09	17.79	16.4	18.2
29.14	13.44	14.63	15.16	15.24	20.8	15.14	14.93	15.91
29.11	13.46	14.86	14.72	14.7	20.55	14.48	14.6	16
29.13	13.45	14.88	14.89	14.8	20.63	14.59	14.67	15.99

T_aeo17[i] [C]	T_aeo18[i] [C]	T_aeo19[i] [C]	T_aeo2[i] [C]	T_aeo20[i] [C]	T_aeo21[i] [C]	T_aeo22[i] [C]	T_aeo23[i] [C]	T_aeo24[i] [C]
15.22	15.13	14.91	14.67	14.63	14.55	14.67	14.48	14.35
18.26	17.67	16.6	13.62	14.37	12.51	14.02	13.76	13.7
18.65	17.63	16.74	13.76	14.33	12.62	14.17	13.96	13.83
15.87	15.85	15.52	15.79	14.03	12.73	14.89	14.94	14.34
15.83	15.51	15.31	16.14	14.05	12.71	14.98	15.36	14.62
15.77	15.41	15.24	16.12	14.03	12.65	14.94	15.23	14.58

T_aeo25[i] [C]	T_aeo3[i] [C]	T_aeo4[i] [C]	T_aeo5[i] [C]	T_aeo6[i] [C]	T_aeo7[i] [C]	T_aeo8[i] [C]	T_aeo9[i] [C]	T_aeo_ave[i] [C]
13.62	14.87	15.11	17.49	14.53	14.71	14.6	13.83	14.9
11.18	13.74	13.58	14.35	14.59	14.6	14.32	13.3	15.01
11.16	13.88	13.69	14.51	14.82	14.72	14.46	13.71	15.04
11.78	15.65	15.99	15.46	15.05	15.03	14.78	13.86	14.83
12.06	16.06	16.16	15.67	15.18	15.21	15.12	14.1	14.87
12.01	15.93	16.16	15.68	15.19	15.19	14.94	13.97	14.85

T_chwallin[i] [C]	T_chwallout[i] [C]	T_cri[i] [C]	T_cro[i] [C]	T_dew[i] [C]	T_erin[i] [C]	T_ero[i] [C]	T_ers1[i] [C]	T_ers10[i] [C]
27.63	25.73	79.67	47.16	14.01	12.04	21.52	22.14	21.45
27.82	25.77	74.96	47.18	13.33	11.16	14.93	11.28	12.45
27.76	25.82	75.24	47.12	13.21	11.32	15.69	11.34	13.07
27.75	25.99	79.09	47.2	13.69	11.86	20.22	19.28	19.28
27.76	25.99	78.89	47.17	13.74	11.91	19.93	20.13	19.9
27.71	25.96	78.87	47.14	13.73	11.87	19.98	20.12	19.54

T_ers11[i] [C]	T_ers12[i] [C]	T_ers2[i] [C]	T_ers3[i] [C]	T_ers4[i] [C]	T_ers5[i] [C]	T_ers6[i] [C]	T_ers7[i] [C]	T_ers8[i] [C]
21.95	20.61	20.72	20.57	20.97	21.13	21.25	22.34	21.16
11.41	10.69	15.79	18.61	21.13	20.67	19.76	20.44	19.89
12.01	10.88	16.39	19.11	21.92	20.84	19.48	19.79	20.09
21.06	20.35	18.88	19.46	20.69	20.46	20.47	20.37	20.02
21.47	20.77	19.26	19.52	20.5	19.91	19.34	17.62	19.71
21.31	20.65	19.28	19.55	20.49	19.93	19.57	18.51	19.63

T_ers9[i] [C]	T_ers_ave[i] [C]	T_noz1[i] [C]	T_noz2[i] [C]	T_noz3[i] [C]	T_sat_cond[i] [C]	T_sat_evap[i] [C]	T_shellbot[i] [C]	T_shelltop[i] [C]
20.45	21.23	14.62	13.64	14.36	47.52	12.12	49.7	75.19
16.91	16.59	16.71	15.41	16.69	47.56	11.24	45.79	71.18
17.55	16.87	16.61	15.35	16.03	47.53	11.39	45.52	71.74
19.38	19.97	15.02	14.73	14.66	47.57	11.93	49.28	75.14
19.86	19.83	15.01	14.54	13.93	47.57	11.99	49.31	74.96
19.53	19.84	15.05	14.6	13.99	47.57	11.94	49.19	74.88

Data for Figs 2.10, 2.11, 2.12

T_sh_sl[i] [C]	T_steam[i] [C]	T_wi[i] [C]	T_wo[i] [C]	UA[i] [kW/C]	UA_r[i] [kW/C]	V_eai[i] [m/s]	V_noz[i] [m/s]	W_auxhtr[i] [kW]
9.402	26.39	18.6	51.22	3.246	3.363	1.572	25.34	3.259
3.693	26.74	18.58	50.48	1.963	1.976	1.561	25.17	3.249
4.3	26.75	18.51	50.45	2.051	2.081	1.56	25.15	3.234
8.287	27.03	18.58	51.26	2.905	2.971	1.561	25.16	3.24
7.94	27.06	18.22	51.3	2.848	2.928	1.56	25.15	3.236
8.035	27.05	18.38	51.2	2.859	2.932	1.561	25.16	3.251

W_comp[i] [kW]	W_fan[i] [kW]	W_h1[i] [kW]	W_outlet[i] [kW]	W_plugin[i] [kW]	x_din[i]	x_dout[i]	Y[i]
4.174	3.884	5.563	1.413	2.46	0.2607	0.288	0.996
4.189	3.869	5.216	1.412	2.46	0.2643	0.2929	0.996
4.181	3.875	5.17	1.407	2.46	0.2635	0.2915	0.996
4.17	3.873	5.386	1.408	2.46	0.2574	0.2845	0.996
4.181	3.872	5.677	1.406	2.46	0.2571	0.2838	0.996
4.164	3.876	5.162	1.414	2.46	0.256	0.2831	0.996

Data for Figures 2.3, 2.6, 2.9

		Sigma	epsilon	LMTD	NTU	UA
baseline	1	0.5749221	0.9495	4.87	2.924	3.254
10% vertical	0.9	0.6097193	0.9448	5.274	2.701	2.998
20% vertical	0.8	0.6505313	0.9354	6.044	2.342	2.592
30% vertical	0.7	1.0808857	0.927	6.653	2.128	2.345
40% vertical	0.6	1.7151312	0.9173	7.479	1.884	2.064
50% vertical	0.5	1.824199	0.905	8.378	1.666	1.808
10% H	0.9	2.8351723	0.9174	6.946	2.028	2.254
10% H improved	0.9	0.5792302	0.9432	4.966	2.909	3.235
15% H	0.85	3.8767682	0.6544	9.989	1.385	1.536
15% H improved	0.85	1.079084	0.9335	5.77	2.44	2.71
baseline	1	0.6054177	0.9473	4.857	2.931	3.246
+corners	0.6770594	3.9244967	0.9007	7.959	1.785	1.963
+center	0.5296456	3.8427554	0.9061	7.598	1.866	2.051
improved corners	0.6770594	0.6615449	0.9382	5.418	2.64	2.905
(improved corners) + center	0.5296456	0.8983237	0.9363	5.495	2.59	2.848
improved (corners & center)	0.5296456	0.6949595	0.9366	5.497	2.599	2.859